Wave propagation methods for the experimental characterization of soft biomaterials and tissues

By

Siavash Kazemirad

Doctor of Philosophy

Department of Mechanical Engineering

McGill University

Montreal, Quebec

August 2013

A dissertation submitted to McGill University in partial fulfillment of the requirements for the degree of Doctor of Philosophy

To my family,

specially

my father and mother

who have devoted their lives to me.

Abstract

A good understanding of the viscoelasticity of soft biomaterials and tissue is needed to predict their mechanical response under loads in biological conditions. For example, the viscoelastic properties of hydrogels used in cell culturing and tissue engineering should approximately match those of the tissue they replace. These properties are strongly dependent on the excitation frequency. This has important implication for voice production. The human vocal folds oscillate at a fundamental frequency around 125, 200, 300 and 500 Hz in normal phonation for male, female, children and infants, respectively. Vibration frequencies can reach up to a few kHz, specially in singing. Vocal fold oscillations, essential to voice production, are significantly affected by the mechanical (viscoelastic) properties of the vocal fold mucosa.

A novel characterization method based on Rayleigh wave propagation was developed for the quantification of frequency-dependent viscoelastic properties of soft biomaterials over a broad frequency range; i.e., up to 4 kHz. Synthetic silicone rubber and gelatin samples were fabricated and tested to evaluate the proposed method. The shear and elastic moduli and the loss factor obtained from the Rayleigh wave propagation method were compared with results from two other methods, as well as results from an independent study. The proposed method was found to be accurate and cost effective for the measurement of viscoelastic properties of soft biomaterials, such as phonosurgical biomaterials and hydrogels, over a wide frequency range.

A non-invasive method was developed to measure the shear modulus of human vocal fold tissue *in vivo* during phonation. This is needed for the development of injectable biomaterials for vocal fold augmentation and repair, and to evaluate voice treatment procedures. The mucosal wave propagation speed was measured for four human subjects at different phonation frequencies using high speed endoscopic images of the larynx and image processing methods. The transverse shear modulus of the vocal fold mucosa was then calculated from a surface wave propagation dispersion equation using the measured

wave speeds. The results were found to be in good agreement with those from other studies obtained via *in vitro* measurements, thereby supporting the validity of the proposed measurement method.

Hyaluronic acid-gelatin hydrogels with varying concentrations of cross-linker are other constituents were fabricated. These biomaterials are for use as synthetic extracellular matrix in vocal fold tissue engineering. The Rayleigh wave propagation method was used to quantify the frequency-dependent viscoelastic properties of these hydrogels, including shear and viscous moduli, over a broad frequency range; i.e., from 40 to 4000 Hz. The viscoelastic properties of the designed hydrogels were similar to those of human vocal fold tissue obtained from *in vivo* and *in vitro* measurements. It was shown that the cross-linker concentration is the most common parameter to tune the viscoelastic properties of designed hyaluronan-based hydrogels. The hyaluronic acid and gelatin contents of these hydrogels are the main parameters to adjust their biochemical and biological properties, considering the changes in the viscoelastic properties of the hydrogels.

Résumé

Les propriétés viscoélastiques des biomatériaux et des tissus mous déterminent leur comportement mécanique sous charge dans des conditions biologiques. Par exemple, les propriétés viscoélastiques des hydrogels utilisés dans la culture cellulaire et l'ingénierie tissulaire doivent approximativement correspondre à ceux du tissu qu'ils remplacent. La quantification précise des propriétés dépendant de la fréquence de tissus de cordes vocales et des biomatériaux mous est importante pour la reconstruction de la voix. Les cordes vocales humaines oscillent à une fréquence fondamentale autour de 125, 200, 300 et 500 Hz pour une phonation normale chez les hommes, femmes, enfants et nourrissons, respectivement. Les fréquences de vibration peuvent atteindre jusqu'à plusieurs kHz, spécialement dans le chant. Les oscillations des cordes vocales, essentielles à la production de la voix, sont significativement affectées par les propriétés mécaniques (viscoélastiques) de la muqueuse des cordes vocales.

Une méthode de caractérisation nouvelle basée sur la propagation des ondes de Rayleigh a été développée pour la quantification des propriétés viscoélastiques dépendant de la fréquence des biomatériaux moux sur une large gamme de fréquences, soit jusqu'à 4 kHz. Des caoutchouc de silicone synthétique et des échantillons de gélatine ont été fabriqués et testés pour évaluer la méthode proposée. Les modules de cisaillement et élastique et le facteur de perte obtenu à partir de la méthode de propagation des ondes de Rayleigh ont été comparés avec ceux obtenus à l'aide de deux autres méthodes, ainsi qu'a des résultats présentés dans une étude indépendante. La méthode proposée semblé fiable, précise et pratique rentable pour la mesure des propriétés viscoélastiques des biomatériaux mous, comme les biomatériaux de phonosurgical et d'hydrogels, sur une large gamme de fréquences.

Une méthode non-invasive a été développée pour mesurer le module de cisaillement des tissus de cordes vocales humaines *in vivo* au cours de la phonation. Ceci est nécessaire pour le développement de biomatériaux injectables pour l'augmentation des

cordes vocales et de réparation, et pour évaluer les procédures de traitement de la voix. La vitesse de propagation de l'onde muqueuse a été mesurée pour quatre sujets humains à des fréquences différentes en utilisant des images endoscopiques à grande vitesse du larynx et des méthodes de traitement d'image. Le module de cisaillement transversal de la muqueuse des cordes vocales a ensuite été calculé à partir d'une équation de dispersion de propagation des ondes de surface en utilisant les vitesses d'ondes mesurées. Les résultats sont en bon accord avec ceux d'autres études obtenus par des mesures *in vitro*, confirmant ainsi la précision de la méthode de mesure proposée.

Les hydrogels acide hyaluronique-gélatine avec des concentrations de cross-linker diverses et d'autres composants ont été fabriqués. Ces biomatériaux sont pour une utilisation comme matrice extracellulaire synthétique dans l'ingénierie tissulaire des cordes vocales. La méthode de propagation des ondes de Rayleigh a été utilisée pour quantifier les propriétés viscoélastiques dépendant de la fréquence de ces hydrogels, y compris les modules de cisaillement et visqueux, sur une large gamme de fréquences, c'est à dire de 40 à 4000 Hz. Les propriétés viscoélastiques des hydrogels conçus sont similaires à celles du tissu pli vocal humain obtenu à partir *in vivo* et des mesures *in vitro*. Il est observé que la concentration de réticulation est le paramètre le plus commun pour régler les propriétés viscoélastiques des hydrogels basés sur l'acide hyaluronique conçus. L'acide hyaluronique et le contenu de gélatine de ces hydrogels sont les principaux paramètres à ajuster leurs propriétés biochimiques et biologiques, en tenant compte des changements dans les propriétés viscoélastiques des hydrogels.

Acknowledgements

I would like to sincerely thank my supervisor, Professor Luc Mongeau. The present research study could not be accomplished without his valuable guidance and support over the past four years, while this work has been developed.

I would like to thank all my colleagues in the Biomechanics and Acoustics laboratories, specially Dr. Hossein K. Heris and Dr. Hani Bakhshaee who collaborated in different parts of my PhD research project.

Financial support from McGill University, through the McGill Engineering Doctoral Award (MEDA), McGill International Doctoral Award (MIDA), and Clifford Pang Doctoral Fellowship, is gratefully acknowledged. Canadian institute of health research (CIHR) and national institute of health on deafness and other communication disorders (NIDCD) are acknowledged for providing funding for this experimental research study.

TABLE OF CONTENTS

LIST OF TABLES

LIST OF FIGURES

Nomenclature

Roman symbols

$\mathbf{u}$	Displacement vector
A_i	Amplitude of the wave potential
B_i	Amplitude of the wave potential
C_1	Amplitude of the wave potential
D_1	Amplitude of the wave potential
$\hat{H}(i\omega)$	Transfer function
L	Distance between two locations on the surface of the sample
c_m	Mucosal wave speed
$\hat{c}_c$	Compressional wave speed
$\hat{c}_s$	Shear wave speed
$\hat{c}_l$	Longitudinal wave speed
$\hat{k}_c$	Compressional wavenumber
$\hat{k}_s$	Shear wavenumber
$\hat{k}_R$	Rayleigh wavenumber
$\hat{k}_l$	Longitudinal wavenumber
$\mathbf{C}$	Coefficient matrix
h	Sample thickness
m	Specimen mass
M	Termination mass
$\hat{G}(\omega)$	Complex shear modulus
$\hat{E}(\omega)$	Complex elastic modulus

E'	Real part of the elastic modulus
E''	Imaginary part of the elastic modulus
G'	Real part of the shear modulus
G''	Imaginary part of the shear modulus
f	Frequency
f_0	Fundamental frequency
Re	Real part of a complex value
Im	Imaginary part of a complex value
a	Curve fitting coefficient
b	Curve fitting coefficient
R^2	Coefficient of determination,

Greek Symbols

σ_{ij}	Stress tensor components
ε_{ij}	Strain tensor components
δ_{ij}	Kronecker delta
ω	Angular frequency
$\hat{\lambda}(\omega)$	Frequency-dependent Lame function
$\hat{\mu}(\omega)$	Frequency-dependent Lame function
ν	Poisson's ratio
ρ	Density
ϕ	Compressional wave potential
ψ	Shear wave potential
φ	Phase of the transfer function
η	Loss factor

λ	Real part of the Rayleigh wavenumber
γ	Imaginary part of the Rayleigh wavenumber
β	Real part of the longitudinal wavenumber
α	Imaginary part of the longitudinal wavenumber
μ'	Shear elasticity
μ''	Shear viscosity

Abbreviations

HA	Hyaluronic acid
ECM	Extracellular matrix
Ge	Gelatin
MR	Magnetic resonance
MRI	Magnetic resonance imaging
HSDI	High speed digital imaging
LDV	Laser Doppler vibrometer
SH	Shear horizontal
IRB	Research Ethics office
dB	Decibel
PEGDA	Polyethylene glycol diacrylate
AFM	Atomic force microscopy

CHAPTER 1
Introduction

1.1. Overview

Voice is the essential part of singing and speech communication. Voice disorders significantly affect the quality of life. According to the National Institute on Deafness and other Communication Disorders (NIDCD), about 7.5 million people suffer from a voice disorder in the United States. This approximately costs $2.5 billion for the US economy annually (Verdolini and Ramig, 2001). Human voice is produced by airflow expelled from the lungs through the airway and modulated by the self-sustained oscillation of the vocal folds, two membranes located within the trachea at the level of Adam's apple. The oscillation involves mainly medial and lateral wavy motion of the vocal fold mucosa, commonly referred to as the mucosal wave. This structural wave travels from the lower to upper vocal fold lip over the medial and superior surfaces of the vocal folds at a speed that is commensurate with the elasticity of the tissue. The generation and propagation of the mucosal wave depends on the shear viscoelastic properties of the mucosa. Vocal fold disorders significantly affect the viscoelasticity of vocal fold tissue, and consequently hamper the self-sustained oscillations of the folds essential to voice production.

One common example of vocal fold disorders is vocal fold scarring, resulting from voice abuse or surgery. Scarring increases the overall stiffness of the tissue, presumably because of the appearance of high intensity cross-linked collagen fibers. Scarred vocal fold lamina propria is commonly treated using injectable biomaterials such as hydrogels and commercial phonosurgical biomaterials. The viscoelastic properties of implants, biomaterials and tissue engineering scaffold materials designed for voice restoration must be compatible with the vibrating tissue throughout the frequency range of vocalization.

Consequently, A knowledge of the viscoelastic properties of biomaterials and vocal fold tissue is needed to create mathematical models and to perform numerical simulations of phonation (Becker *et al.*, 2009; Link *et al.*, 2009), for therapeutic applications such as the development of injectable biomaterials for vocal fold augmentation and repair (Caton *et al.*, 2007; Heris *et al.*, 2012), for diagnostic purposes to distinguish between scarred and healthy tissue (Thibeault *et al.*, 2002; Rousseau *et al.*, 2004), and to evaluate surgical methods used in vocal fold treatment (Thibeault et al., 2011). The fundamental frequency of vocal fold vibrations can reach up to a few kHz in singing (Titze, 1994). Data obtained from electroglottography (EGG) and laser Doppler velocimetry of the human vocal folds during phonation has shown that there is significant vibration energy at frequencies up to 3 kHz (Chan *et al.*, 2013). Therefore, the mechanical properties of vocal fold tissue and injectable biomaterials need to be characterized at frequencies up to 3 kHz.

1.2. Background and literature review

1.2.1. Mechanical characterization of injectable biomaterials

The injectable biomaterials are mostly gel-like materials, and thus standard measurement techniques such as dynamic mechanical analysis are not suitable to quantify their mechanical properties. Parallel-plate rheometry has mostly been used to characterize the viscoelastic properties of phonosurgical biomaterials (Chan and Titze, 1998; 1999a; Klemuk and Titze, 2004; Titze *et al.*, 2004; Caton *et al.*, 2007; Kimura *et al.*, 2010). Chan and Titze (1998; 1999) employed a parallel-plate shear rheometer to measure the viscoelastic properties of commonly used phonosurgical biomaterials and hyaluronic acid. Measurements were performed at frequencies up to 10 Hz. Klemuk *et al*. (2004) used a parallel-plate rheometer to measure the viscoelastic properties of three vocal fold injectable biomaterials at low frequencies, i.e. 0.1 to 100 Hz. Titze *et al*. (2004)

introduced a method for the rheological characterization of biomaterials with approximate vocal fold tissue properties at low frequencies within the audible range, i.e. from 20 to 250 Hz. Sample geometry, phase corrections, and compensation for the system inertia were taken into account to extend the frequency range of a commercially available rheometer. Caton *et al*. (2007) measured the shear and viscous moduli of five commonly used vocal fold injectable biomaterials using a parallel-plate shear rheometer at frequencies up to 150 Hz. Results were compared with viscoelastic properties of cadaveric vocal fold tissue. Kimura *et al*. (2010) used a controlled-strain simple-shear rheometer to measure the viscoelastic properties of currently or potentially used vocal fold injectable biomaterials at frequencies up to 250 Hz. Based on the literature, methods developed so far for the quantification of the viscoelastic properties of vocal fold injectable biomaterials are limited to frequencies lower than 250 Hz.

Hyaluronic acid (HA) is a glycosaminoglycan. It is one of the main components of the extracellular matrix (ECM) of the human vocal fold lamina propria (Butler *et al.*, 2001; Lebl *et al.*, 2007). It has been postulated that HA helps to maintain the viscosity and stiffness of the vocal fold tissue within an optimal range that eases phonation and helps the control of the fundamental frequency (Chan *et al.*, 2001). Shear thinning of HA, i.e. the decrease in viscosity as the frequency of oscillation is increased, is assumed to play a role in wide bandwidth of phonation, specially in singing (Chan *et al.*, 2001; Ward *et al.*, 2002). In addition to HA's viscoelastic properties, its shock absorption and space filling characteristics make it to be a good injectable biomaterial for vocal fold tissue augmentation and repair (Ward *et al.*, 2002). Clinical studies on vocal fold treatment using HA based injectable biomaterials showed significant improvements in glottal closure and the quality of voice, as well as less resorption compared with collagen based injectable biomaterials (Hertegård *et al.*, 2002; 2004). Several investigations have been performed on the measurement of the viscoelastic properties of HA hydrogels (Chan and Titze, 1999a; Ghosh *et al.*, 2005; Jha *et al.*, 2009). For example, Chan and Titze (Chan and Titze, 1999a) measured the viscoelastic shear properties of HA gels at different concentrations, with and without fibronectin, at frequencies up to 15 Hz and compared them with those of the human vocal fold mucosa.

Gelatin (Ge), obtained from partially hydrolyzed collagen, is composed of a heterogeneous mixture of proteins (Benton *et al.*, 2009). It is an excellent substrate for cell attachment, proliferation, and differentiation. Gelatin and HA has been cross-linked to fabricate synthetic ECM hydrogels for tissue engineering, three-dimensional cell culture, and wound repair (Shu *et al.*, 2003; Shu and Prestwich, 2004). Cross-linked HA-Ge hydrogels were produced for vocal fold tissue repair and tested on rabbit vocal folds that underwent biopsy bilaterally (Duflo *et al.*, 2006a; Duflo *et al.*, 2006b). The viscoelastic properties of the tissue were measured at frequencies up to 10 Hz, three weeks after biopsy and injection. The viscoelastic properties of the injected HA-Ge hydrogels, however, were not measured. The presented results suggested that a gelatin concentration of 5% provided a better wound-healing environment for tissue regeneration, which improved the tissue viscoelastic properties. The shear modulus of a variety of cross-linked HA-Ge hydrogels with different concentrations of HA, Ge, and the cross-linker were measured using a shear rheometer at 1 Hz (Vanderhooft *et al.*, 2009). The frequency-dependency of the viscoelastic properties of the fabricated hydrogels was not investigated.

1.2.2. Mechanical characterization of vocal fold tissue

In vitro measurements of the viscoelastic shear properties of human vocal fold tissue have mostly been performed using parallel plate or linear skin rheometry (Chan and Titze, 1999b; Goodyer *et al.*, 2003; Chan, 2004; Hess *et al.*, 2006; Chan and Rodriguez, 2008; Dailey *et al.*, 2009; Goodyer *et al.*, 2009). For example, Chan and Titze (1999) used a parallel plate rotational rheometer to measure the linear viscoelastic shear properties of 15 excised human vocal fold mucosa samples. The elastic and viscous shear moduli of the samples were determined at frequencies up to 15 Hz using shear stresses and strains obtained from the rheometer. Chan and Rodriguez (2008) designed a custom-built, controlled-strain, linear, simple-shear rheometer for the measurement of the viscoelastic properties at frequencies up to 250 Hz. The viscoelastic shear moduli of seven human vocal fold cover specimens were measured. Hess and Goodyer et al. (2003; 2006; 2009) used a linear skin rheometer to measure the vocal fold viscoelastic properties. The stiffness and the viscosity of porcine, canine and human vocal folds were measured using a simple shear rheometer at a frequency of 0.3 Hz. Local stiffness measurements were also made. These existing methods are inaccurate for frequencies greater than at most 250 Hz, and cannot be used for in vivo measurements.

In vivo measurements of the vocal fold elastic modulus have been performed (Berke, 1992; Berke and Smith, 1992; Tran et al., 1993; Goodyer et al., 2006; Goodyer et al., 2007a; Goodyer et al., 2007b). Berke and Tran et al. (1992; 1993) constructed an apparatus, which worked based on direct lateral force and displacement measurements, to obtain the vocal folds elastic modulus in vivo. This invasive measurement technique had a limited range of application due to its cumbersome apparatus. Goodyer et al. (2006; 2007a; 2007b) developed a custom built instrument to measure the vocal folds elastic properties in vivo. The shear modulus of eight patients' vocal folds was measured along the transverse direction at the mid-membranous point. This measurement technique is invasive, and is performed in a quasi-static manner; i.e., the frequency-dependent properties of human vocal fold tissue were not obtained at different phonation frequencies.

1.2.3. Wave propagation based characterization methods

Wave propagation methods have been recently introduced to measure the viscoelastic properties of soft materials and tissues (Greenleaf *et al.*, 2003; Catheline *et al.*, 2004; Chen *et al.*, 2004; Kanai, 2005; Sinkus *et al.*, 2005; Chen *et al.*, 2009; Vappou *et al.*, 2009; Nenadic *et al.*, 2011a; Nenadic *et al.*, 2011b). The excitation of the waves has been performed using either external or internal methods. The former has usually been done by a mechanical actuator, and the later by means of the radiation force of ultrasound. Three general methods have been used for tracking and detecting the waves; namely acoustic, ultrasound, and magnetic resonance (MR) methods. Acoustic methods measure the sound produced by the vibrating sample. Ultrasound methods measure the displacement using either Doppler or pulse-echo methods. MR methods use a phase-sensitive MR machine to measure the displacement distribution (Greenleaf *et al.*, 2003). For example, Catheline *et al*. (2004) investigated an inverse problem algorithm to estimate the viscoelastic properties of soft materials. Transient elastography experiments were performed using plane shear wave propagations in the medium. Experimental results were compared to predictions from two simple rheological models.

Chen *et al*. (2004; 2009) developed a method to calculate the viscoelastic properties of homogeneous materials via shear wave speed dispersion measurements. An ultrasound transducer was used to generate cylindrical shear waves at different frequencies in a medium. The propagation speed was determined from the phase shift of the propagating shear wave along the propagation direction. The shear elasticity and viscosity of the medium were calculated by fitting the Voigt viscoelastic model to the measured data. This method was used to measure the viscoelastic properties of gelatin phantoms, bovine muscle *in vitro*, and swine liver *in vivo*. Following a similar approach, Nenadic *et al*. (2011b) developed a measurement method based on Lamb wave propagation for quantifying the viscoelastic properties of soft materials and tissues with plate-like geometries. The viscoelastic properties of urethane rubber, gelatin, and excited porcine myocardium samples were measured. Dispersion equations for cylindrical Lamb and Rayleigh waves propagated in a viscoelastic plate submerged in a nonviscous fluid were presented by Nenadic *et al.* (2011a). Wave propagation velocities were measured in gelatin plates, excised porcine spleen, and left ventricular free-wall myocardium samples; the corresponding viscoelastic properties were determined. However, these methods use rheological models that assume *one constant value* for the shear modulus and viscosity and do not take the dependence of viscoelastic properties of the material on frequency into consideration. In these studies, only the phase of the propagating wave was measured at different locations along the propagation direction. The decrease in the amplitude of the propagating wave with distance, which takes place in viscoelastic media due to dissipation, was not measured and considered in the modeling. Thus real values were obtained for the wave propagation speeds. The wave speeds and consequently the wavenumbers in viscoelastic media should be complex (Borcherdt, 2009). In the end, an approximate rheological model was used to perform the regression of the measured data to obtain the complex shear modulus of the medium. This yields only a *constant value* for the shear elasticity and viscosity over the frequency range of interest.

1.3. Research objectives

The literature review presented in previous section suggests that more sophisticated methods are required to characterize the *frequency-dependent* viscoelastic properties of injectable biomaterials and vocal fold tissue over a *broad frequency range*. The main objective of this study was to develop an integrated methodology to characterize the frequency-dependent properties of human vocal fold tissue and fabricate an optimum injectable hydrogel with desirable biomechanical and biological properties required for the treatment of any specific patient's vocal fold tissue. The following specific aims were defined to achieve the main objective.

The first aim was to develop a model-independent characterization method based on wave propagation approaches for quantifying the frequency-dependent viscoelastic properties of soft biomaterials. The developed method should be optimized for the characterization of expensive injectable phonosurgical biomaterials and hydrogels used for vocal fold augmentation and repair.

The second aim was to develop a methodology for non-invasive *in vivo* measurement of the shear modulus of human vocal fold mucosa during phonation. This enables physicians to select the best available injectable biomaterial for the treatment of any specific patients' vocal fold tissue. Furthermore, the post surgery assessment of the treated tissue can be provided.

The third aim was to fabricate and characterize various hydrogels with viscoelastic properties similar to those of human vocal fold tissue. The application of these hydrogels with tuned mechanical and biological properties is for use as a synthetic extracellular matrix (ECM) in vocal fold tissue engineering.

1.4. Thesis organization

The theoretical modelling of the developed wave propagation based methods for quantifying the frequency-dependent viscoelastic properties of soft biomaterials and the shear modulus of human vocal fold tissue is presented in Chapter 2. The experimental methods and considerations used in this study to fabricate the test samples and implement the developed characterization methods are described in Chapter 3. The results obtained from different parts of this study is presented and comprehensively discussed in Chapter 4. The evaluation of the proposed characterization methods versus other independent well-established methods and studies is also presented in the same chapter. Finally, a summary of this study, some concluding remarks, and the perspectives for future works is described Chapter 5.

CHAPTER 2
Theoretical modelling

2.1. Rayleigh wave propagation method

A novel model-independent characterization method is developed based on Rayleigh wave propagation for the quantification of *frequency-dependent* viscoelastic properties of soft biomaterials. Planar harmonic Rayleigh waves at different frequencies, up to 4 kHz, are launched on the surface of a sample using an actuator. In contrast with previous studies, both the phase and amplitude of the propagating surface (Rayleigh) wave are measured at different locations. These two independent parameters are simultaneously considered in the modelling via a transfer function method, and thus complex values for the Rayleigh wavenumber (or propagation speed) are obtained at each excitation frequency. The complex wavenumber includes information about both the *propagation* and *dissipation* of the wave at different frequencies. Therefore, it is not required to fit any approximate rheological model to the measured data. Eventually, the frequency-dependent complex shear and elastic moduli are calculated using a dispersion relation obtained from the solution of the inverse wave propagation problem.

2.1.1. Mathematical modelling

Rayleigh waves are surface waves which are confined near stress-free boundaries in half spaces. They involve interactions between compressional and shear waves (Achenbach, 1973). To model their propagation in viscoelastic materials, the medium is assumed to be linear, isotropic, and macroscopically homogeneous. The constitutive equations may be written as

$$\sigma_{ij} = \hat{\lambda}(\omega)\delta_{ij}\varepsilon + 2\hat{\mu}(\omega)\varepsilon_{ij}\,, \tag{2.1}$$

where σ_{ij} and ε_{ij} are stress and strain tensor components, δ_{ij} is the Kronecker delta symbol, ω is the angular frequency, and $\hat{\lambda}(\omega)$ and $\hat{\mu}(\omega)$ are complex, frequency-dependent Lame functions. These are determined according to the relations

$$\hat{\lambda}(\omega) = \frac{2\nu}{1-2\nu}\hat{G}(\omega), \tag{2.2a}$$

$$\hat{\mu}(\omega) = \hat{G}(\omega), \tag{2.2b}$$

in which $\hat{G}(\omega) = G'(\omega) + i\,G''(\omega)$ is the complex shear modulus, and ν is the Poisson's ratio of the medium. Wave motion in the medium is governed by Navier's equation (Achenbach, 1973)

$$\rho\frac{\partial^2\mathbf{u}}{\partial t^2} = \hat{\mu}\nabla^2\mathbf{u} + \left(\hat{\lambda} + \hat{\mu}\right)\boldsymbol{\nabla}\left(\boldsymbol{\nabla}\cdot\mathbf{u}\right), \tag{2.3}$$

subject to the appropriate boundary conditions. Here, ρ is the density of the specimen, and **u** is the displacement vector that can advantageously be expressed as the sum of the gradient of a scalar potential and the curl of a vector potential

$$\mathrm{u} = \boldsymbol{\nabla}\phi + \boldsymbol{\nabla}\times\boldsymbol{\psi}, \tag{2.4}$$

with the condition $\boldsymbol{\nabla}\cdot\boldsymbol{\psi} = 0$. Because of the two-dimensional nature of the problem; i.e., the translational invariance of the problem geometry along the x_3-axis of the coordinate system (see Figure 2-1), we may assume $\boldsymbol{\psi} = (0,0,\psi)$. Applying the above decomposition, Eq. (2.4), into Eq. (2.3) allows separation of the governing equation of motion into the classical Helmholtz equations

$$\left(\nabla^2 + \hat{k}_c^2\right)\phi = 0, \tag{2.5a}$$

$$\left(\nabla^2 + \hat{k}_s^2\right)\psi = 0, \tag{2.5b}$$

where the quantities ϕ and ψ are the compressional and the shear wave potentials (Graff, 1975). The complex wavenumbers, $\hat{k}_c$ and $\hat{k}_s$, are expressed as (Graff, 1975)

$$\hat{k}_c = \frac{\omega}{\hat{c}_c} = \frac{\omega}{\sqrt{\left(\hat{\lambda} + 2\hat{\mu}\right)/\rho}}, \tag{2.6a}$$

$$\hat{k}_s = \frac{\omega}{\hat{c}_s} = \frac{\omega}{\sqrt{\hat{\mu}/\rho}}, \tag{2.6b}$$

in which $\hat{c}_c$ and $\hat{c}_s$ are complex compressional and shear wave speeds, respectively. The relevant displacement components in a Cartesian coordinate system are expressed in terms of these potentials through

$$u_1 = \frac{\partial\phi}{\partial x_1} + \frac{\partial\psi}{\partial x_2}, \tag{2.7a}$$

$$u_2 = \frac{\partial\phi}{\partial x_2} - \frac{\partial\psi}{\partial x_1}, \tag{2.7b}$$

and the corresponding stresses in the viscoelastic medium are

$$\sigma_{11} = 2\hat{\mu}\frac{\partial u_1}{\partial x_1} + \hat{\lambda}\varepsilon, \tag{2.8a}$$

$$\sigma_{22} = 2\hat{\mu}\frac{\partial u_2}{\partial x_2} + \hat{\lambda}\varepsilon, \tag{2.8b}$$

$$\sigma_{12} = \hat{\mu}\left(\frac{\partial u_1}{\partial x_2} + \frac{\partial u_2}{\partial x_1}\right), \tag{2.8c}$$

where $\varepsilon = \nabla \cdot \mathbf{u} = \nabla^2 \phi = -\hat{k}_c^2 \phi$.

The quantities ϕ and ψ must satisfy the boundary conditions on the surface of the medium. One proper set of potentials is (Kundu, 2004)

$$\phi = A_1 e^{i\hat{k}_R x_1 - k_1 x_2}, \tag{2.9a}$$

$$\psi = A_2 e^{i\hat{k}_R x_1 - k_2 x_2}, \tag{2.9b}$$

in which A_1 and A_2 are the amplitudes of the existing potentials, and $\hat{k}_R$ is the complex Rayleigh wavenumber. Harmonic time variation was assumed with the $e^{-i\omega t}$ factor omitted for simplicity. Note that ϕ and ψ decrease as x_2 increases, which satisfies the requirement that the Rayleigh waves must be confined to regions near the medium surface. Substitution of Eq. (2.9) into Eq. (2.5) yields

$$k_1^2 = \hat{k}_R^2 - \hat{k}_c^2, \tag{2.10a}$$

$$k_2^2 = \hat{k}_R^2 - \hat{k}_s^2. \tag{2.10b}$$

The specific boundary conditions that need to be satisfied on the stress-free boundary (i.e., at $x_2 = 0$) are $\sigma_{12} = 0$ and $\sigma_{22} = 0$. Consequently, utilization of the stress relations in the boundary conditions yields

$$\hat{\mu}\left(-2iA_1 k_1 \hat{k}_R e^{i\hat{k}_R x_1 - k_1 x_2} + A_2 k_2^2 e^{i\hat{k}_R x_1 - k_2 x_2} + A_2 \hat{k}_R^2 e^{i\hat{k}_R x_1 - k_2 x_2}\right) = 0, \tag{2.11a}$$

$$\begin{aligned} &\left(\hat{\lambda} + 2\hat{\mu}\right)\left(A_1 k_2^2 e^{i\hat{k}_R x_1 - k_1 x_2} + iA_2 \hat{k}_R k_2 e^{i\hat{k}_R x_1 - k_2 x_2}\right) \\ &\qquad + \hat{\lambda}\left(-A_1 \hat{k}_R^2 e^{i\hat{k}_R x_1 - k_1 x_2} - iA_2 \hat{k}_R k_2 e^{i\hat{k}_R x_1 - k_2 x_2}\right) = 0. \end{aligned} \tag{2.11b}$$

Manipulation and simplification of Eqs. (2.11a) and (2.11b) lead to the following dissipation equation, ensuring nontrivial solutions for A_1 and A_2

$$\left(2-\xi^2\right)^4 - 16\left(1-\xi^2\right)\left(1-\frac{\xi^2}{\kappa^2}\right) = 0, \tag{2.12}$$

where

$$\kappa^2 = \left(\frac{\hat{c}_c}{\hat{c}_s}\right)^2 = \left(\frac{\hat{k}_s}{\hat{k}_c}\right)^2 = \frac{\hat{\lambda}+2\hat{\mu}}{\hat{\mu}} = \frac{2-2\nu}{1-2\nu}, \tag{2.13}$$

and $\xi = \dfrac{\hat{k}_s}{\hat{k}_R}$.

It can easily be shown that if $\xi = \xi_R < 1$, then k_1 and k_2 are real values. In this case, a Rayleigh wave with a velocity $\hat{c}_R = \xi_R\,\hat{c}_s$ propagates near the free surface of the medium. From the Rayleigh wavenumber, and after substitution of Eqs. (2.9) into Eqs. (2.7), the displacement components at the free surface of the medium ($x_2 = 0$) are obtained as

$$\hat{u}_1\left(i\omega, x_1\right) = i\hat{k}_R A_1\left(3-\frac{\xi_R^2}{2}\right)e^{i\hat{k}_R x_1}, \tag{2.14a}$$

$$\hat{u}_2\left(i\omega, x_1\right) = ik_1 A_1\left(1+\frac{2\hat{k}_R^2-\hat{k}_s^2}{2k_1k_2}\right)e^{i\hat{k}_R x_1}. \tag{2.14b}$$

2.1.2. The transfer function method

The transfer function is the complex ratio of the vibration displacements of two different locations of the sample along the wave propagation direction. Transfer function method was developed and used along with a standing longitudinal wave propagation method to obtain the complex modulus of rod-like specimens (Pritz, 1982). It has never been used in characterization methods based on surface wave propagations. In this study, the transfer function method was employed to calculate the complex Rayleigh wavenumber from the measured amplitude and phase of the propagated wave at different locations. The transfer function between the vertical displacement components, u_2, at two different locations along the propagation direction, x_1, on the surface of the sample is defined as

$$\hat{H}(i\omega)=\left|\hat{H}(i\omega)\right|e^{i\varphi}=\frac{\hat{u}_2(i\omega)\big|_{x_1=x_{12}}}{\hat{u}_2(i\omega)\big|_{x_1=x_{11}}}, \tag{2.15}$$

where $\left|\hat{H}(i\omega)\right|$ and φ are the amplitude and phase of the transfer function. Consequently, the real and imaginary parts of the Rayleigh wavenumber were calculated from substitution of Eq. (2.14b) into Eq. (2.15) as

$$\hat{H}(i\omega)=\frac{\hat{u}_2(i\omega)\big|_{x_1=x_{12}}}{\hat{u}_2(i\omega)\big|_{x_1=x_{11}}}=e^{i\hat{k}_R(x_{12}-x_{11})}=e^{\gamma L}e^{i\lambda L}\Rightarrow\left|\hat{H}(i\omega)\right|=e^{\gamma L},\ \varphi=\lambda L, \tag{2.16}$$

where $\hat{k}_R=\lambda-\gamma i,$ and L is the distance between two locations on the surface of the sample; i.e., $x_{12}-x_{11}=L$.

The shear wavenumber was obtained from Eqs. (2.12) and (2.13) in terms of the Rayleigh wavenumber. Finally, the complex shear and elastic moduli and the loss factor of the medium were calculated from (Pao and Mow, 1973; Graff, 1975; Lakes, 2009)

$$\hat{G}=\frac{\omega^2\rho}{\hat{k}_s^2}, \tag{2.17a}$$

$$\hat{E}=2(1+\nu)\hat{G}, \tag{2.17b}$$

$$\eta = \frac{E''}{E'} = \frac{G''}{G'} \,. \tag{2.17c}$$

2.2. Rayleigh wave propagation in layered media

The Rayleigh wave propagation method developed in previous section is a fairly straight-forward method in the case of performing the experiments and analyzing the obtained data, and thus very useful for the characterization of a large variety of soft biomaterials. However, it is based on the assumption of no reflection from sample boundaries; hence, the propagated waves should dissipate before reaching the boundaries. It requires a relatively large volume of sample material, which is very expensive for many phonosurgical biomaterials and hydrogels. To reduce the volume of material needed, another model-independent characterization method based on Rayleigh wave propagation for quantifying the *frequency-dependent* viscoelastic properties of *a thin layer of biomaterials* is developed. A thin layer of the soft material under study is applied on a substrate made from another soft material with known viscoelastic properties. As of the previous case, Rayleigh waves are produced on the sample surface. A transfer function method is used to obtain the complex Rayleigh wavenumber and the velocity dispersion curves from measured vibration amplitudes and phases at different locations on the sample surface. An inverse wave propagation problem is solved, and a complex nonlinear dispersion equation for Rayleigh wave propagation in layered media is obtained. The dispersion equation is solved numerically to calculate the complex shear and elastic moduli of the thin samples from the measured wavenumbers.

2.2.1. Mathematical modelling

The interactions between body waves (i.e., compressional and shear waves) propagating inside a layered medium may cause Rayleigh waves to propagate parallel to the stress-free boundary of the medium, as shown in Figure 2-2. The amplitude of the propagating surface wave decreases as x_2 increases in the substrate, while there is a standing wave in the top layer. The wave amplitude decreases as x_1 increases because of dissipation in the viscoelastic materials. General governing equations such as Navier's equation, Helmholtz equations, complex wavenumbers, and displacement and corresponding stress components are similar to those described in previous section.

The specific boundary conditions that had to be satisfied on the stress-free boundary, $x_2 = 0$, and at the interface of the two media, $x_2 = h$, are

$$\sigma_{12}^1\Big|_{x_2=0} = 0, \quad \sigma_{22}^1\Big|_{x_2=0} = 0, \tag{2.18a}$$

$$\sigma_{12}^1\Big|_{x_2=h} = \sigma_{12}^2\Big|_{x_2=h}, \quad \sigma_{22}^1\Big|_{x_2=h} = \sigma_{22}^2\Big|_{x_2=h}, \quad u_1^1\Big|_{x_2=h} = u_1^2\Big|_{x_2=h}, \quad u_2^1\Big|_{x_2=h} = u_2^2\Big|_{x_2=h}. \tag{2.18b}$$

where superscripts 1 and 2 refer to the parameters associated with the top layer and the substrate, respectively. One proper set of compressional and shear wave potentials propagating inside the substrate and the top layer, which satisfies the boundary conditions, is (Kundu, 2004)

$$\phi_1 = \left(A_1 e^{-ik_1x_2} + A_2 e^{ik_1x_2}\right) e^{i\hat{k}_R x_1}, \tag{2.19a}$$

$$\psi_1 = \left(B_1 e^{-ik_2x_2} + B_2 e^{ik_2x_2}\right) e^{i\hat{k}_R x_1}, \tag{2.19b}$$

$$\phi_2 = C_1 e^{i\hat{k}_R x_1 - k_3 x_2}, \tag{2.19c}$$

$$\psi_2 = D_1 e^{i\hat{k}_R x_1 - k_4 x_2}, \tag{2.19d}$$

where $\hat{k}_R$ is the complex Rayleigh wavenumber, and A_1, A_2, B_1, B_2, C_1, and D_1 are the unknown amplitudes of the corresponding potentials. The harmonic time variation factor, $e^{-i\omega t}$, is omitted throughout the formulations for simplicity. Substitution of the field potentials, Eqs. (2.19), into the Helmholtz equations yields

$$k_1^{\ 2} = \hat{k}_{c1}^{\ 2} - \hat{k}_R^{\ 2}, \quad k_2^{\ 2} = \hat{k}_{s1}^{\ 2} - \hat{k}_R^{\ 2}, \tag{2.20a}$$

$$k_3{}^2 = \hat{k}_R{}^2 - \hat{k}_{c2}{}^2, \quad k_4{}^2 = \hat{k}_R{}^2 - \hat{k}_{s2}{}^2. \tag{2.20b}$$

Substitution of Eqs. (2.19) and (2.20) into the boundary conditions, Eqs. (2.18), yields

$$2\hat{k}_R k_1 \left(A_1 - A_2\right) + \left(2\hat{k}_R^2 - \hat{k}_{s1}^2\right)\left(B_1 - B_2\right) = 0, \tag{2.21a}$$

$$\left(2\hat{k}_R^2 - \hat{k}_{s1}^2\right)\left(A_1 + A_2\right) + 2\hat{k}_R k_2 \left(B_2 - B_1\right) = 0, \tag{2.21b}$$

$$\begin{aligned} &2\hat{k}_R k_1 \hat{\mu}_1 \left(A_1 e^{-ik_1 h} - A_2 e^{ik_1 h}\right) + \left(2\hat{k}_R^2 - k_2^2\right)\hat{\mu}_1 \left(B_1 e^{-ik_2 h} + B_2 e^{ik_2 h}\right) \\ &\qquad + 2i\hat{k}_R k_3 \hat{\mu}_2 C_1 e^{-k_3 h} - \left(2\hat{k}_R^2 - \hat{k}_{s2}^2\right)\hat{\mu}_2 D_1 e^{-k_4 h} = 0, \end{aligned} \tag{2.21c}$$

$$\begin{aligned} &\left(2\hat{k}_R^2 - \hat{k}_{s1}^2\right)\hat{\mu}_1 \left(A_1 e^{-ik_1 h} + A_2 e^{ik_1 h}\right) + 2\hat{k}_R k_2 \left(B_2 e^{ik_2 h} - B_1 e^{-ik_2 h}\right) \\ &\qquad - \left(2\hat{k}_R^2 - \hat{k}_{s2}^2\right)\hat{\mu}_2 C_1 e^{-k_3 h} - 2i\hat{k}_R k_4 \hat{\mu}_2 D_1 e^{-k_4 h} = 0, \end{aligned} \tag{2.21d}$$

$$i\hat{k}_R \left(A_1 e^{-ik_1 h} + A_2 e^{ik_1 h}\right) + ik_2 \left(B_2 e^{ik_2 h} - B_1 e^{-ik_2 h}\right) - i\hat{k}_R C_1 e^{-k_3 h} + k_4 D_1 e^{-k_4 h} = 0, \tag{2.21e}$$

$$ik_1 \left(A_2 e^{ik_1 h} - A_1 e^{-ik_1 h}\right) - i\hat{k}_R \left(B_1 e^{-ik_2 h} + B_2 e^{ik_2 h}\right) + k_3 C_1 e^{-k_3 h} + i\hat{k}_R D_1 e^{-k_4 h} = 0. \tag{2.21f}$$

In situation where the Rayleigh wavenumber is measured and the viscoelastic properties of the media are known, Equations (2.21) form a set of six coupled equations with six unknown; i.e., the amplitudes of the field potentials. The unknown amplitudes, and subsequently the displacement field and the corresponding stress and strain components, can be defined within the two media. In the current study, however, the viscoelastic properties of the substrate are known, but those of the top layer material are not.

2.2.2. The transfer function method

Substitution of the field potentials, Eq. (2.19), into Eq. (2.7) yields the displacement component in the top layer as

$$\hat{u}_1(i\omega, x_1)\Big|_{x_2=0} = \Big[i\hat{k}_R(A_1 + A_2) + ik_2(B_2 - B_1)\Big]e^{i\hat{k}_R x_1}, \tag{2.22a}$$

$$\hat{u}_2(i\omega, x_1)\Big|_{x_2=0} = \Big[ik_1(A_2 - A_1) - i\hat{k}_R(B_1 + B_2)\Big]e^{i\hat{k}_R x_1}. \tag{2.22b}$$

Consequently, the real and imaginary parts of the Rayleigh wavenumber were calculated from substitution of Eq. (2.22b) into Eq. (2.15) as

$$\hat{H}(i\omega) = \frac{\hat{u}_2(i\omega)\big|_{x_1=x_{12}}}{\hat{u}_2(i\omega)\big|_{x_1=x_{11}}} = e^{i\hat{k}_R(x_{12}-x_{11})} = e^{\gamma L}e^{i\lambda L} \Rightarrow \left|\hat{H}(i\omega)\right| = e^{\gamma L}, \ \varphi = \lambda L, \tag{2.23}$$

where $\hat{k}_R = \lambda - \gamma i,$ and L is the distance between two locations on the surface of the sample; i.e., $x_{12} - x_{11} = L$.

Considering the following relation between the shear and compressional wavenumbers for each of the media

$$\kappa^2 = \left(\frac{\hat{c}_{ci}}{\hat{c}_{si}}\right)^2 = \left(\frac{\hat{k}_{si}}{\hat{k}_{ci}}\right)^2 = \frac{\hat{\lambda}_i + 2\hat{\mu}_i}{\hat{\mu}_i} = \frac{2-2\nu_i}{1-2\nu_i}, \ i = 1, 2, \tag{2.24}$$

the components of the coefficient matrix of the system of equations developed in Eq. (2.21) become $\mathbf{C}_{i,j} = f_{i,j}\left(\hat{k}_R, \hat{k}_{s1}, \hat{k}_{s2}, \mu_2, \nu_1, \nu_2, \rho, \omega, h\right); \quad i, j = 1, 2, ..., 6$. The coefficient matrix, $\mathbf{C}$, is presented in the Appendix A. To ensure nontrivial solutions for the unknown coefficients in Eq. (2.21), the determinant of the coefficient matrix must vanish. Accordingly, a complex dispersion equation for the propagating Rayleigh waves was obtained by equating the determinant of the coefficient matrix with zero, Eq. (A.3). The dispersion equation relates the measured Rayleigh wavenumbers to shear wavenumbers. In contrast to a uniform (non-layered) medium, the Rayleigh wave is dispersive in a layered media. It means that the relation between the Rayleigh and shear wavenumbers depends on the frequency, and thus the dispersion equation must be solved separately for each set of data at each frequency. The real and imaginary parts of the dispersion equation form two coupled nonlinear equations. The real and imaginary parts of the shear wavenumber propagated in the top layer were calculated from the numerical solution of these equations:

$$\mathrm{Re}\{\det(\mathbf{C})\} = 0, \tag{2.25a}$$

$$\mathrm{Im}\{\det(\mathbf{C})\} = 0, \tag{2.25b}$$

where "det" represents the determinant of matrix **C**, and "Re" and "Im" are the real and imaginary parts of the determinant. The subroutines of commercial computational softwares, such as MATLAB, for solving nonlinear algebraic equations did not yield accurate solutions, due to the presence of many local minimums. Thus, the results depended on the initial guess. A code based on the iterative Rayleigh-Ritz method was developed in Mathematica and numerical analysis tools were used, yielding reliable robust results for different initial guesses. Finally, the complex shear and elastic moduli and the loss factor of the medium (top layer) were calculated from

$$\hat{G}_1 = \hat{\mu}_1 = \frac{\omega^2 \rho_1}{\hat{k}_{s1}^2}, \tag{2.26a}$$

$$\hat{E}_1 = 2(1+\nu_1)\hat{G}_1, \tag{2.26b}$$

$$\eta_1 = \frac{E_1''}{E_1'} = \frac{G_1''}{G_1'}. \tag{2.26c}$$

2.3. Longitudinal wave propagation method

A longitudinal wave propagation method was implemented for evaluation purposes. In this method, a standing longitudinal compression wave is generated in rod-shaped test specimens. A uniform displacement is assumed in the direction transverse to that of wave propagation (Pritz, 1982; Madigosky and Lee, 1983). The solution of the longitudinal wave propagation problem with appropriate boundary conditions relates the measured transfer function to the imaginary and real parts of the wavenumber through (Pritz, 1982)

$$\mathrm{Re}\left\{\frac{1}{\hat{H}(i\omega)}\right\} = \cosh\alpha L\cos\beta L + \left(\frac{M}{m}\right)\left(\alpha L\sinh\alpha L\cos\beta L - \beta L\cosh\alpha L\sin\beta L\right), \tag{2.27a}$$

$$\mathrm{Im}\left\{\frac{1}{\hat{H}(i\omega)}\right\} = \sinh\alpha L\sin\beta L + \left(\frac{M}{m}\right)\left(\alpha L\cosh\alpha L\sin\beta L + \beta L\sinh\alpha L\cos\beta L\right), \tag{2.27b}$$

where $\hat{k}_l = \beta - \alpha i$ is the complex longitudinal wavenumber, $\hat{H}(i\omega) = \frac{\hat{w}(L)}{\hat{w}(0)}$ is the transfer function between the velocity at the two ends of the sample, L is the length of the sample, and m and M are the specimen and termination masses, respectively. The iterative Newton-Raphson method was used to solve Eq. (2.27) to calculate the imaginary and real parts of the wavenumber.

Based on the definition of the wavenumber, the frequency-dependent relation between the complex wavenumber and the elastic modulus may be written as

$$\hat{k}_l = \frac{\omega}{\hat{c}_l} = \sqrt{\frac{\omega^2\rho}{\hat{E}}}, \tag{2.28}$$

in which $\hat{c}_l$ is the complex longitudinal wave speed, $\hat{c}_l = \sqrt{\frac{\hat{E}}{\rho}}$, and $\hat{E}(\omega) = E'(\omega) + i\,E''(\omega)$ is the frequency-dependent complex elastic modulus (dynamic modulus) of the viscoelastic sample, determined using

$$\hat{E} = \frac{\omega^2\rho\left[\left(\beta^2 - \alpha^2\right) + 2i\alpha\beta\right]}{\left(\beta^2 + \alpha^2\right)^2}. \tag{2.29}$$

The loss factor is proportional to the ratio of the energy dissipated and the energy stored for dynamic loading (Lakes, 2009). It was calculated as the ratio of the imaginary part of the complex elastic modulus to its real part as follows,

$$\eta = \frac{E''}{E'} = \frac{2\alpha\beta}{\beta^2 - \alpha^2}. \tag{2.30}$$

2.4. Voigt viscoelastic model

The Voigt model, commonly used for soft viscoelastic materials (Royston *et al.*, 1999), was used to obtain an approximate mean value for the shear elasticity (modulus), μ', and the shear viscosity, μ'', of the tested soft materials and tissue for comparison purposes with the results presented in other studies. The viscoelastic properties of the medium with a complex shear modulus $\hat{G} = \hat{\mu} = G' + iG'' = \mu' + i\omega\mu''$ are related to the shear wave speed via the following equation (Yamakoshi *et al.*, 1990)

$$c_s = \sqrt{\frac{2\left(\mu'^2 + \omega^2\mu''^2\right)}{\rho\left(\mu' + \sqrt{\mu'^2 + \omega^2\mu''^2}\right)}}. \tag{2.31}$$

For an elastic medium with negligible dissipation, where $\mu' >> \omega\mu''$, Eq. (2.31) reduces to Eq. (2.6b). The shear wave speed can be obtained for a medium with known viscoelastic properties at different frequencies using Eq. (2.31). In the present study, the shear wave speed is known at several different frequencies, allowing the calculation of the complex shear modulus of the tested media.

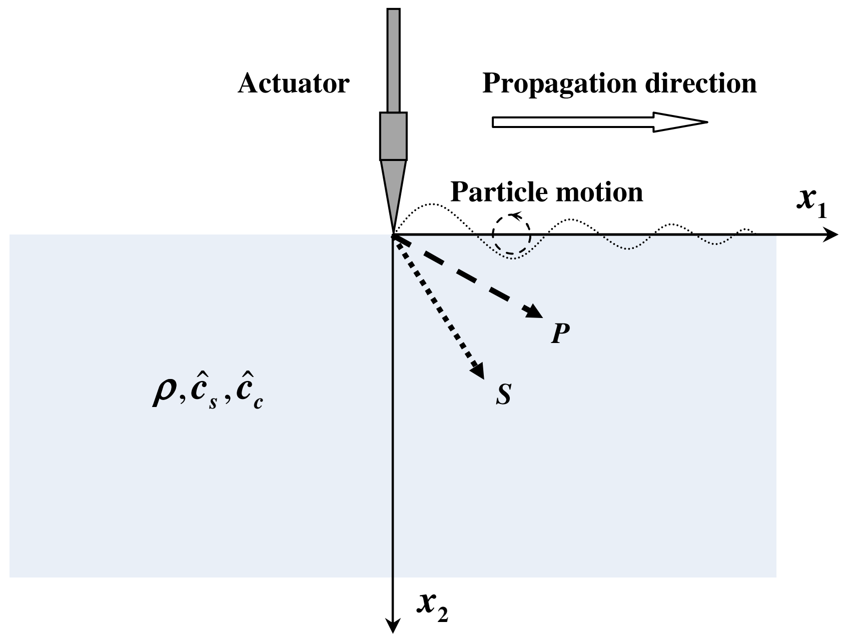

Figure 2-1. Schematic of the Rayleigh wave propagation concept. The interactions between compressional and shear waves propagating inside the medium cause Rayleigh waves near stress-free boundaries. Because of the dissipative behavior of the medium, the amplitude of the propagating surface wave decreases with distance.

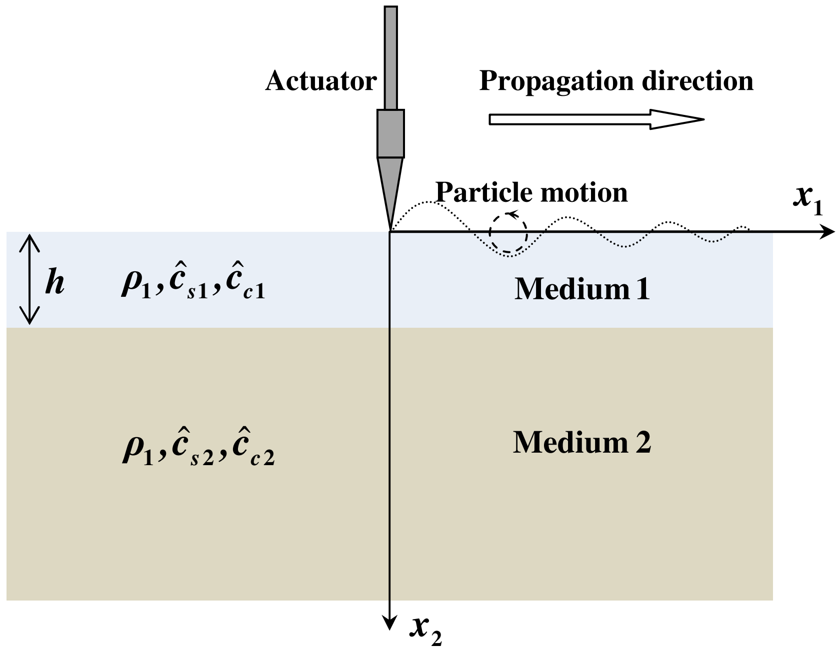

Figure 2-2. Schematic of the Rayleigh wave propagation concept in a layered half-space. In the substrate, the amplitude of the propagating surface wave decreases as x_2 increases. The amplitude decreases as x_1 increases because of the dissipative behavior of the viscoelastic medium. The particles undergo elliptical motion. The motion direction is counter clockwise when the wave propagates from left to right.

CHAPTER 3
Experimental methods

3.1. Rayleigh wave propagation method

3.1.1. Sample preparation

Silicone rubber samples were made from Ecoflex 10 Platinum Cure Silicone Rubber (Smooth-On, Inc). The mixing ratio of the two parts (part A and part B) was unity. Silicone thinner was added to achieve viscoelastic properties similar to values reported for commercial phonosurgical biomaterials and cadaveric human vocal fold cover; i.e., a few kPa over the low frequency range (Chan and Rodriguez, 2008; Kimura et al., 2010). A vacuum pump was used to evacuate the mixture and remove air bubbles after mixing of the components and after casting. It was cured at room temperature for around ten to twelve hours. Two rubber samples with component ratios 1:1:0.5 and 1:1:1 (i.e., part A: part B: silicone thinner), all by weight, were used as the test specimens.

3.1.2. Poisson ratio estimation

One of the advantages of the Rayleigh wave propagation method for characterization purposes is that the obtained values for viscoelastic properties of the medium are very robust with respect to the variation of the Poisson's ratio. For example, if the assumed Poisson's ratio of the medium is changed from 0.4 to 0.5 in the calculation procedure, the difference in the obtained shear modulus will surprisingly be only about 2%. This is verified by the error analysis of Eqs. (2.12), (2.13) and (2.17a). The Poisson's ratio of silicone rubbers depends on their composition, molecular entanglement and so on. Different values have been reported in the literature for the Poisson's ratio of different polymers ranging from 0.33 to 0.49 (Van Krevelen and Hoftyzer, 1972). Reported values for the silicone rubber used in the current study (EcoflexTM Platinum Cure Silicone Rubber) were in the range of 0.36 to 0.42 (Drechsel, 2007; Zörner et al., 2010), and 0.44 (Bufi et al., 2011). The mean value of the above mentioned range, 0.40, was assumed as the Poisson's ratio of the silicone rubber samples in the present study. The maximum error in the Poisson's ratio value was 0.04, which could result in a maximum error of 0.8 and 2.8 percent in the obtained values for the shear and elastic moduli, respectively.

For evaluation purposes, simple uniaxial tension tests were performed to obtain the Poisson's ratio of silicone rubber samples used in the present study. Cubic rod-shaped silicone rubber samples with component ratios 1:1:0.5 and 1:1:1 were fabricated; the samples' dimensions are given in Table 3-1. The changes in the width and the thickness of the samples were measured, while the samples underwent a known elongation. An area in the center of the samples with an approximately uniform elongation was considered for the strain measurements along the longitudinal and transverse directions. The Poisson's ratios of the samples were obtained using the measured strains for the width, ε_w, and the thickness, ε_t, of the samples divided by that of the longitudinal direction, ε_l, as following:

$$\nu_1 = -\frac{\varepsilon_w}{\varepsilon_l}, \tag{3.1a}$$

$$\nu_2 = -\frac{\varepsilon_t}{\varepsilon_l}. \tag{3.1b}$$

The average of these values was considered as the Poisson's ratio of each sample such as

$$\nu_{avg.} = \frac{\nu_1 + \nu_2}{2}. \tag{3.2}$$

As seen in Table 3-1, the Poisson's ratios obtained for silicone rubber samples with component ratios 1:1:0.5 and 1:1:1 were 0.4090 and 0.4105, which are in good agreement with that assumed in the present study, 0.40. If the assumed Poisson's ratio of the medium is changed from 0.40 to 0.41 in the calculation procedure, the differences in the obtained shear wave speed and shear modulus will be only about 0.1% and 0.2%, respectively.

3.1.3. Experiments

A schematic of the experimental apparatus is shown in Figure 3-1. A linear actuator, with a width of 2.54 cm, connected to a shaker was used to generate a planar harmonic Rayleigh wave with a known frequency on the surface of a sample, as shown in Figure 3-1. The sample was mounted on an optical table to reduce the influence of extraneous seismic vibration. The input vibrations of the actuator and the motion of the sample surface were measured using an attached accelerometer and a laser Doppler vibrometer (LDV), respectively. Reflection of the laser beam from some of the samples was poor. To enhance the reflection, a very small amount of a titanium dioxide powder was deposited onto the samples at measurement locations where the strength of the reflected signal was not sufficient. The titanium dioxide is a very fine powder that did not change the mechanical properties of the medium. The frequency of the excitation was increased step by step from 20 Hz to 4 kHz. The amplitude and phase of the propagating wave were measured at each excitation frequency at several locations (at least five) along the propagation direction. These measurement locations were 1 and 0.5 cm apart for the frequency ranges of 20 to 500 Hz and 500 to 4000 Hz, respectively. The measured data from at least one thousand cycles of excitation were saved. The data from the first one hundred cycles were removed to exclude possible transient effects. Each experiment was repeated at least five times. The real and imaginary parts of the Rayleigh wavenumber were calculated from the transfer function between vertical displacements at two different locations on the surface of the sample, using Eq. (2.16).

Long-term exposure of the samples to the LVD beam may cause local heating, which changes the local viscoelastic properties of that specific spot. To account for that, the duration of each set of measurement at each location on the sample surface was less than 30 seconds. The temperature of the samples was monitored using a thermocouple and kept approximately constant; i.e., $22 \pm 1^{\circ} C$. Although the local temperature of the spots exposed to the laser beam may be slightly increased, but the measured wave speeds and the obtained viscoelastic properties using the Rayleigh wave propagation method are representative over the distance of the wave propagation and measurement. Therefore, the effects of the slight changes in the local temperature of the LDV measurement spots were assumed to be negligible on the obtained global viscoelastic properties of the samples.

The real part of the wavenumber, calculated from the phase difference between any two locations from Eq. (2.16), was consistent; i.e., the standard deviation of obtained values was within 8%. The imaginary part of the wavenumber has a significant effect on the value of the imaginary part of the complex elastic/shear moduli and consequently the loss factor. The results did vary with the measurement location in this case. To deal with this variation, measurements were performed at several locations along the propagation direction and an exponential decay function was used to obtain a regression of the oscillation amplitudes. The imaginary part of the wavenumber was calculated from the regression and Eq. (2.16). In the following, the elastic/shear moduli mean the real part of the complex moduli (storage moduli).

The method developed for this study is based on the assumption of no reflection; hence, the propagated waves should dissipate before reaching the boundaries. The dissipation is a function of frequency (wavelength), the distance across which the wave is propagated (i.e., sample size), and the loss factor (intrinsic dissipation coefficient) of the medium. The propagated surface waves are generally dissipated over a shorter propagation distance at higher frequencies, where the wavelength is smaller. Therefore, the sample size can be smaller if the characterization at higher frequencies is the aim or the sample material has a greater loss factor. Experiments were performed for evaluation purposes. The motion of the sample surface was measured at different frequencies and locations to ensure that the propagating waves dissipated before reaching the sample boundaries. The motion of the mold was also measured at different frequencies to determine if the propagating waves have reached the bottom or lateral boundaries of the sample. Motion of the sample surface at locations near the boundaries and that of the mold were negligible at frequencies greater than 80 Hz, proving no reflection from the boundaries at those frequencies. Therefore, the assumed model is accurate for frequencies greater than 80 Hz. Therefore, the frequency range of validity of the experimental results was between 80 and 4000 Hz. This frequency limit might be slightly different for different materials. The motion of the sample surface was negligible in directions other than the assumed propagation direction (i.e., perpendicular to the actuator, x_1 direction). This confirms the accuracy of the proposed model for a planar Rayleigh wave propagation. Furthermore, the measurements were performed for different actuation amplitudes at certain frequencies. The obtained relative surface vibrations at different locations on the sample surface; i.e., the transfer function between the measured vibration of the sample surface and that of the actuator, were similar for different actuation amplitudes at each frequency. It assures the negligibility of the nonlinear effects.

3.2. Rayleigh wave propagation in layered media

3.2.1. Sample preparation

Silicone rubber and gelatin samples were fabricated and tested. Silicone rubber samples were similar to those used in previous section. Gelatin samples were fabricated from 70% water, 15% glycerol, and 15% 300 Bloom gelatin (Sigma-Aldrich), all by volume. The mixture used in (Nenadic *et al.*, 2011a) was fabricated to allow the comparison of the viscoelastic properties of gelatin samples found in this study with those previously reported. The mixture was molded and evacuated in the same manner as for the silicone rubber samples. It was cured at room temperature shortly after casting, but was kept under water to ensure constant mechanical properties over a twenty four hours period prior to the experiments. The specimens' dimensions and properties are given in Tables 3-2 to 3-4.

The substrate was made of silicone rubber with component ratio 1:1:1. A thin layer of either gelatin or silicone rubber with component ratio 1:1:0.5 was added on the top. A silicone rubber sample with component ratio 1:1:0.5 was used as the substrate for the case with a top layer of silicone rubber with component ratio 1:1:1.

3.2.2. Experiments

A schematic of the experimental apparatus is shown in Figure 3-2. The experimental set-up and procedure is similar to that described in previous section, where the only difference is in the tested sample. The top layer of the sample to be characterized can be very thin, as long as the precise measurement of the thickness, h, is possible. However, the length and the width of the sample cannot be smaller than a certain limit for accurate measurements (no reflection) based on the frequency range of interest and the loss factor of the media.

A systematic investigation is performed to confirm the appropriate use of the name "Rayleigh waves" for the waves generated and propagated within the top layer of the layered media using the present experimental set-up. Rayleigh waves do propagate in parallel to the surface of layered half-space media with the mathematical model (wave potentials) presented in this study (Ewing *et al.*, 1957; Kundu, 2004). The difference between the Rayleigh wave propagation in isotropic (non-layered) and layered half-space media is that in a non-layered medium the Rayleigh wave is not dispersive but in a layered media it is (Kundu, 2004). The other types of surface and interface waves have been discussed in the following to explain why none of them are valid for the case investigated in the present study:

- The motion of medium particles in Rayleigh wave propagations is in the plane of propagation, x_1 and x_2 directions. In contrast, the medium particles move perpendicular to the plane of propagation, x_3 direction, in Love wave propagations. So, the Love wave is a *shear horizontal (SH) surface wave* (Achenbach, 1973; Kundu, 2004). In the present study, the harmonic excitation was in x_2 direction. The motion of the sample surface was also measured in x_2 direction (in the plane of propagation). Therefore, the Love wave modelling cannot be valid for the current study.
- Lamb (plate) waves propagate in plate-shaped media with *two stress free boundaries* that is not valid for the present study (Achenbach, 1973; Kundu, 2004).
- Stoneley waves can propagate in the interface of *two half-space media* which is not the case in the present study (Achenbach, 1973). The Stoneley wave is also called "generalized Rayleigh wave" (Ewing *et al.*, 1957). The Stoneley wave is mostly propagated in the interface a fluid and a solid half-space medium. It is rarely propagated in the interface of two solid half-space media; i.e., only under certain conditions (Scholte, 1947).
- Scholte waves are surface waves (interface waves) of the Stoneley wave type associated with the interface between a fluid and a solid medium, which is not the case in the current study (Cagniard, 1962).

3.3. Longitudinal wave propagation method

A schematic of the experimental apparatus is shown in Figure 3-3. Rod-shaped silicone rubber samples with a square cross-section were attached at one end of a PCB accelerometer, which was connected to a linear actuator. The actuator generated longitudinal compressional waves in the sample at a known frequency. A LDV was used to measure the velocity of a lumped mass attached to the other end of the sample. The effect of the attached mass on the vibration of the sample was taken into consideration through the use of the appropriate boundary conditions in the analytical model.

To minimize noise, the measurements were performed independently at single frequencies. Small experimental errors (i.e., noise) may cause large deviations in the measured viscoelastic properties (Park *et al.*, 2003). Mechanical vibrations were generated by the actuator and transmitted through the set-up structure. This contaminated the LDV-measured motion of the sample bottom, especially at high frequencies. To address this problem, the LDV was decoupled from the experimental set-up through the use of a vibration isolation support. Because of wave dissipation within the material, the length of the sample did not exceed a few wavelengths to obtain a sufficiently high vibration signal at the mass end. With no external mass attached, the vibration amplitude decreases exponentially with distance as $\frac{\hat{w}(x_2)}{\hat{w}(x_1)} = e^{-\alpha(x_2 - x_1)}$. The relationship between sample length and vibration amplitude is more complex when an external mass is attached to the sample.

3.4. Measurement of the shear modulus of human vocal fold tissue

A non-invasive method is developed for *in vivo* measurement of the shear modulus of the human vocal fold mucosa during phonation. To the author's knowledge, this is the first method presented in the literature for *in vivo* measurement of the mechanical properties of the human vocal fold tissue during phonation. Images of four human subjects' vocal folds were captured using high speed digital imaging (HSDI) and magnetic resonance imaging (MRI) for different phonation pitches, specifically fundamental frequencies between 110 to 440 Hz. The pixel size of each set of high-speed images was determined by overlapping images of specific anatomical features obtained from HSDI and MRI. Vocal fold oscillation involves mainly a wavy motion of the vocal fold mucosa. The wave propagated on the surface of the mucosa during the oscillation is called the mucosal wave. An automatic image processing algorithm was developed to detect and track the mucosal wave propagating on the superior surface of the vocal folds, through which the speed of mucosal wave propagations at different pitches were obtained for different subjects (Bakhshaee, 2013). An inverse surface (Rayleigh) wave propagation problem was solved to calculate the shear modulus of the subjects' vocal folds mucosa in the transverse direction from the measured wave speeds. In addition, a Voigt viscoelastic model was fitted to the obtained shear wave velocities to calculate an approximate value for the complex shear modulus of vocal fold mucosa over the pitch range of interest.

3.4.1. Human subjects

The Research Ethics office (IRB) of McGill University approved the protocol and consent procedure for the high speed digital and magnetic resonance imaging experiments. Three male and one female adult subjects, aged between 22 to 29, participated in the imaging experiments. The subjects were healthy, non-smoker, with no major medical history, and no voice disorders. None of the subjects were trained voice users. Each subject underwent the HSDI and MRI experiments within two different clinical sessions.

3.4.2. High speed digital imaging (HSDI)

A Color high-speed camera (Fastcam MC2- Model 10K; Photron Limited, San Diego, CA) attached to an endoscope was used for high speed imaging experiments. A sampling rate of 4000 frame/s was found to be the optimum one for all the experiments. Smaller frame rates produced insufficient number of images in which the mucosal wave was observed. In contrast, very high frame rates resulted in smaller camera field of view and lower image quality. The high speed imaging experiments were performed by a surgeon at the voice clinic of the Montreal General Hospital. The high speed images were recorded for at most five seconds each time to prevent heating of the subjects' larynx by the powerful endoscope light. The human subjects were asked to sustain vowel /i/ at different pitches with fundamental frequencies of $f_0 = 110, 130, 165, 220, 260$ for male and $f_0 = 220, 330, 440$ Hz female subjects. A musical note at the target pitch was produced for the subjects prior to recording the images to adjust their voice during phonation. A sound pressure level meter was held 30 cm away from the subjects' mouth to monitor radiated sound level. The subjects were asked to phonate with an approximate steady volume intensity of 80 dB.

3.4.3. Magnetic resonance imaging (MRI)

MRI experiments were performed to scale the images obtained from HSDI experiments and establish the pixel size in each set of high-speed images. The subjects were asked to phonate at different pitches with fundamental frequencies similar to those of the HSDI experiments. The pixel size was then obtained for each set of high-speed images by comparing a known anatomical feature in images from MRI and HSDI experiments, e.g. the anterior-posterior length of the vocal folds in the MRI and HSDI images. The details of the MRI experiments are given in (Bakhshaee, 2013) and (Kazemirad *et al.*, in review).

3.4.4. Estimation of the shear modulus

The length and the thickness of human vocal folds are approximately 10-15 and 3-5 mm, respectively (Hahn *et al.*, 2006). The thyroarytenoid muscle is approximately 7-8 mm thick (Figure 3-4). It is involved in maintaining tension in the vocal fold tissue to adjust phonation pitch. The vocal fold muscle is covered laterally by the lamina propria and the epithelium (Stevens and Hirano, 1981; Titze, 1994). The lamina propria is a layered nonmuscular structure that may be subdivided into three different layers. The superficial layer is approximately 0.5 mm thick (Stevens and Hirano, 1981), and is made of loosely organized elastin fibers. The intermediate layer consists mostly of unidirectional (longitudinal) oriented elastin fibers. The deep layer is made of collagen fibers oriented primarily along the longitudinal direction (Titze, 1994). The thickness of the intermediate and the deep layers of the lamina propria is around 1-2 mm (Stevens and Hirano, 1981).The self-sustained oscillations of human vocal folds are mostly confined within the mucosa, which consists of the epithelium and the superficial layer of the lamina propria. The frequency of the vocal folds vibrations, and consequently the mucosal wave propagation, is the same as phonation pitch. An inverse wave propagation problem, where the displacement or velocity field is known and the mechanical properties of the medium are unknown, is solved based on the wave propagation model described in the following section to calculate the mechanical properties of the human vocal mucosa.

3.4.5. Wave propagation model

It was shown that the movement of the medial and superior surfaces of vocal folds, featuring the mucosal wave propagation, are respectively elliptical and circular in general (Boessenecker *et al.*, 2007). This suggests that, mucosal waves include motion in both the longitudinal and transverse directions (Figure 3-4), with respect to the propagation direction. This behavior is similar to that of Rayleigh waves that propagates near stress-free surfaces. Therefore, the Rayleigh wave propagation model was employed to calculate the shear modulus of the vocal fold mucosa from the measured mucosal wave speeds, assuming ideal Rayleigh waves. The Rayleigh wave dispersion equation for a macroscopically homogeneous and isotropic medium is developed in Chapter 2; i.e., Eq. (2.12). The Poisson's ratio of the vocal fold tissue, ν, was assumed to be 0.495. The mucosal wave propagation speed at different pitches was obtained from the image processing procedure for each of the subjects, c_m, and treated as the Rayleigh wave propagation speed, c_R. Then, the shear wavenumber, k_s, and consequently the shear wave speed, c_s, were obtained from Eqs. (2.12) and (2.13). Finally, the shear modulus of the vocal fold mucosa was calculated from $G = \frac{\omega^2 \rho}{k_s^2}$. The vocal fold mucosa density, ρ, was assumed to be 1060 and 1075 kg/m^3 for male and female subjects, respectively (Titze, 1994).

The shear modulus obtained from such surface wave propagation method is representative over the depth of wave penetration. The mucosal wave propagates mainly within the mucosa during phonation. Therefore, the obtained shear modulus is believed to be that of the vocal fold mucosa.

3.5. Viscoelasticity of hyaluronic acid-gelatin hydrogels

A variety of cross-linked HA-Ge hydrogels with tuned mechanical and biological properties were fabricated for use as synthetic ECM hydrogels in vocal fold tissue engineering. The shear and viscous moduli of the synthesized hydrogels were measured over a broad frequency range; i.e., from 40 to 4000 Hz, using the Rayleigh wave propagation method. The effects of HA, Ge, and cross-linker concentrations on the frequency-dependent viscoelastic properties of these hydrogels were investigated.

3.5.1. Materials

Thiolated HA (CMHA-S or Glycosil, Mn~200kDa, thiolatation: 40% of carboxyl groups), thiolated Ge (Gtn- DTPH or Gelin-S, Mn~25kDa, thiolatation: 40% of carboxyl groups), and polyethylene glycol diacrylate (PEGDA, mw~3400g/mol) were generously donated by Glycosan Biosystems, Inc. (Salt Lake City, UT).

3.5.2. Hydrogel fabrication

Hydrogels were cast in a variety of compositions where a mixture of thiol-modified HA, thiol-modified Ge, and PEGDA cross-linker was prepared with various concentrations of these constituents. A schematic of thiol-modified HA and Ge cross-linked by PEGDA and the cross-linked network of HA-Ge hydrogels is shown in Figure 3-5. Samples were cured at room temperature after casting, and were kept hydrated prior to the experiment. Although 20 minutes was sufficient to ensure cross-linking, a 12 hours period was considered before performing the experiments to ensure a fully cured hydrogel and consistent mechanical properties.

3.5.3. Experiments

The characterization method based on Rayleigh wave propagation in layered media was used for the quantification of the frequency-dependent viscoelastic properties of the fabricated hydrogels. Planar harmonic Rayleigh waves were produced on the surface of a sample composed of a substrate with known material properties coated with a thin layer of the hydrogel to be characterized. A schematic of the fabricated layered sample and the Rayleigh wave propagation concept is shown in Figure 3-6. The substrate was made of a silicone rubber material, Ecoflex 10 Platinum Cure Silicone Rubber (Smooth-On, Inc), with a component ratio 1:1:3 (i.e., part A: part B: silicone thinner), by weight. The viscoelastic properties of the substrate material were measured using the Rayleigh wave propagation method. A transfer function method was used to obtain the complex Rayleigh wavenumbers at each excitation frequency through the phase and amplitude of the propagating waves measured at different locations along the propagation direction. An inverse wave propagation problem was solved; yielding a complex nonlinear dispersion equation, Eq. (2.25). The complex shear modulus, $\hat{G} = G' + i\omega G''$, where G' and G'' are the shear and viscous moduli of the hydrogel were calculated at frequencies up to 4 kHz through the numerical solution of the dispersion equation using the measured Rayleigh wave speeds (wavenumbers) propagating on the sample surface.

Table 3-1. Dimensions silicone rubber sample and the obtained strains and Poisson's ratio values.

Material	Length [10^{-3} m]	Width [10^{-3} m]	Thickness [10^{-3} m]	$-\varepsilon_w$	$-\varepsilon_t$	ε_l	ν_1	ν_2	$\nu_{avg.}$
Silicone rubber 1:1:0.5	2.85	0.96	0.64	0.3085	0.3342	0.7857	0.3926	0.4254	0.4090
Silicone rubber 1:1:1	2.85	0.96	0.64	0.2893	0.3057	0.7247	0.3992	0.4218	0.4105

Table 3-2. Dimensions and properties of the layered sample for the case with the silicone rubber with component ratio 1:1:0.5 as the material to be characterized.

Material	Length [10^{-3} m]	Width [10^{-3} m]	Height [10^{-3} m]	Mass (m) [10^{-3} kg]	Density ρ [kg/m^3]
Silicone rubber 1:1:0.5	102	51	5	28.17	1083
Silicone rubber 1:1:1	102	51	46	241.9	1011

Table 3-3. Dimensions and properties of the layered sample for the case with the silicone rubber with component ratio 1:1:1 as the material to be characterized.

Material	Length [10^{-3} m]	Width [10^{-3} m]	Height [10^{-3} m]	Mass (m) [10^{-3} kg]	Density ρ [kg/m^3]
Silicone rubber 1:1:0.5	102	51	46	259.9	1086
Silicone rubber 1:1:1	102	51	5	26.27	1010

Table 3-4. Dimensions and properties of the layered sample for the case with the gelatin as the material to be characterized.

Material	Length [10^{-3} m]	Width [10^{-3} m]	Height [10^{-3} m]	Mass (m) [10^{-3} kg]	Density ρ [kg/m^3]
Gelatin	102	51	5	27.96	1075
Silicone rubber 1:1:1	102	51	46	242.2	1012

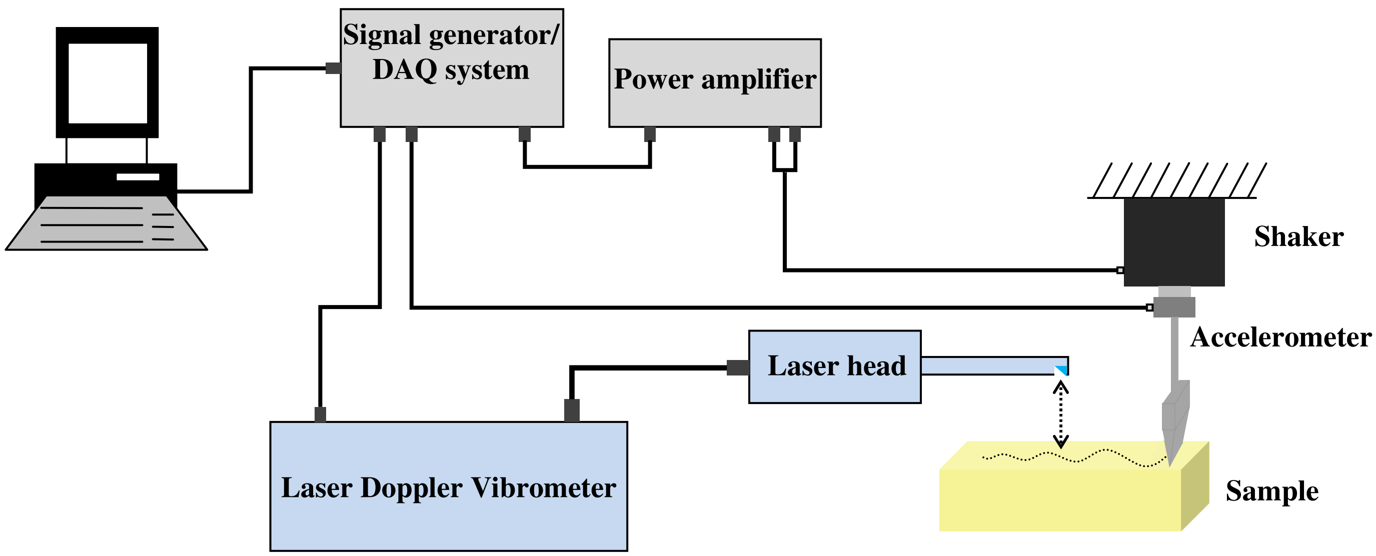

Figure 3-1. Schematic of the test setup for the Rayleigh wave propagation experiments. A linear actuator was used to produce Rayleigh waves on the surface of a rubber sample. The sample is fixed to the superior surface of an optical table to minimize extraneous disturbances. The input vibrations of the actuator and the motion of the sample surface were measured using an accelerometer and a Polytec laser Doppler vibrometer, respectively.

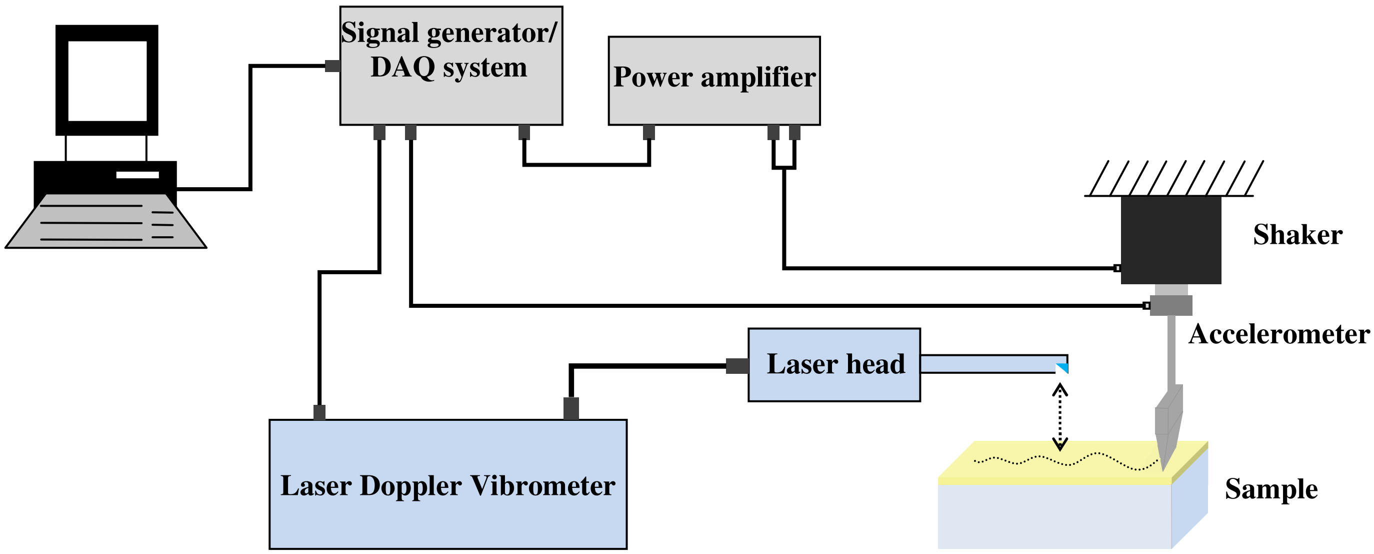

Figure 3-2. Schematic of the test setup. Single frequency harmonic excitation signals were generated using a signal generator (Data Translation) and amplified before being fed to a shaker. A linear actuator connected to the shaker was used to produce planar Rayleigh waves on the surface of a sample fixed, mounted on an optical table. A PCB accelerometer and a laser Doppler vibrometer were used to measure the vibrations of the actuator and the sample surface, respectively.

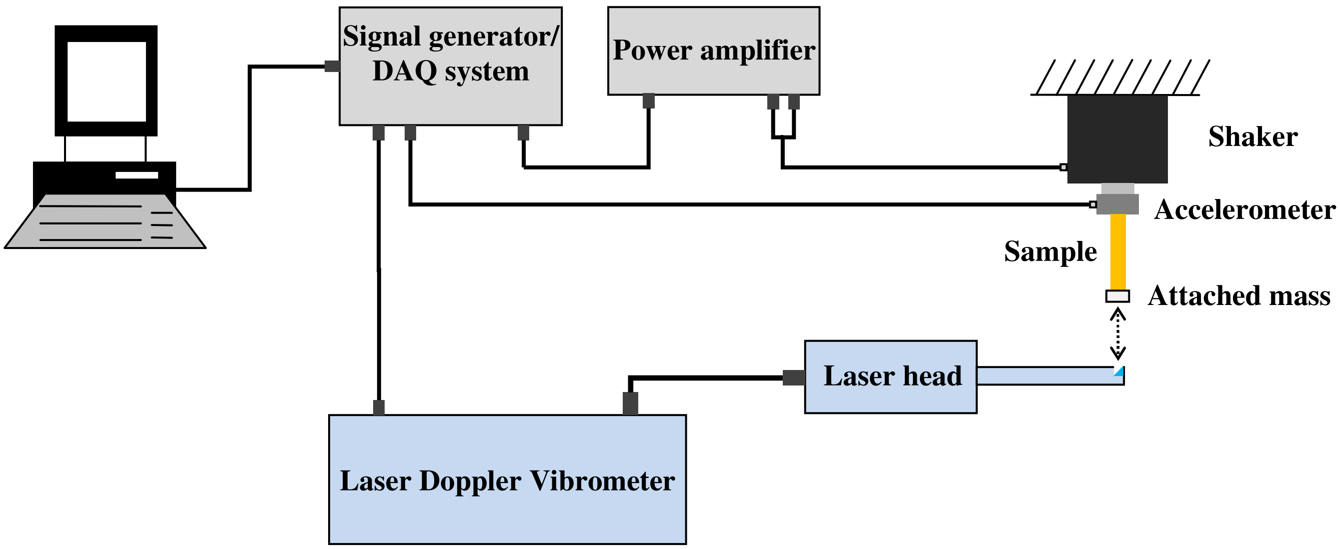

Figure 3-3. Schematic of the test setup for the longitudinal wave propagation experiments. A linear actuator produced longitudinal waves in rod-shaped rubber samples with a square cross section at a known frequency. The vibrations of the two ends of the sample were measured using an accelerometer and a laser Doppler vibrometer.

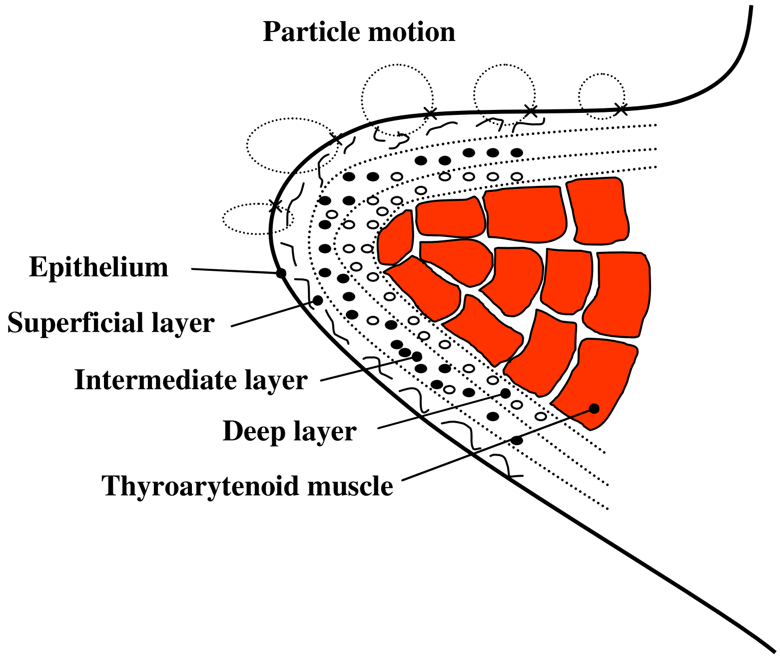

Figure 3-4. Simplified schematic of a coronal section structure of human vocal fold tissue, and the motion of different locations of the vocal fold surface due to the mucosal wave propagation. ● and ○ denote the cross section of elastin and collagen fibers, respectively.

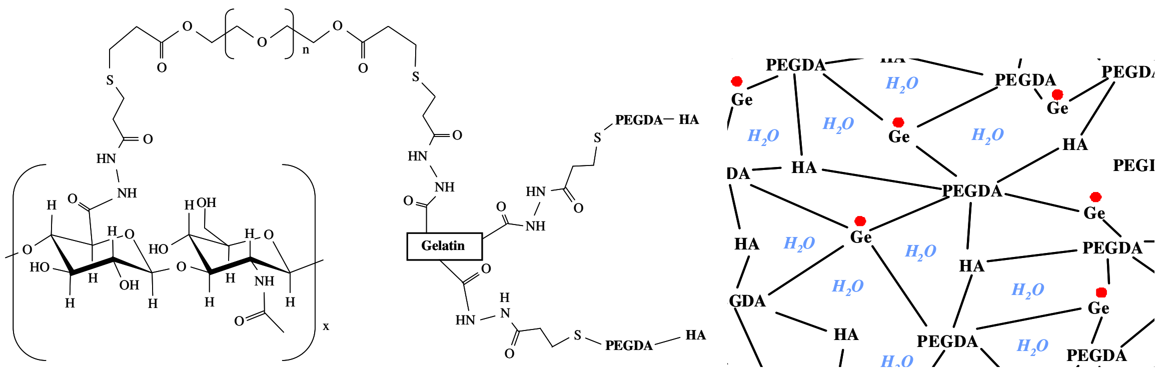

(a) (b)

Figure 3-5. (a) schematic of thiol-modified HA and Ge cross-linked by PEGDA(Shu *et al.*, 2003). (b) cross-linked network of HA-Ge hydrogels (Heris *et al.*, 2012).

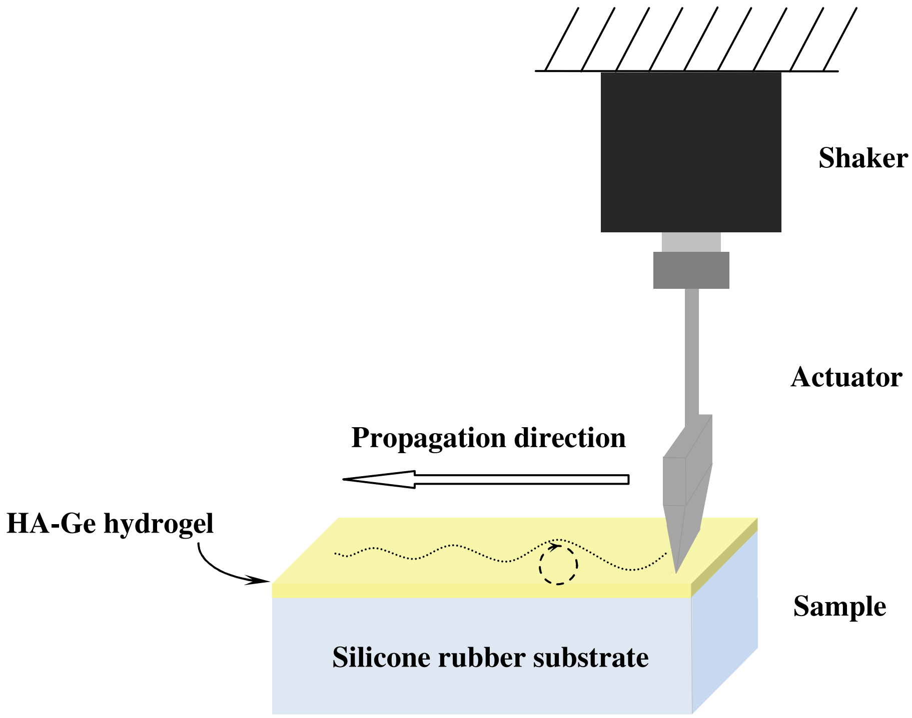

Figure 3-6. Schematic of the fabricated layered sample and Rayleigh wave propagation concept. A linear actuator was used to produce Rayleigh waves on the surface of the sample. The sample is fixed to the superior surface of an optical table to minimize extraneous disturbances. The input vibrations of the actuator and the motion of the sample surface were measured using an accelerometer and a laser Doppler vibrometer, respectively.

CHAPTER 4
Results and discussion

4.1. Longitudinal wave propagation method

4.1.1. Results

In this section, the results obtained from the longitudinal wave propagation method are first evaluated *qualitatively* versus trends reported in the literature for the frequency-dependent properties of polymers. This is performed through the investigation of the variations of obtained viscoelastic properties of silicone rubber samples by frequency, composition, and pre-tension. In a separate, related investigation, dynamic indentation tests using atomic force microscopy (AFM) were performed at frequencies up to 300 Hz (Heris, 2013). No systematic verification study is available for the AFM-based method, which can be used when the dimensions of the test samples are too small for other existing testing methods. The results obtained from the Rayleigh wave propagation and AFM-based indentation methods were compared *quantitatively* with those from the longitudinal wave propagation method. The results were cross validated in the following sections and qualitatively confirmed theoretical expectations presented in the literature for the frequency-dependence of polymers. Wave propagation experiments were repeated at least five times for each sample. AFM experiments were repeated three times for each sample. The mean value and standard deviation of the results were calculated. The standard deviation values were too small to be shown as error bars in Figures 4-1 to 4-4; thus they are presented in Tables 4-1 and 4-2.

Two samples with component ratios 1:1:0.5 and 1:1:1 were used for the longitudinal wave propagation experiments. The specimens' dimensions, properties and attached mass values are listed in Table 4-3.

Figure 4-1 shows the elastic modulus and loss factor of the two silicone rubber samples. Measurements were done at frequencies up to 4 kHz with no external masses attached (i.e., zero pre-elongation). The viscoelastic behavior of rubbers is highly dependent on their molecular entanglement network, i.e., the coupled configurational motion of neighboring molecules (Lakes, 2009). The magnitude of rubber elastic moduli depends on the configurational rearrangements that occur within the time period of one dynamic loading cycle (Ferry, 1980). The loss factor peaks at a frequency within a region called the transition zone, during which an increase in frequency causes the material to undergo a transition from a rubber- to glass-like consistency. The elastic modulus increases rapidly during the transition, while the loss factor decreases after reaching a maximum value. At frequencies below the transition zone, polymer molecular chains move and slide alongside each other. At higher frequencies (i.e., in the glassy region), only minor molecular adjustment and thus energy dissipation can take place within the period of deformation. In this region, the mechanical behavior of the material is similar to that of elastic solids (Ferry, 1980). As shown in Figure 4-1, the addition of silicone thinner yields a lower elastic modulus at low frequencies (below 300 Hz), as expected. Thinning also results in a slight decrease in the frequency of the peak loss factor, which coincides with a lower point of rapid elastic modulus increase. The elastic moduli of the two samples with different ratios are nearly equivalent at high frequencies (above 300 Hz). This is consistent with the fact that the viscoelastic properties in the transition region depend on the rearrangements of sufficiently short molecular segments. Thus, the cross links between the molecular chains, and consequently the molecular weight or its distribution, do not significantly affect the viscoelastic behavior of the rubber at high frequencies (Lakes, 2009).

The elastic modulus and loss factor of silicone rubber with a component ratio of 1:1:0.5 are shown in Figure 4-2 for different pre-elongations. At low frequencies (below 300 Hz), the pre-elongation caused a small decrease in the elastic modulus because of the strain-softening behavior of the material. Greater pre-elongations caused the frequency of the peak loss factor to migrate at slightly lower frequencies. This resulted in inflection points of elastic modulus to occur at lower frequencies and therefore a greater elastic modulus at high frequencies (above 300 Hz). This is because the increasing pre-stress increases the viscoelastic relaxation time (Ferry, 1980), which is inversely related to the frequency of the peak loss factor. The segmental mobility of polymer molecular chains depends on the fractional free volume. As the free volume decreases with pre-stress, the mobility of the segments and thus the energy loss decreases within the loading cycle period. As a result, the overall loss factor decreased with increased pre-elongation.

4.1.2. Discussion

For evaluation purposes, a characterization method that involves the generation of standing longitudinal compression waves in a rod-shaped test specimen was adopted from an earlier study (Park *et al.*, 2003). The transfer function between the velocities at the two ends of the sample was used to determine the complex wavenumber. The complex elastic modulus was calculated analytically from the measured complex wavenumber. The longitudinal wave propagation method was evaluated *qualitatively* via investigation of the variations of obtained viscoelastic properties of silicone rubber samples by frequency, composition, and pre-tension. The consistency and quality of the results, presented in this section, suggested the use of results from this method to verify the accuracy of other characterization methods. Therefore, the results obtained from the Rayleigh wave propagation method were compared *quantitatively* with those obtained from the longitudinal wave propagation method and cross validated in the following sections.

4.2. Rayleigh wave propagation method

4.2.1. Results

Silicone rubber with a component ratio of 1:1:1 was used for Rayleigh wave propagation experiments. Table 4-4 shows specimen dimensions and properties.

Figure 4-3 shows the elastic modulus and loss factor of silicone rubber samples obtained from both experimental methods. Results from the Rayleigh wave propagation method were obtained at frequencies between 80 Hz and 4 kHz. The elastic modulus and loss factor values were found to be in good agreement with those obtained from the longitudinal wave method. The discrepancies were less than 10% for the loss factor and 17% for the elastic modulus (except at 200 Hz). Silicone rubber with a component ratio of 1:1:0.5 was also tested. The differences between the results from the two methods were within the same range as for the previous case.

An error analysis was performed to investigate the sensitivity of the results obtained from the wave propagation methods to the experimental errors from different sources such as the data acquisition system, accelerometer, LDV, scale, vernier and so on. As seen in Table 4-5, the maximum error was about 12% at the lowest investigated frequency, 20 Hz, for the longitudinal wave method. As the frequency was increased, the error generally decreased for both methods and was less than 1% at frequencies greater than 100 Hz. This is because the error in frequency measurements (ω) was smaller at higher frequencies, where the sampling frequency was the same. Furthermore, the magnitudes of the measured vibrations were greater at higher frequencies, which reduced the error in measured velocities and accelerations from the LDV and accelerometer. The errors were slightly smaller for the Rayleigh wave method, due to smaller errors in the sample dimension and density measurements; i.e., samples had greater dimensions and weights in this case. The errors were comparable for other silicone compositions and sample pre-elongations.

The viscoelastic properties of a silicone rubber sample with a component ratio of 1:1:0.5 were measured using the atomic force microscope at frequencies up to 300 Hz. The results were compared to those from the wave propagation methods, as shown in Figure 4-4. The trends in elastic modulus and loss factor values obtained from AFM are in good agreement with those from the wave propagation methods. Variations were found in the results obtained from stiff and soft tips. The oscillation amplitude also affected the results. The average of the values obtained from the AFM-based indentation method using different probes and oscillation amplitudes (at each frequency) was compared to averages from the wave propagation methods. The differences between these values were less than 10% for the elastic modulus and 15% for the loss factor, except at 20 Hz where it was 40%.

4.2.2. Discussion

The results obtained from the Rayleigh wave propagation method were found to be in good agreement with those from the longitudinal wave propagation and AFM-based nano-indentation methods. Therefore, this method is reliable and useful for the quantification of the *frequency-dependent* viscoelastic properties of soft biomaterials at *high frequencies*.

In isotropic elastic media, the amplitudes of compressional and shear components of Rayleigh waves decrease with depth exponentially by a factor of $e^{k_1 x_2}$ and $e^{k_2 x_2}$, respectively. In viscoelastic media, these amplitudes decrease even further by a factor of $e^{\lambda x_1}$ and $e^{\lambda x_2}$ in x_1 and x_2 directions, respectively. Consequently, the rate of decrease is a function of frequency and of the viscoelastic properties of the medium at the frequency of interest. At higher frequencies (greater Rayleigh wavenumbers) the amplitude of longitudinal and transverse motions corresponding to Rayleigh waves generally decreases faster with depth. For example, the calculated amplitude of the propagated Rayleigh waves in the silicone rubber sample under study at a location 1 cm below the sample surface is about 28%, 10% and 8% of that of the surface at 100, 500 and 1000 Hz, respectively. The obtained overall (bulk) mechanical properties are representative over a depth commensurate with the Rayleigh wave penetration.

The depths probed by the Rayleigh wave propagation and AFM-based indentation methods are different. Thus these two methods may not necessarily yield the same results for layered or anisotropic materials. The probing depth was generally in the range of several millimetres (at high frequencies) to a few centimetres (at low frequencies) for the Rayleigh wave propagation method, and few micrometers for the AFM method. However, the used silicone rubber was isotropic and macroscopically homogeneous. Therefore, the results were comparable regardless of the depth probed by these methods.

4.3. Rayleigh wave propagation in layered media

4.3.1. Results

The mean values and standard deviations of the measured data were calculated. The standard deviation values of the measured elastic and shear moduli and loss factor were less than 10 percent of the mean values except for the loss factor of the silicone rubber sample with component ratio 1:1:0.5 at 500 Hz, where it was 12 percent. Thus, only mean values are shown.

Rayleigh and shear wave propagation speeds versus frequency for silicone rubber samples with component ratios 1:1:0.5 and 1:1:1 and a gelatin sample in the frequency range from 80 Hz to 4 kHz are shown in Figures 4-5, 4-6 and 4-7, respectively. The results obtained from layered samples were compared to those from uniform (non-layered) ones; i.e., presented in previous section. Shear wave speeds obtained from layered samples were those of the top layer, $\hat{c}_{s1}$. As seen in these figures, the wave propagation speeds increased with the frequency. This is consistent with the expected trend of greater elastic and shear moduli at higher frequencies. The measured wave speeds for the silicone rubber sample with component ration 1:1:1 were smaller than those for component ratio 1:1:0.5 at low frequencies (below 300 Hz). This is consistent with the fact that the addition of silicone thinner yields lowers elastic and shear moduli at low frequencies. In contrast, wave speeds for the silicone rubber sample with component ratio 1:1:1 were greater than those with component ratio 1:1:0.5 at high frequencies. One possible reason for this observation is that the elastic and shear moduli of the two samples with different ratios are nearly equal at high frequencies. Therefore, the smaller density of the sample with component ratio 1:1:1 resulted in greater wave speeds.

The results obtained from the layered samples were slightly smaller than those from uniform samples, the difference being less than 15 percent. It is noteworthy that the Rayleigh wave speeds in a layered medium are not necessarily the same as those in a uniform medium. But, the shear wave speed and elastic and shear moduli are only *frequency-dependent*, at a fixed experiment temperature, and should be the same for uniform and layered samples. However, there were differences between shear wave speeds obtained from a layered sample and those from a non-layered sample in the order of 10 percent or less. This discrepancy was the source of differences between the calculated values for the elastic and shear moduli and loss factor from layered and non-layered samples. The discrepancy is believed to be caused by experimental errors in the data and variability in the fabrication procedures and the resulting elastomer mechanical properties.

Theoretically, the Rayleigh wave propagation speed is slightly smaller than the shear wave propagation speed at each frequency, which is consistent with the results presented in this study. For a uniform sample, the ratio of the Rayleigh wave speed to shear wave speed is a constant value that is a function of the Poisson's ratio of the medium. In this case, the approximate relation between the Rayleigh and shear wave speeds (or the corresponding wavenumbers) obtained from the Rayleigh wave model is expressed as (Achenbach, 1973)

$$\hat{c}_R = \frac{0.862 + 1.14\nu}{1+\nu}\hat{c}_s \ , \tag{4.1}$$

where c_R is the Rayleigh wave speed. The Poisson's ratio of the used silicone rubber was assumed to be 0.4, while that of the gelatin sample was assumed to be 0.495 (Nenadic *et al.*, 2011a). Equation (4.1) yields wave speed ratios of 0.94 and 0.95 for silicone rubber and gelatin samples, respectively. As shown in Figures 4-5 to 4-7, the wave speeds measured in a uniform sample are in good agreement with the calculated values. In the case of a layered sample, the measured wave speed ratio was found to vary for different materials and different frequencies. For example, for the silicone rubber sample with component ratio 1:1:0.5, this ratio was 0.93 and 0.90 at 3 and 4 kHz, respectively.

The measured Rayleigh and shear wave propagation speeds in the uniform and layered gelatin samples are shown in Figure 4-7. The measured wave speeds were slightly greater than those measured by Nenadic *et al*. (2011a) in the range of 6 to 17 percent. This discrepancy can be due to several reasons. First, the measurements were performed on samples with slightly different properties. Attempts were made to use gelatin samples similar to those in Nenadic et al. (2011a); however, the necessary fabrication procedures are unpublished. For example, it was unknown whether Nenadic *et al.*, (2011a) evacuated the mixture to remove air bubbles after component mixing and casting. If not, the samples would likely have been less stiff, yielding slightly lower wave propagation speeds than found in the present study, where evacuation was performed. The sample dimensions can also be another source of error. Nenadic *et al.*, (2011a) used gelatin samples with a plate-shaped geometry, which is not the most appropriate geometry for Rayleigh wave propagation modelling.

The elastic/shear moduli and loss factor of silicone rubber samples with component ratios 1:1:0.5 and 1:1:1 and the gelatin sample are shown in the frequency range from 80 Hz to 4 kHz in Figures 4-8, 4-9 and 4-10, respectively. The values obtained from the layered samples were compared with those of the corresponding uniform sample. The difference between the results was generally less than 10 percent for the elastic and shear moduli, and 20 percent for the loss factor except at few frequencies. The elastic and shear moduli appeared to be more consistent, maybe because the real part of the wavenumbers was more accurately measured than the imaginary part.

The elastic and shear moduli of all materials tested increased with frequency, as illustrated in Figures 4-8 to 4-10. The rate of change increased beyond a specific frequency, where the materials undergo a transition from a rubber- to glass-like consistency (glass transition phenomenon). The loss factor peak, which is an important characteristic of the dissipative behavior of viscoelastic materials, occurred within the transition zone. A comparison between Figures 4-8 and 4-9 suggests that the addition of silicone thinner yielded a lower elastic modulus at low frequencies. Thinning also resulted in a slight decrease in the frequency of the peak loss factor, which corresponds to the onset of rapid elastic modulus increase. As a result, the elastic moduli for the two samples of different ratios were nearly equivalent at high frequencies. This is consistent with the hypothesis that the wave speed and, consequently, the elastic and shear moduli are governed by the matrix at low frequencies (rubber-like consistency) and by the polymer fibers at high frequencies (glass-like consistency). A comprehensive discussion of the viscoelastic behavior of rubbers and its dependency on their molecular entanglement; i.e., the coupled configurational motion of neighboring molecules, is available in the literature (Ferry, 1980; Lakes, 2009).

The shear modulus and loss factor of the gelatin sample were obtained from a layered and a uniform sample and compared with those obtained by Nenadic *et al*. (2011a) in Figure 4-10 (a, b). The mechanical properties of soft biomaterials are highly dependent on frequency. For instance, the shear modulus of the gelatin sample at high frequencies (few kHz) was two orders of magnitude greater than that at low frequencies. This accentuates the importance of the characterization of *frequency-dependent* viscoelastic properties of soft biomaterials. In the study by Nenadic *et al*. (2011a), a Voigt material frequency response with a complex shear modulus $\hat{\mu} = \mu' + i\omega\mu''$ was fitted to the measured wave speeds, where μ' and μ'' are the shear elasticity (modulus) and viscosity of the medium, respectively. This method yields *one constant value* for the shear modulus and viscosity of the material over the entire frequency range of interest. As Figure 4-10 (a) shows, the constant value in Nenadic *et al.*, (2011a) is approximately equivalent to the mean shear modulus of the gelatin sample in the present study, obtained for the same frequency range (i.e., 40 to 500 Hz) using the Rayleigh wave propagation method. As seen in Figure 4-10 (b), the loss factor predicted by the Voigt model increased linearly with frequency, such as $\eta = \frac{\omega\mu''}{\mu'}$, and did not capture the loss factor peak obtained from the present method. The loss factor peak is an important feature of the viscoelastic response. This highlights limitations of rheological models to describe the viscoelastic behavior of soft biomaterials accurately. Therefore, development of model-independent characterization methods, such as the Rayleigh wave propagation method presented in this study, is required to accurately quantify the frequency-dependent viscoelastic properties of such materials. For evaluation purposes, the Voigt model was fitted to the wave speeds measured in the present study at frequencies up to 500 Hz; i.e., the maximum measurement frequency in (Nenadic *et al.*, 2011a). The obtained shear modulus and viscosity were found to be in good agreement with those of Nenadic *et al.* (2011a). The differences between the values obtained in the present study, $\hat{\mu} = 11750 + 3.26\, i\omega$, and those obtained in Nenadic *et al.*, (2011a), $\hat{\mu} = 10700 + 3.7\, i\omega$, are 10% for the shear modulus (elasticity) and 12% for the viscosity.

4.3.2. Discussion

An experimental method based on Rayleigh wave propagation was developed for quantifying the *frequency-dependent* viscoelastic properties of *a small volume of expensive biomaterials* over a *broad frequency range*. The results were found to be in good agreement with those from the previously mentioned methods and improved upon those of Nenadic *et al*. (2011a).

The measured propagation wave speeds increased with frequency at a greater rate at high frequencies, which confirms the rapid increase of elastic and shear moduli beyond the transition zone. The results emphasize the need for the characterization of *frequency-dependent* viscoelastic properties of soft biomaterials over a broad frequency range. This is needed to accurately characterize the viscoelastic properties of injectable phonosurgical biomaterials and hydrogels used for vocal fold treatment.

This characterization method is based on the assumption of no reflection from the boundaries of the sample and cannot, therefore, be used to quantify the mechanical properties of materials with a negligible loss factor, such as elastic materials. In addition, the propagated surface waves are generally dissipated over a greater propagation distance at low frequencies, where the wavelength is greater. Samples with small dimensions do not allow accurate measurements at low frequencies. In the present study, there was no reflection from the boundaries at frequencies higher than 80 Hz, and thus results were presented in the frequency range of 80 to 4000 Hz.

4.4. Measurement of the shear modulus of human vocal fold tissue

4.4.1. Results

Data were obtained for different phonation pitches in the range from 110 to 260 Hz and 220 to 440 Hz for male and female subjects, respectively. The mean value and standard deviation of the measured data obtained from each subject at each pitch were calculated. The standard deviation values of the measured mucosal wave speed and shear modulus were less than 6 and 12 percent of the corresponding mean values, respectively. Thus, only the mean values are shown.

The mucosal wave propagation on the medial and superior surfaces of Subject 1's vocal folds during the open phase at a fundamental frequency of 130 Hz, obtained from high speed imaging, is shown in Figure 4-11. As seen in this figure, the mucosal wave mainly propagates in the medial-lateral direction and vanishes before reaching the boundaries of the vocal folds. Therefore, the assumption of 1D (one-directional) Rayleigh wave propagation with no reflection from the boundaries is satisfied. The maximum horizontal (lateral) displacement of vocal fold upper edge at different pitches from 110 to 440 Hz is shown in Figure 4-12. The vocal folds edge position and glottal area depend on to the viscoelastic mechanical properties of the tissue, as well as lung air pressure, vocal folds geometry, vocal tract inertance, and other parameters that can vary from one subject to another. Therefore, it is not possible to compare the results obtained from different subjects without additional information. Nevertheless, the edge position obtained from each specific subject's vocal fold is expected to decrease with pitch, due to the decrease in the vocal folds width and the expected increase in the shear modulus. This is consistent with the results shown in Figure 4-12. A Depth-kymography technique (George et al., 2008) yielded values between 1.2 and 1.6 mm with a mean value of 1.4 mm at 149 Hz. It is in very good agreement with the mean value of those of the three male subjects, 1.39 mm. The differences were expected to be much higher than only 0.7 percent.

The speed of mucosal wave propagation on the superior surface of vocal folds for four human subjects at different pitches is shown in Figure 4-13. As seen in this figure, the mucosal wave propagation speed increased with pitch except for Subject 3 where it was almost constant. This is consistent with the expected trend of greater overall stiffness (shear modulus) of the tissue at higher frequencies. There were significant differences between the values of the mucosal wave propagation speed obtained from different subjects. For example, it was 466 and 1164 mm/s for Subjects 1 and 3, respectively, at 110 Hz with a difference of 150 percent. Average values of 510 and 810 mm/s were obtained by George *et al*. (2008) at 149 Hz, which were in good agreement with the results shown in Figure 4-13, specially those for Subjects 1 and 2.

The shear modulus of human vocal fold mucosa in the transverse direction at fundamental frequencies from 110 to 440 Hz is shown in Figures 4-14. The same trends as those of mucosal wave propagation speed were observed as expected. The frequency-dependent behavior of mechanical properties of human vocal fold tissue is influenced by two main parameters, namely the inherent viscoelastic properties of the tissue and the longitudinal tension.

As shown in Figure 4-14, considerable differences were observed between the obtained shear modulus vales from different subjects' vocal folds. The rate of increase of shear modulus values with pitch was also different for different subjects. The extension of the vocal fold length varied with pitch. For example, the length of the vocal folds of Subject 1 at 260 Hz was 45 percent greater than that at 110 Hz. For a relative elongation of 45 %, the increase in shear modulus values was 225 % between the corresponding pitches. For Subject 3, for which the rate of increase of the shear modulus was the least, the values for the relative elongation of vocal folds and the increase in shear modulus were 19 % and only 13 %, respectively.

The complex shear modulus values of subjects' vocal fold mucosa obtained from the Voigt viscoelastic model are shown in Table 4-6. The Voigt model yields constant values for the shear elasticity and viscosity averaged over all frequencies. The real part of the complex shear modulus, the shear modulus, was found to be a good approximate mean value of the shear modulus values shown in Figure 4-14. The imaginary part of the obtained complex shear modulus, the viscous modulus, increased linearly with frequency accordingly with the Voigt model, $G'' = \omega\mu''$. This is in good agreement with data obtained by Chan and Rodriguez (2008) from *in vitro* measurements. The mean value of shear modulus of four subjects' vocal fold mucosa was 1378 Pa, which is in excellent agreement with those obtained by Goodyer *et al.* (2007b) from *in vivo* measurements; i.e, 1371 Pa. The difference is surprisingly small, only 0.5 percent, considering the data is for different human subjects and is obtained with different measurement methods. In the present study, the shear modulus is obtained during phonation using a dynamic method. Goodyer *et al.* (2007b) implemented a simple-shear technique in a semi-static manner.

The mean value and standard deviations of the shear modulus of three subjects' vocal fold mucosa, Subjects 1 to 3, were compared with those obtained by (Chan and Rodriguez, 2008) from *in vitro* measurements in Figure 4-15. As seen in this figure, the results fall within the same range while those from *in vivo* measurements were generally greater than *in vitro* ones. Chan and Rodriguez (2008), used a parallel rheometer to measure the shear modulus of the human vocal fold cover with no extension (tension). The method used in the present study, however, yields data during phonation, while the vocal folds underwent large extensions. This allowed the effect of vocal fold tension to be taken into account.

4.4.2. Discussion

A non-invasive method was developed to determine the shear modulus of human vocal fold tissue *in viv*o via measurements of the mucosal wave propagation speed during phonation. The obtained shear modulus from four human subjects' vocal fold tissue were found to be in good agreement with those obtained by Chan and Rodriguez (2008) *in vitro*, and thus support the validity of the proposed *in vivo* measurement method for clinical applications.

The vocal fold tissue includes a large concentration of fibers such as elastin and collagen within interstitial fluid (Titze, 1994), and thus feature a highly viscoelastic mechanical behavior. The magnitude of the tissue shear modulus depends on the configurational rearrangements that occur within the time period of one dynamic loading cycle. At low frequencies, the fibers have sufficient time to adjust themselves with the applied deformation by sliding alongside each other. Therefore, the tissue stiffness is relatively small. At higher frequencies, only minor adjustment can take place within the period of deformation, and thus the tissue is stiffer. A longitudinal tension is required for the self-oscillation of vocal folds. This tension is applied by the thyroarytenoid muscle and sustained by collagenous fibers of the ligament, which consists of the intermediate and deep layers of the lamina propria (Titze, 1994). The global (effective) stiffness of the tissue is directly related to vocal fold tension (Titze, 1994). Greater tensions are applied to the vocal folds at higher pitches, which results in greater stiffnesses.

The vocal fold mucosa was advantageously assumed as a transversely isotropic material. This assumption was justified based on the unidirectional orientation of elastin and collagen fibers in the superficial, intermediate, and deep layers of the lamina propria. The axis of symmetry was in the anterior-posterior direction; i.e., parallel with the fibers, and thus the mechanical properties of the tissue was assumed to be constant in any cross-sectional planes normal to this axis, which are called planes of isotropy. This assumption was evaluated by the calculation of the mucosal wave speed at different locations along the anterior-posterior direction, and different distances from the vocal fold edge. Similar values were obtained, and thus the assumption of transversely isotropic material for the vocal fold mucosa was proved to be effective.

Several assumptions have been made in the present study, and thus the obtained mucosal wave speed and shear modulus were estimates of such values. For example, the phonation frequency was not measured in MRI experiments, although the musical note was produced to help them to phonate at the required frequencies each time. The actual phonation frequency in MRI experiments, and consequently the vocal fold dimensions, could be slightly different from those of the assumed frequency. Differences between the visible anatomical features from one set of HSDI data to another made it more challenging to overlap these features with the corresponding ones in MRI images. It was done with the help of experienced professionals who were familiar with laryngeal anatomy. Furthermore, ideal Rayleigh wave propagation was assumed on the superior surface of the vocal folds, which might not precisely model the mucosal wave propagation due to the complex geometry.

4.5. Viscoelasticity of hyaluronic acid-gelatin hydrogels

4.5.1. Results

The experiments were repeated at least five times for each hydrogel sample. The mean value and standard deviation of the results were calculated. The standard deviation values of the measured shear and viscous moduli were less than 10 percent of the mean values. Thus, only the mean values are presented in the following sections.

The silicone rubber substrate and hydrogel specimens' dimensions and properties are given in Tables 4-7. The shear and viscous moduli of the substrate in the frequency range from 40 Hz to 4 kHz are shown in Figure 4-16. As seen in this figure, a very soft silicone rubber material was used as the substrate to ensure the Rayleigh wave propagation in the top layer. The amplitude of the Rayleigh wave was insufficiently small when there was a significant difference between the stiffness of the substrate and that of the top layer.

The shear and viscous moduli and the loss factor of Sample 2, measured three and twelve hours after fabrication, are shown in the frequency range from 40 Hz to 4 kHz in Figure 4-17. The results are compared with those obtained from the shear rheometry in the frequency range from 1 to 12 Hz (Heris *et al.*, 2012). As seen in this figure, the values obtained from the wave propagation method at high frequencies are consistent with those obtained from the rheometry at low frequencies. The shear and viscous moduli of the hydrogel increased with the frequency throughout the frequency range of interest. The rate of increase in the moduli, however, changed in different frequency ranges. The greatest rate of increase occurred in the frequency range from 40 to 200 Hz where the loss factor, which is defined as the ratio of the viscous (loss) modulus to the shear (storage) modulus, reached a local maximum value. This is qualitatively consistent with the theoretical expectations presented in the literature for the frequency-dependence of polymeric biomaterials (Ferry, 1980; Lakes, 2009). The shear and viscous moduli values obtained twelve hours after fabrication were greater than those obtained only three hours after fabrication. The trends in the measured values were smoother, suggesting that the molecular chains of the hydrogel were more uniformly cross-linked and entangled over the measurement area after twelve hours.

Figure 4-18 shows the shear and viscous moduli of three hydrogels with different cross-linker concentrations, namely Samples 1, 2 and 3. The viscoelastic properties of human vocal tissue from *in vitro* and *in vivo* measurements, respectively obtained by Chan and Rodriguez (2008) and those presented in the previous section, are also shown in the same figure. The viscoelastic properties of the designed hydrogels were in the same range of those of human vocal fold tissue. More specifically, the shear moduli of Samples 1 and 2 were in good agreement with those from *in vitro* and *in vivo* measurements, respectively, and the viscous modulus of Sample 3 was the most similar to that from *in vivo* and *in vitro* measurements. The shear and viscous moduli of the hydrogels increased approximately linearly with an increase in the cross-linker concentration, while the trends of increase in values obtained for each hydrogel with frequency remained the same. By doubling the cross-linker concentration, the shear modulus of Sample 2 increased by a factor in the range between 1.54 and 2.02 compared to that of Sample 1 at different frequencies, with a mean value of 1.89. This factor was in the range between 1.47 and 2.53 with a mean value of 2.06 for the shear modulus of Sample 3 compared to that of Sample 2. This is in very good agreement with data presented by Vanderhooft *et al.* (2009). The average of increase rates in the shear modulus values by doubling the cross-linker concentration was reported to be 2.03 at 1 Hz in that study; please see Table 1 of Vanderhooft *et al.* (2009). The viscous modulus also increased by average factors of 2.19 and 2.81 for Samples 2 and 3 compared to Samples 1 and 2, respectively.

The shear and viscous moduli of three hydrogels with different Ge concentrations are shown in Figure 4-19. Samples 4 and 5 were fabricated by the substitution (replacement) of 10 and 20 percent of the HA content of Sample 2 with Ge, respectively. As seen in Figure 4-19, the moduli of the hydrogels decreased by increasing the Ge concentration. This is in good agreement with data presented by Vanderhooft *et al*. (2009). Regardless of the decreases in the moduli, the shear modulus remained in a range similar to those obtained for human vocal fold tissue. The increase in Ge concentration resulted in a slight increase in the frequency at which the slope of shear and viscous moduli trends changes. The differences between the moduli of hydrogels with different Ge concentrations were consequently smaller at high frequencies (above 400 Hz). For example, the shear and viscous moduli of Sample 2 were 1.74 and 1.55 times greater than those of Sample 5 at low frequencies (between 40 and 400 Hz), respectively. These values were 1.53 and 1.21 at high frequencies (between 500 and 4000 Hz).

The frequency-dependency of shear and viscous moduli of the fabricated hydrogels were parameterized using linear least-squares regressions. A power law relation between the frequency and moduli was assumed to perform the regression (curve fitting) as following:

$$G' = a f^{b} \quad \Rightarrow \quad \log G' = \log a + b \log f\,, \tag{4.2}$$

$$G'' = a f^{b} \quad \Rightarrow \quad \log G'' = \log a + b \log f\,, \tag{4.3}$$

where f is the frequency, and a and b are the curve fitting coefficients. These coefficients were separately calculated for the shear and viscous moduli of each tested hydrogel and shown in Table 4-8. The coefficient of determination, R^2, was greater than 0.95 for all cases. This confirms that the assumed power law relation was an ideal model to parameterize the data presented in this study.

For arbitrary concentrations of HA, Ge, and cross-linker, a predictive second order polynomial curve fitting procedure was introduced to obtain the curve fitting parameters for a variety of hydrogels for two following cases: 1) HA hydrogels with fixed 0.5% thiol-modified HA and a variable concentration of the cross-linker (PEGDA); 2) HA-Ge hydrogels with initial concentrations of 0.5% thiol-modified HA and 0.5% PEGDA, in which a variable concentration of HA is replaced with Ge. The curve fitting parameters are obtained from the following relations:

$$a = a_1 + a_2 x + a_3 x^2\,, \tag{4.4}$$

$$b = b_1 + b_2 x + b_3 x^2, \tag{4.5}$$

in which a_i and b_i $(i = 1,2,3)$ were calculated separately for the two mentioned cases using the curve fitting coefficients obtained for the tested hydrogels (Table 4-8) and given in Table 4-9. The variable x is the cross-linker concentration for the first case and the concentration of HA replaced with Ge for the second case. The shear and viscous moduli of an assumed case with 0.475% thiol-modified HA, 0.025% thiol-modified Ge, and 0.5% PEGDA; i.e., the second case where 0.025% of HA concentration is replaced with Ge, was obtained from Eqs. (4.2) to (4.5) and shown in Figure 4-19. As seen in this figure, the viscoelastic properties were accurately predicted by these parametric equations at frequencies higher than 100 Hz.

4.5.2. Discussion

Among different available hydrogels and commercial phonosurgical biomaterials, HA-based hydrogels have clinically been shown to provide considerable improvements in the quality of voice (Hertegård *et al.*, 2002; 2004). In this study, cross-linked HA-Ge hydrogels for vocal fold tissue treatment were fabricated and characterized. The synthesis and characterization of a variety of HA-Ge hydrogels with viscoelastic properties similar to those of human vocal fold tissue provides physicians with the opportunity to choose the best injectable hydrogel for any specific patient.

The Rayleigh wave propagation method used in this study for the characterization of the viscoelastic properties of the fabricated hydrogels was compared and evaluated with two different characterization methods, namely longitudinal wave propagation and AFM-based indentation methods, as well a characterization method based on surface wave propagation presented in an independent study (Nenadic *et al.*, 2011a). The trends and values of the results obtained in this study for the fabricated hydrogels were also in good agreement with those presented in the literature at low frequencies (Vanderhooft *et al.*, 2009; Heris *et al.*, 2012).

The viscoelastic properties of hydrogels are affected by various parameters such as the concentration, entanglement, and molecular weight of the constituents (Vanderhooft *et al.*, 2009). In this study, we varied the cross-linker density and relative concentration of HA and Ge. Cross-link density, which is determined by the cross-linker concentration, is the most common parameter to tune the viscoelastic properties (more specifically the shear modulus) of designed HA-based hydrogels (Ghosh *et al.*, 2005). The shear and viscous moduli of HA-Ge hydrogels tested in this study were increased approximately by a factor of two by doubling the cross-linker concentration suggesting a linear correlation. In most tissue engineering applications, the viscoelastic properties of the injectable biomaterial is matched with those of the native tissue for better structural and functional integrity with the host tissue. In addition to changes in the viscoelastic properties, the increase in cross-linker density decreases porosity and diffusivity of the network and ultimately affects the cellular behaviour such as cell migration in tissue engineering. Furthermore, higher cross-linking increases the *in vivo* residence time of the injectable biomaterial, which also affects the outcome of tissue engineering. On the other hand, the concentration of HA and Ge mainly affects the ligand-integrin mediated cellular response. For instance, HA molecules can reduce the inflammatory response of the host tissue after injection of the biomaterial and Ge increases the rate of cell adhesion to the matrix (Heris *et al.*, 2012). The variation of the mechanical properties with respect to the Ge concentration was assessed to better tune the viscoelastic properties where the addition of Ge is required to improve the cell adhesion characteristics of the injectable biomaterial.

The shear and viscous moduli of tested hydrogels at high frequencies (few kHz) were one order of magnitude (10 times) greater than those at low frequencies. This important result emphasizes the importance of the characterization of *frequency-dependent* viscoelastic properties of the synthesized HA-Ge hydrogels with application for vocal fold tissue treatment. A non-invasive method has been developed for the *in vivo* measurements of the shear modulus of human vocal fold tissue during phonation in in this study. This method can clinically be used to assess the viscoelastic properties of any specific patients' vocal fold tissue. Subsequently, an appropriate injectable HA-Ge hydrogel, with known viscoelastic properties using the frequency-dependent parametric relations provided here, Eqs. (4.2) to (4.5), can be fabricated based on the requirements for the treatment of the specific patient's vocal folds. This integrated methodology to characterize the frequency-dependent properties of human vocal fold tissue and fabricate the optimum injectable hydrogel can potentially have a broad application, specially for singers as the fundamental frequency of their vocal fold oscillation reaches up to a few kHz in singing.

Table 4-1. Standard deviation values of the measured elastic modulus (kPa) using the wave propagation methods. The results of the longitudinal wave propagation method are for the case of zero pre-elongation.

Frequency (Hz)	Rayleigh method, sample 1:1:1	longitudinal method, sample 1:1:0.5	longitudinal method, sample 1:1:1
20	-----	0.764	0.355
40	-----	0.665	0.453
60	-----	0.729	0.250
80	3.007	0.518	0.267
100	2.589	0.543	0.282
200	3.119	1.222	0.623
300	2.145	1.533	1.402
400	2.400	3.016	2.277
500	3.282	3.842	3.683
600	4.550	4.274	4.033
700	4.623	6.060	5.720
800	5.805	5.905	5.938
900	6.432	7.586	7.575
1000	7.209	9.295	9.875
2000	15.86	27.17	42.99
3000	31.06	60.76	64.85
4000	52.17	110.7	115.9

Table 4-2. Standard deviation values of the measured loss factor using the wave propagation methods. The results of the longitudinal wave propagation method are for the case of zero pre-elongation.

Frequency (Hz)	Rayleigh method, sample 1:1:1	longitudinal method, sample 1:1:0.5	longitudinal method, sample 1:1:1
20	-----	0.0136	0.0182
40	-----	0.0121	0.0177
60	-----	0.0120	0.0092
80	0.0103	0.0084	0.0094
100	0.0120	0.0084	0.0096
200	0.0177	0.0186	0.0221
300	0.0250	0.0265	0.0393
400	0.0358	0.0431	0.0362
500	0.0490	0.0375	0.0372
600	0.0552	0.0311	0.0310
700	0.0657	0.0288	0.0291
800	0.0686	0.0218	0.0216
900	0.0731	0.0211	0.0210
1000	0.0744	0.0211	0.0204
2000	0.0628	0.0121	0.0171
3000	0.0516	0.0108	0.0105
4000	0.0527	0.0098	0.0097

Table 4-3. Sample dimensions, properties and attached mass values for the longitudinal wave propagation experiments.

Sample	Length (L) [10^{-3} m]	Cross sectional area [10^{-6} m^2]	Mass (m) [10^{-3} kg]	Density ρ [kg/m^3]	External mass #1 (M_1) [10^{-3} kg]	External mass #2 (M_2) [10^{-3} kg]
1:1:0.5	75	36	2.92	1082	0.55	1.82
1:1:1	75	36	2.76	1007	0.55	1.82

Table 4-4. Sample dimensions and properties for the Rayleigh wave propagation experiments.

Sample	Length [10^{-3} m]	Width [10^{-3} m]	Height [10^{-3} m]	Mass (m) [10^{-3} kg]	Density ρ [kg/m^3]
1:1:0.5	102	51	51	288.6	1088
1:1:1	102	51	51	268.2	1011

Table 4-5. Measured complex elastic modulus and the possible experimentally induced error (kPa) using the wave propagation methods. The results of the longitudinal wave propagation method are for the case of zero pre-elongation.

Frequency (Hz)	Rayleigh method, sample 1:1:1	longitudinal method, sample 1:1:1
20	-----	(8.898+4.059*i*) ± (0.623+0.499*i*)
40	-----	(11.34+5.025*i*) ± (0.381+0.176*i*)
60	-----	(12.54+5.794*i*) ± (0.339+0.222*i*)
80	(14.61+6.714*i*) ± (0.203+0.096*i*)	(13.37+6.345*i*) ± (0.225+0.070*i*)
100	(14.47+6.886*i*) ± (0.164+0.080*i*)	(14.10+6.835*i*) ± (0.193+0.102*i*)
200	(23.33+11.32*i*) ± (0.158+0.059*i*)	(15.57+8.627*i*) ± (0.115+0.092*i*)
300	(27.66+22.22*i*) ± (0.149+0.068*i*)	(28.05+22.07*i*) ± (0.169+0.075*i*)
400	(43.47+31.42*i*) ± (0.146+0.127*i*)	(45.55+33.02*i*) ± (0.172+0.146*i*)
500	(73.49+61.21*i*) ± (0.211+0.177*i*)	(73.67+54.83*i*) ± (0.129+0.124*i*)
600	(90.07+60.07*i*) ± (0.250+0.216*i*)	(100.8+78.14*i*) ± (0.277+0.240*i*)
700	(155.8+99.44*i*) ± (0.324+0.246*i*)	(143.0+104.2*i*) ± (0.385+0.304*i*)
800	(186.6+128.1*i*) ± (0.418+0.307*i*)	(197.9+142.9*i*) ± (0.474+0.377*i*)
900	(211.5+151.6*i*) ± (0.475+0.368*i*)	(252.5+177.3*i*) ± (0.522+0.427*i*)
1000	(274.6+176.1*i*) ± (0.558+0.434*i*)	(329.1+224.8*i*) ± (0.620+0.528*i*)
2000	(1192+600.7*i*) ± (1.841+1.264*i*)	(1433+819.4*i*) ± (2.094+1.473*i*)
3000	(3001+1352*i*) ± (3.097+2.853*i*)	(3242+170.2*i*) ± (3.525+3.250*i*)
4000	(5648+2642*i*) ± (5.483+5.379*i*)	(5795+2838*i*) ± (6.255+6.179*i*)

Table 4-6. The complex shear modulus, $\hat{G}$, of human subjects' vocal fold mucosa obtained from the Voigt viscoelastic model.

Subjects	Shear modulus [Pa]
# 1	$415 + i\omega 0.40$
# 2	$878 + i\omega 0.52$
# 3	$1496 + i\omega 0.67$
# 4	$2722 + i\omega 1.01$

Table 4-7. Dimensions and properties of the silicone rubber substrate and hydrogel specimens. The acronym XL denotes the cross-linker. All the concentrations are given in weight per unit volume (w/v).

Material	Length [10^{-3} m]	Width [10^{-3} m]	Height [10^{-3} m]	Mass (m) [10^{-3} kg]	Density ρ [kg/m^3]
Substrate: silicone rubber 1:1:3	76.2	38.1	38.1	112.2	1014
Sample 1: 0.5% HA + 0.25% XL	76.2	38.1	1.38	4.028	1007
Sample 2: 0.5% HA + 0.5% XL	76.2	38.1	1.38	4.040	1010
Sample 3: 0.5% HA + 1% XL	76.2	38.1	1.38	4.060	1015
Sample 4: 0.45% HA + 0.05% Ge + 0.5% XL	76.2	38.1	1.72	5.050	1010
Sample 5: 0.4% HA + 0.1% Ge + 0.5% XL	76.2	38.1	1.72	5.050	1010

Table 4-8. The curve fitting and determination coefficients obtained from least-squares regressions to parameterize the shear and viscous moduli of the fabricated hydrogels. All the concentrations are given in weight per unit volume (w/v).

Material	Shear modulus $G' = a f^b$			Viscous modulus $G'' = a f^b$		
	a	b	R^2	a	b	R^2
Sample 1: 0.5% HA + 0.25% XL	13.61	0.7034	0.9959	7.157	0.4610	0.9861
Sample 2: 0.5% HA + 0.5% XL	23.26	0.7182	0.9980	13.54	0.4839	0.9928
Sample 3: 0.5% HA + 1% XL	61.64	0.6824	0.9961	67.22	0.3956	0.9596
Sample 4: 0.45% HA + 0.05% Ge + 0.5% XL	19.61	0.7136	0.9960	12.24	0.4827	0.9857
Sample 5: 0.4% HA + 0.1% Ge + 0.5% XL	11.23	0.7601	0.9983	8.496	0.5206	0.9824

Table 4-9. The coefficients obtained from a second order polynomial curve fitting procedure for a variety of hydrogels for two general cases.

Curve fitting case	$a = a_1 + a_2 x + a_3 x^2$			$b = b_1 + b_2 x + b_3 x^2$		
Shear modulus $G' = a f^b$	a_1	a_2	a_3	b_1	b_2	b_3
Case 1	10.32	0.440	50.88	0.667	0.190	-0.174
Case 2	23.26	-25.70	-946.0	0.7182	-0.603	10.22
Viscous modulus $G'' = a f^b$	a_1	a_2	a_3	b_1	b_2	b_3
Case 1	14.41	-56.30	109.1	0.393	0.360	-0.358
Case 2	13.54	-1.56	-488.8	0.484	-0.415	7.820

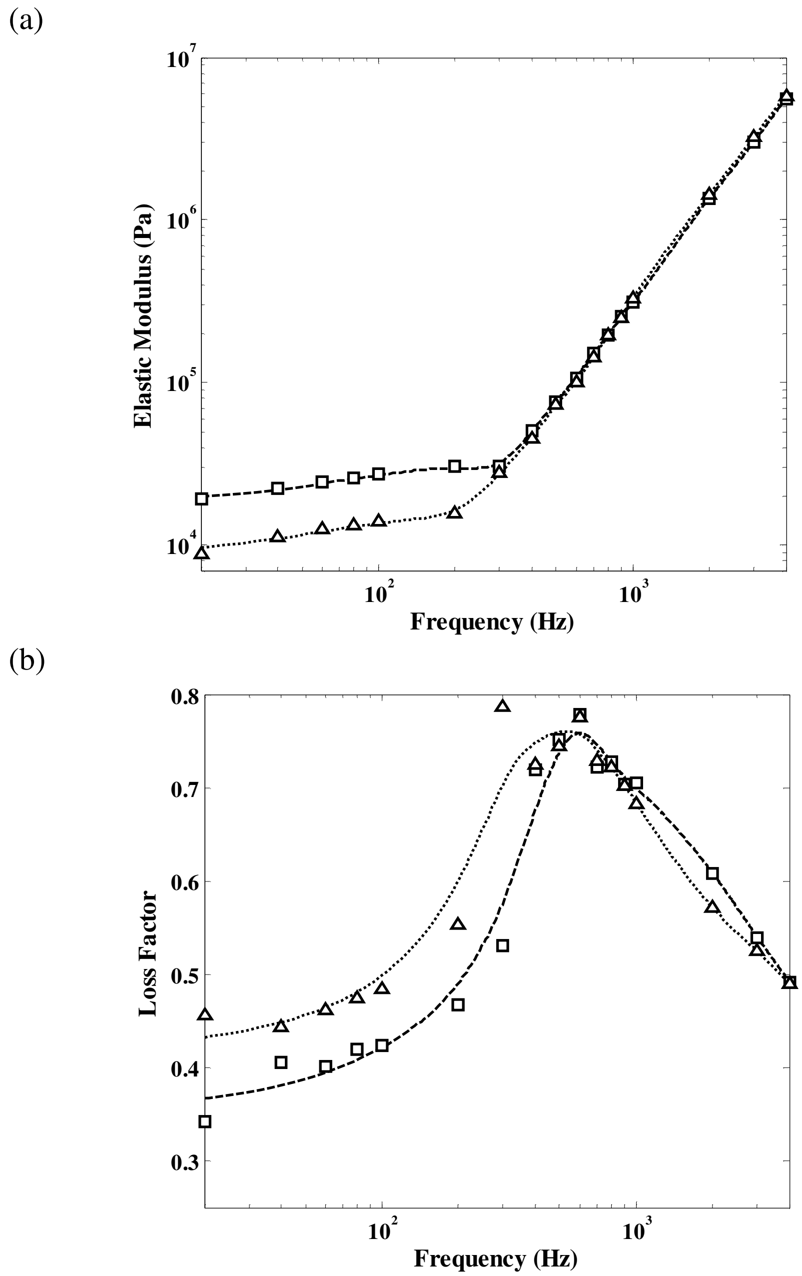

Figure 4-1. (a) Elastic modulus and (b) loss factor versus frequency for two different silicone rubber samples using the longitudinal wave propagation method. The results are for the case of zero pre-elongation in the frequency range from 20 Hz to 4 kHz. ◘: sample 1:1:0.5; ▲: sample 1:1:1; ▬ ▬ ▬: regression for sample 1:1:0.5; ....: regression for sample 1:1:1. (Regressions are to guide the eye)

(a)

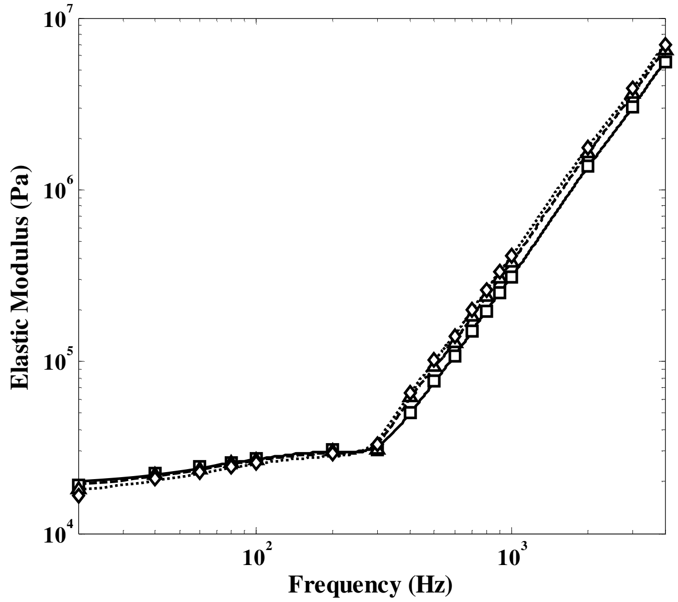

(b)

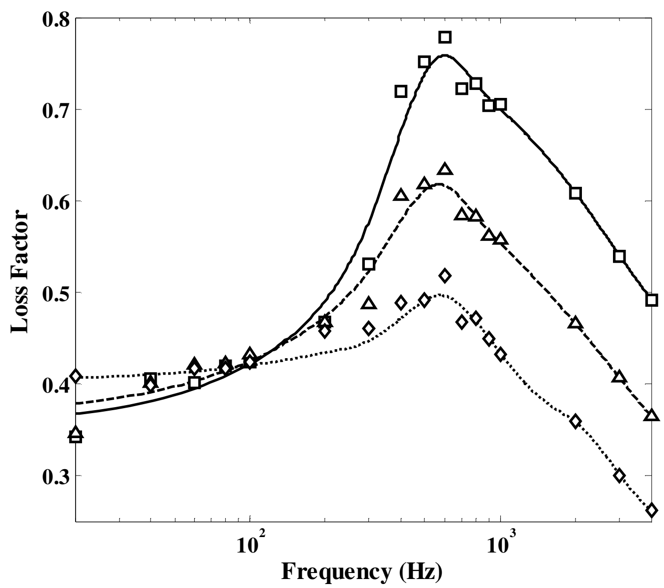

Figure 4-2. (a) Elastic modulus and (b) loss factor versus frequency for a silicone rubber sample with component ratio of 1:1:0.5 using the longitudinal wave propagation method. The results are presented for different pre-elongations in the frequency range from 20 Hz to 4 kHz. □: zero pre-elongation; ▲: 3% pre-elongation; ◇: 7% pre-elongation; ———: regression for zero pre-elongation; – – –: regression for 3% pre-elongation; ....: regression for 7% pre-elongation. (Regressions are to guide the eye)

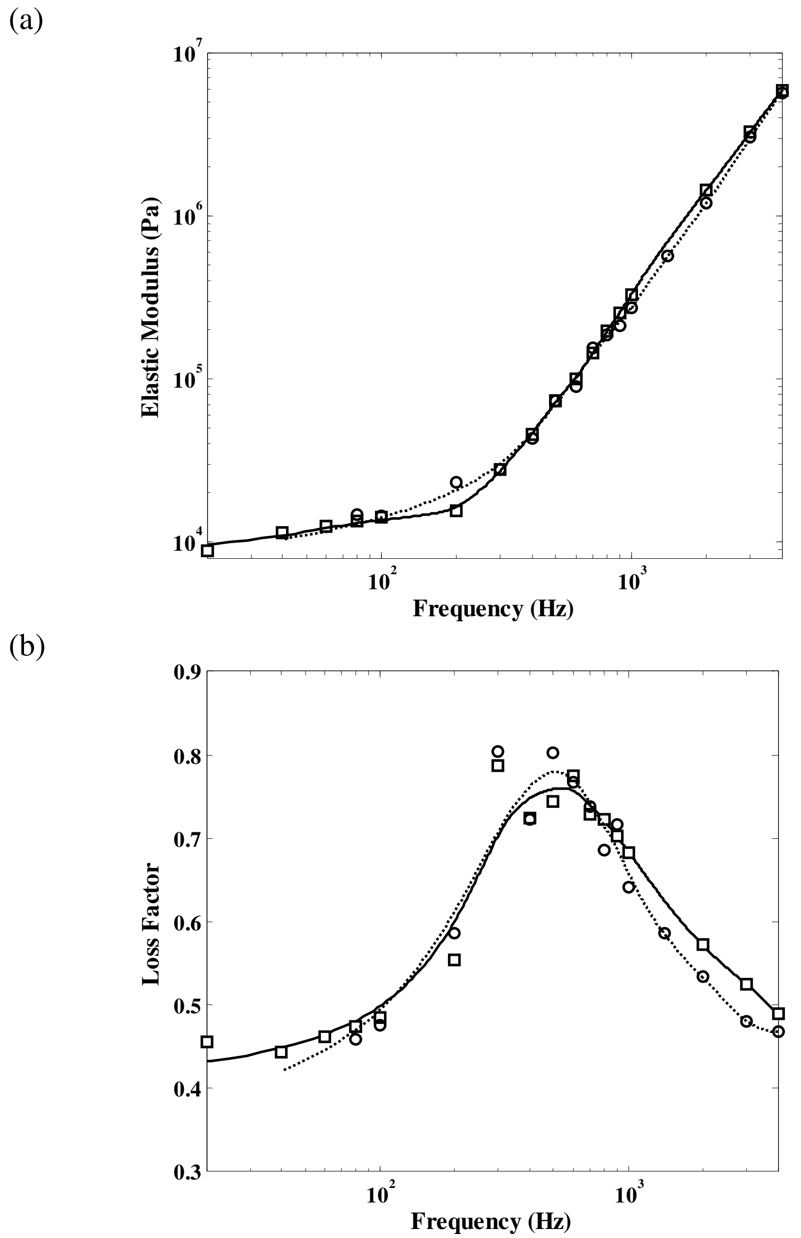

Figure 4-3. (a) Elastic modulus and (b) loss factor versus frequency for silicone rubber samples with component ratio of 1:1:1. The viscoelastic properties were measured in the frequency range from 20 Hz to 4 kHz and 80 Hz to 4 kHz using the longitudinal and Rayleigh wave propagation methods, respectively. □: longitudinal wave propagation method, zero pre-elongation; o: Rayleigh wave propagation method; ——: regression for longitudinal wave propagation method, zero pre-elongation; ....: regression for Rayleigh wave propagation method. (Regressions are to guide the eye)

(a)

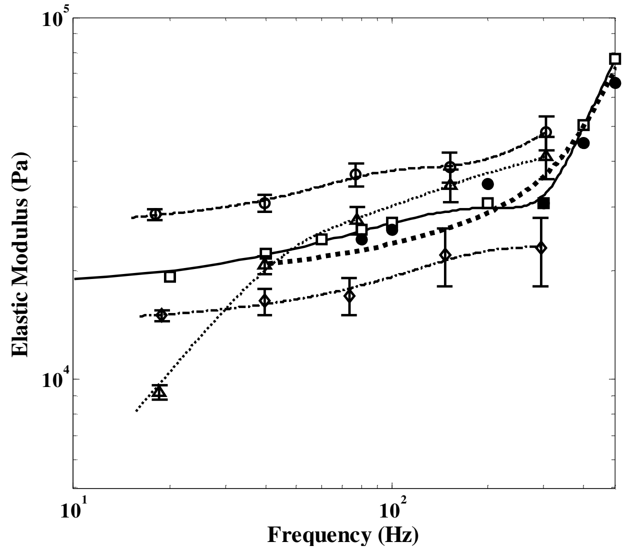

(b)

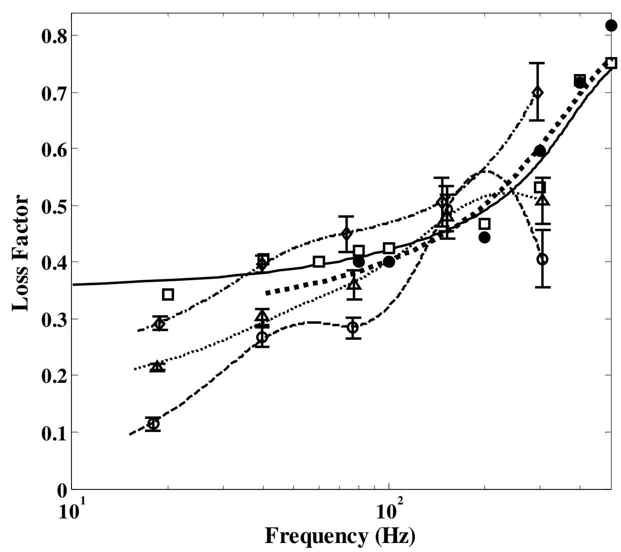

Figure 4-4. (a) Elastic modulus and (b) loss factor versus frequency for silicone rubber samples with component ratio of 1:1:0.5 using wave propagation methods and AFM. □: longitudinal wave propagation method, zero pre-elongation; ● : Rayleigh wave propagation method; o: AFM, stiff spherical tip, small amplitude oscillations (10 nm); ▲: AFM, stiff spherical tip, large amplitude oscillations (30 nm); ◇: AFM, soft spherical tip; ——: regression for longitudinal wave propagation method, zero pre-elongation; ■■■■■ : regression for Rayleigh wave propagation method; – – –: regression for AFM, stiff spherical tip, small amplitude oscillations; ....: regression for AFM, stiff spherical tip, large amplitude oscillations; – · – : regression for AFM, soft spherical tip.

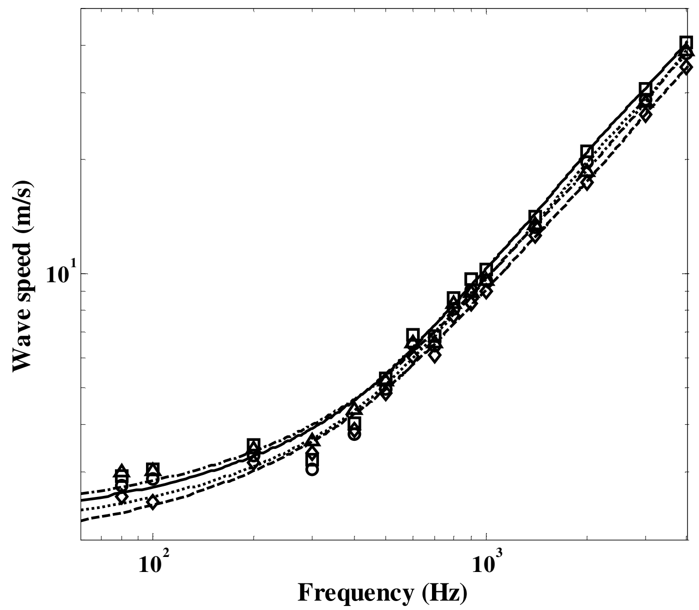

Figure 4-5. Wave propagation speed versus frequency for a silicone rubber sample with component ratio 1:1:0.5 in the frequency range from 80 Hz to 4 kHz. o: Rayleigh wave speed from a uniform sample; □: shear wave speed from a uniform sample; ◊: Rayleigh wave speed from a layered sample; ▲: shear wave speed within the top layer of a layered sample; ....: regression for Rayleigh wave speed from a uniform sample; ——: regression for shear wave speed from a uniform sample; – – –: regression for Rayleigh wave speed from a layered sample; — · —: regression for shear wave speed from a layered sample. (Regressions are to guide the eye)

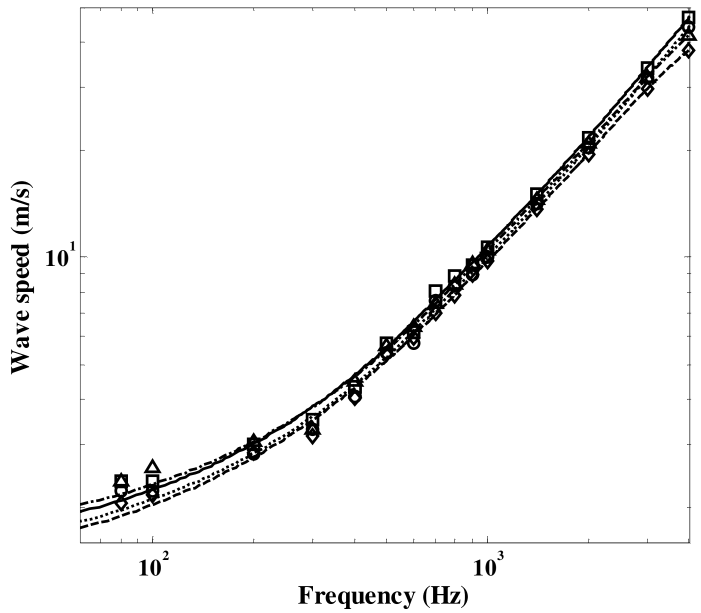

Figure 4-6. Wave propagation speed versus frequency for a silicone rubber sample with component ratio 1:1:1 in the frequency range from 80 Hz to 4 kHz. o: Rayleigh wave speed from a uniform sample; □: shear wave speed from a uniform sample; ◊: Rayleigh wave speed from a layered sample; ▲: shear wave speed within the top layer of a layered sample; ………: regression for Rayleigh wave speed from a uniform sample; ——: regression for shear wave speed from a uniform sample; – – –: regression for Rayleigh wave speed from a layered sample; — · —: regression for shear wave speed from a layered sample. (Regressions are to guide the eye)

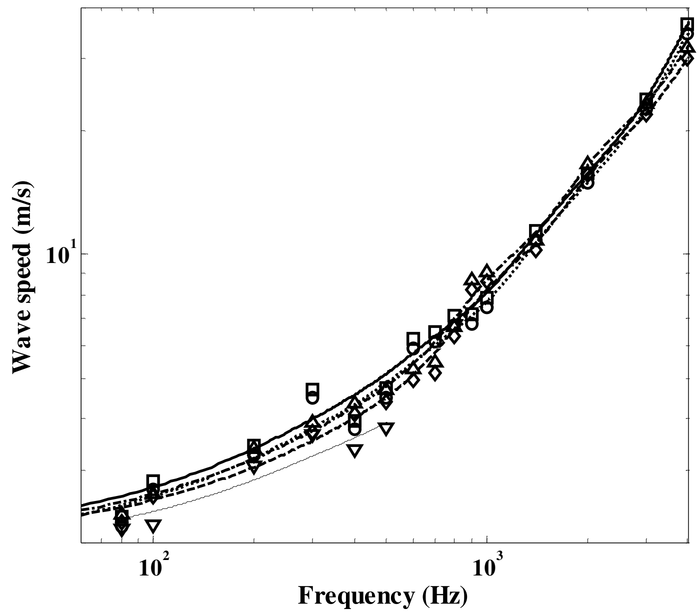

Figure 4-7. Wave propagation speed versus frequency for a gelatin sample in the frequency range from 80 Hz to 4 kHz. o: Rayleigh wave speed from a uniform sample; □: shear wave speed from a uniform sample; ◊: Rayleigh wave speed from a layered sample; ▲: shear wave speed within the top layer of a layered sample; ▽: Rayleigh wave speed (Nenadic *et al.*, 2011a); ....: regression for Rayleigh wave speed from a uniform sample; ——: regression for shear wave speed from a uniform sample; – – –: regression for Rayleigh wave speed from a layered sample; — · —: regression for shear wave speed from a layered sample; ——— : regression for Rayleigh wave speed (Nenadic *et al.*, 2011a). (Regressions are to guide the eye)

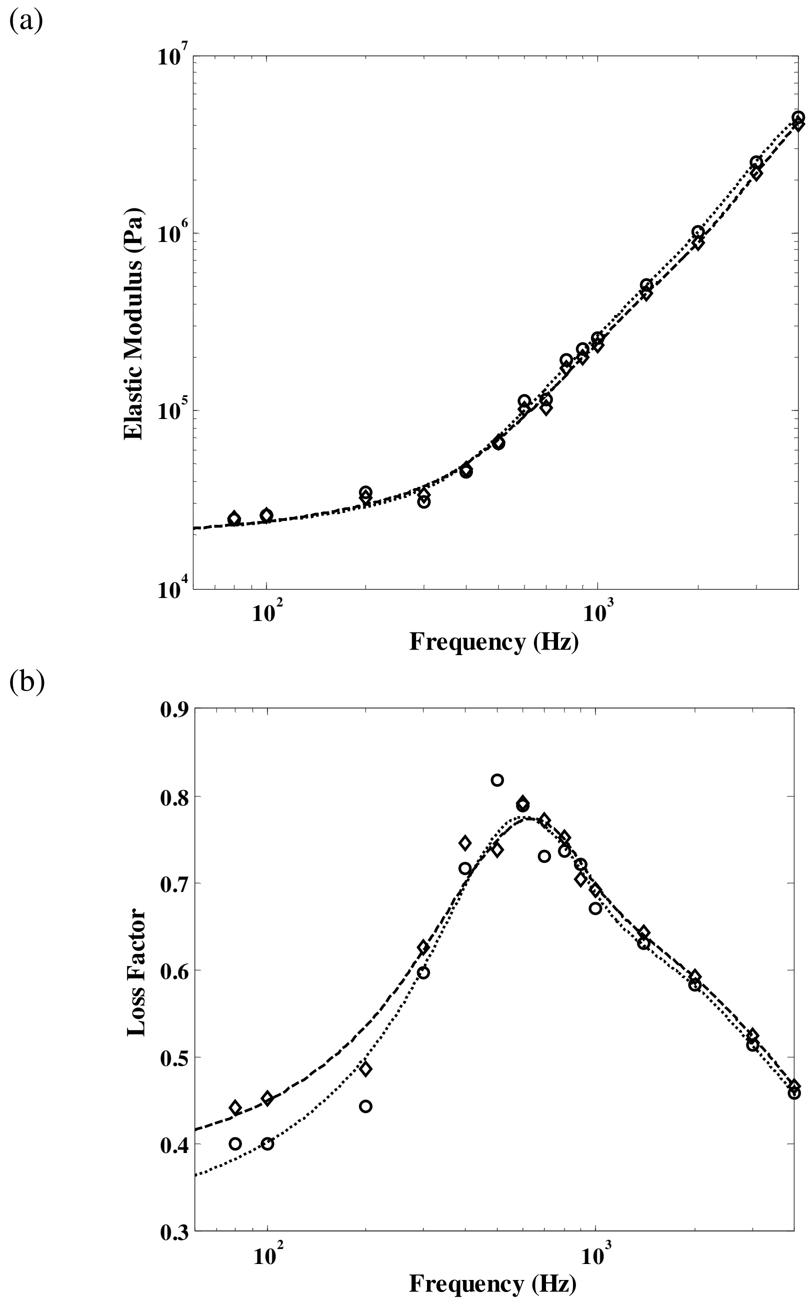

Figure 4-8. (a) Elastic modulus and (b) loss factor versus frequency for a silicone rubber sample with component ratio 1:1:0.5 in the frequency range from 80 Hz to 4 kHz. o: a uniform sample; ◊: a layered sample; ....: regression for a uniform sample; – – –: regression for a layered sample. (Regressions are to guide the eye)

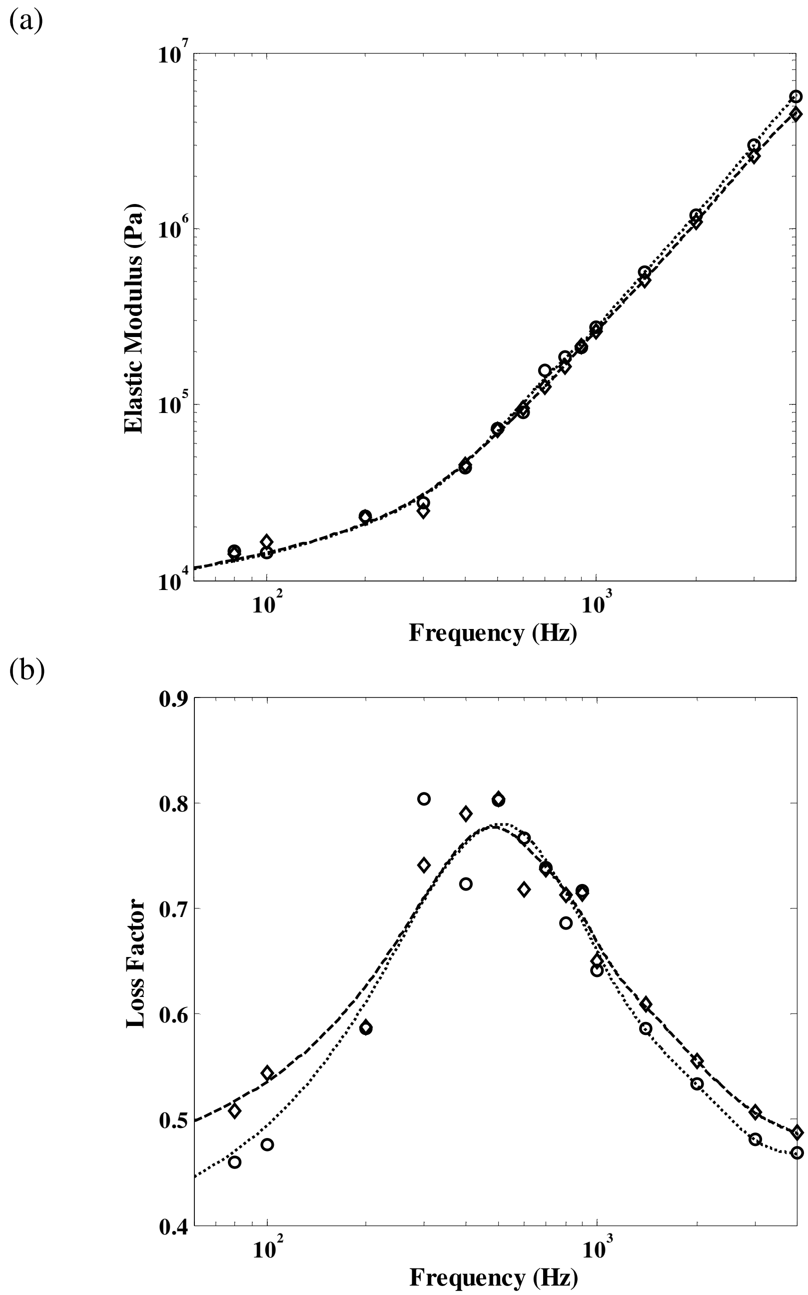

Figure 4-9. (a) Elastic modulus and (b) loss factor versus frequency for a silicone rubber sample with component ratio 1:1:1 in the frequency range from 80 Hz to 4 kHz. o: a uniform sample; ◊: a layered sample; ....: regression for a uniform sample; – – –: regression for a layered sample. (Regressions are to guide the eye)

(a)

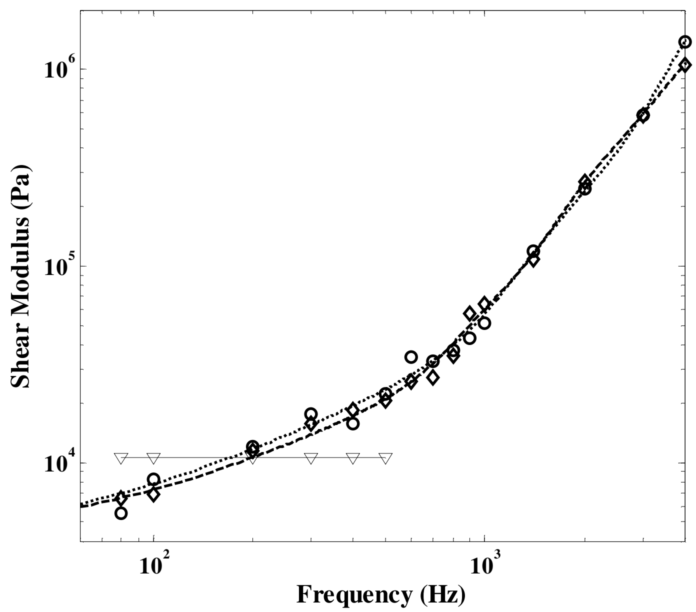

(b)

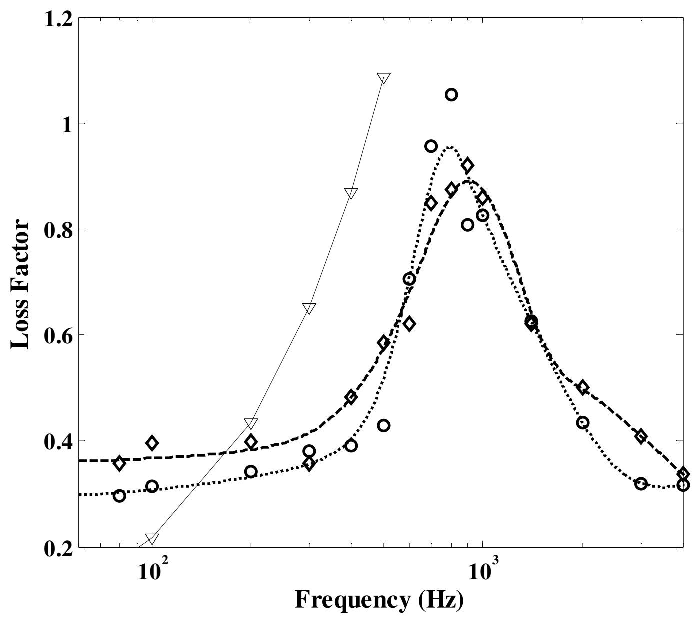

Figure 4-10. (a) Shear modulus and (b) loss factor versus frequency for a gelatin sample in the frequency range from 80 Hz to 4 kHz. o: a uniform sample; ◊: a layered sample; ▽: (Nenadic *et al.*, 2011a); ....: regression for a uniform sample; – – –: regression for a layered sample; ______ : regression for (Nenadic *et al.*, 2011a). (Regressions are to guide the eye)

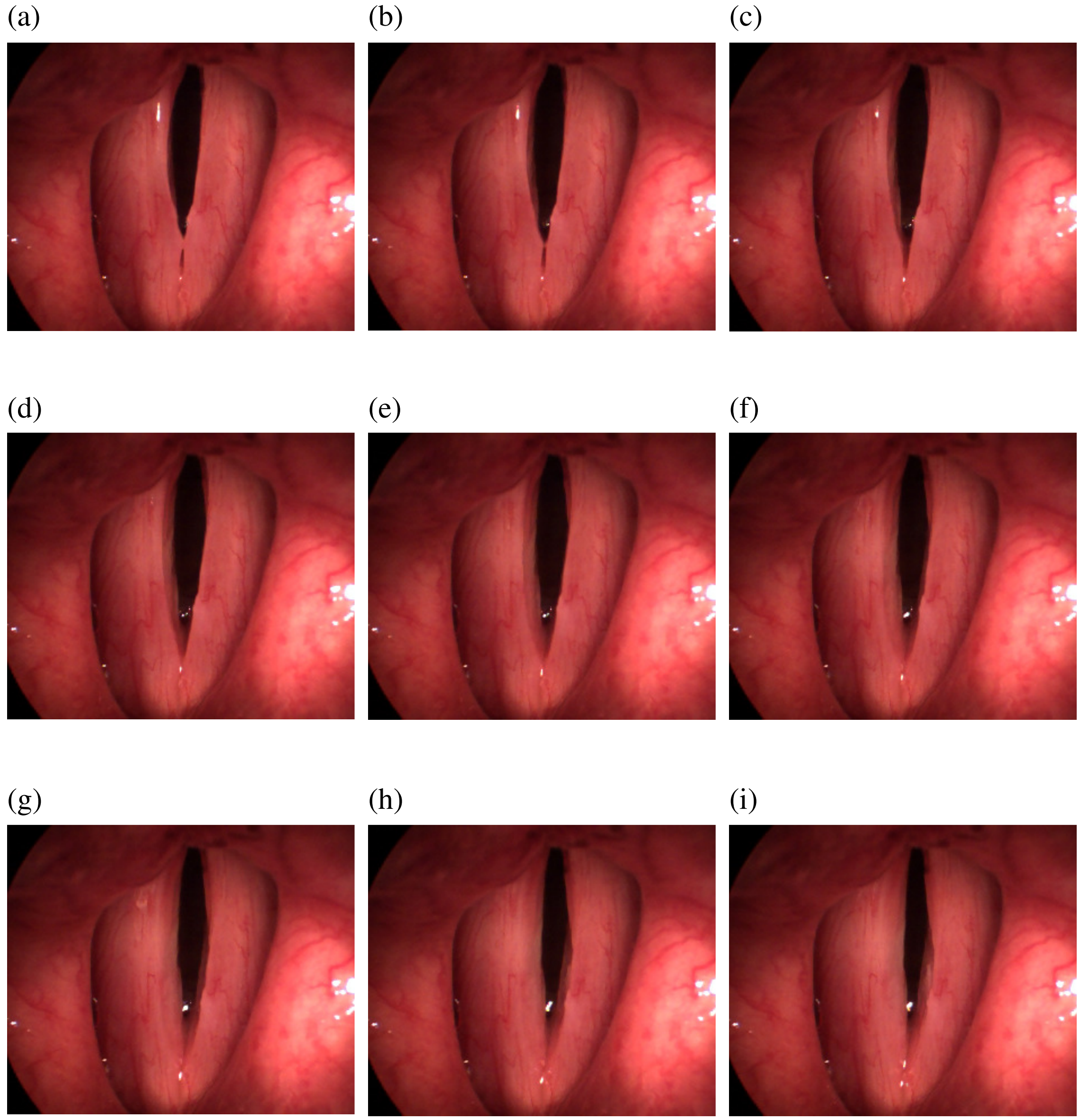

Figure 4-11. (a) to (i) The mucosal wave propagation on the medial and superior surfaces of Subject 1's vocal folds during the open phase at a fundamental frequency of 130 Hz, obtained from high speed imaging.

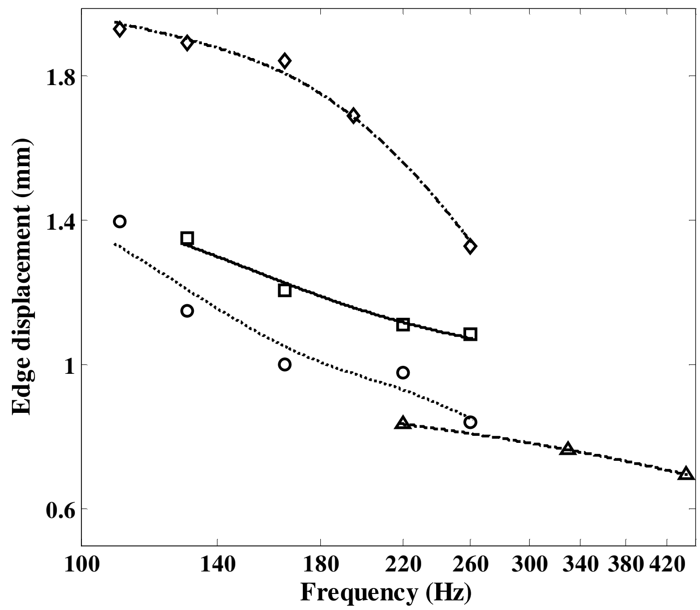

Figure 4-12. The maximum of the horizontal displacement of vocal fold upper edge during the opening phase at different phonation pitches from 110 to 440 Hz. o: Subject 1; ◻: Subject 2; ◇: Subject 3; ▲: Subject 4; ....: regression for Subject 1; ———: regression for Subject 2; — · —: regression for Subject 3; – – – : regression for Subject 4. (Regressions are to guide the eye)

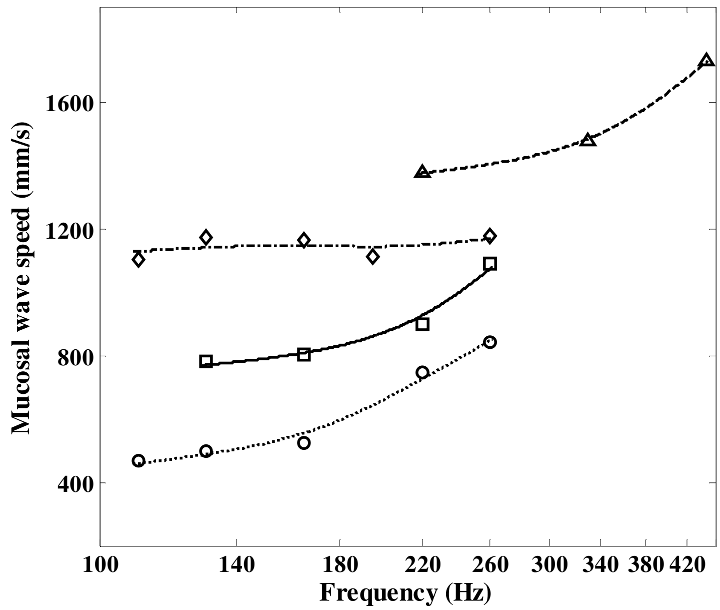

Figure 4-13. The mucosal wave propagation speed at different phonation pitches from 110 to 440 Hz. o: Subject 1; □: Subject 2; ◇: Subject 3; ▲: Subject 4; ....: regression for Subject 1; ——: regression for Subject 2; — · —: regression for Subject 3; – – – : regression for Subject 4. (Regressions are to guide the eye)

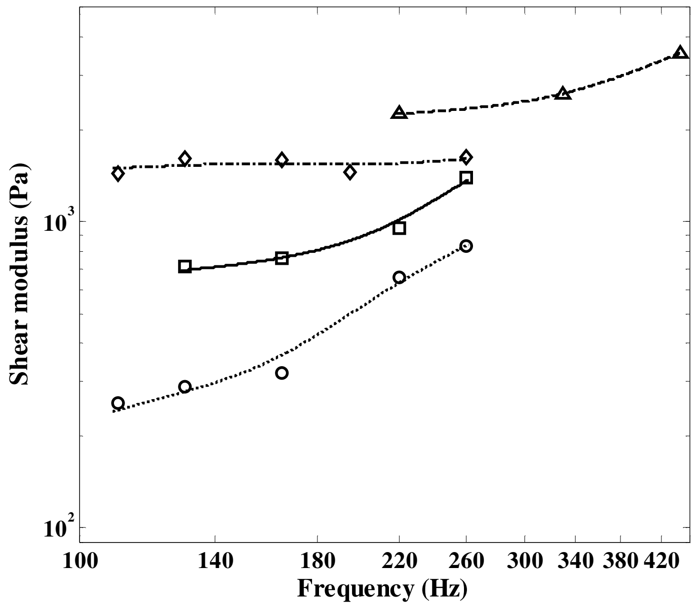

Figure 4-14. The shear modulus of human vocal fold mucosa at different phonation pitches from 110 to 440 Hz. o: Subject 1; □: Subject 2; ◇: Subject 3; ▲: Subject 4; ....: regression for Subject 1; ———: regression for Subject 2; — · —: regression for Subject 3; – – – : regression for Subject 4. (Regressions are to guide the eye)

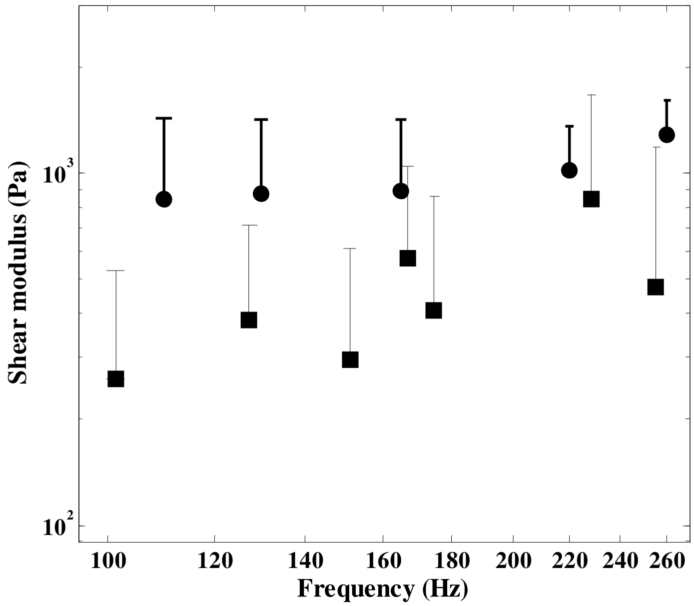

Figure 4-15. The means and standard deviations (upper error bars) of the shear modulus of human vocal fold mucosa versus frequency in the range from 100 to 260 Hz. ■ : the mean value of three male subjects from *in vivo* measurements (present study); ● : the mean value of seven specimens obtained from *in vitro* measurements (Chan and Rodriguez, 2008).

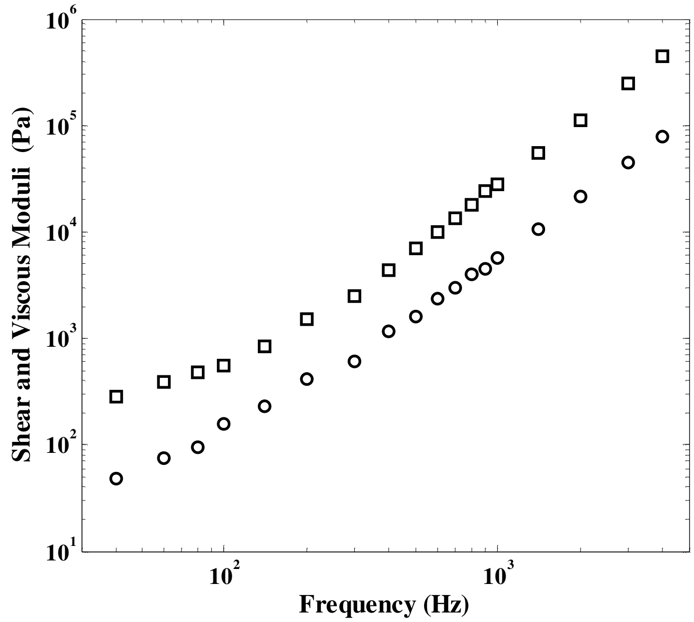

Figure 4-16. Shear and viscous moduli versus frequency for the silicone rubber substrate with component ratio of 1:1:3 using a longitudinal wave propagation method in the frequency range from 40 Hz to 4 kHz. □ : shear modulus; ○ : viscous modulus.

(a)

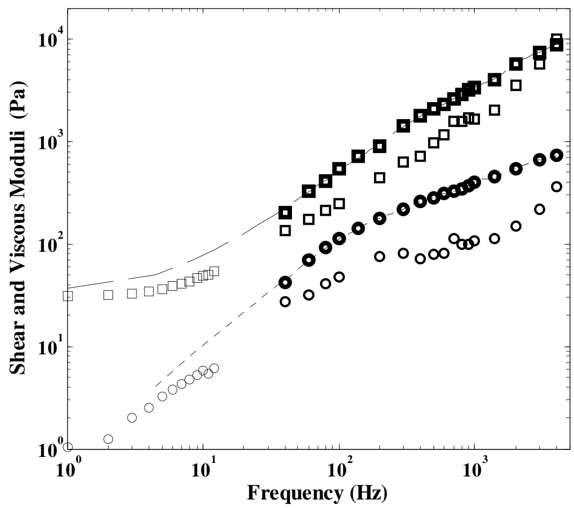

(b)

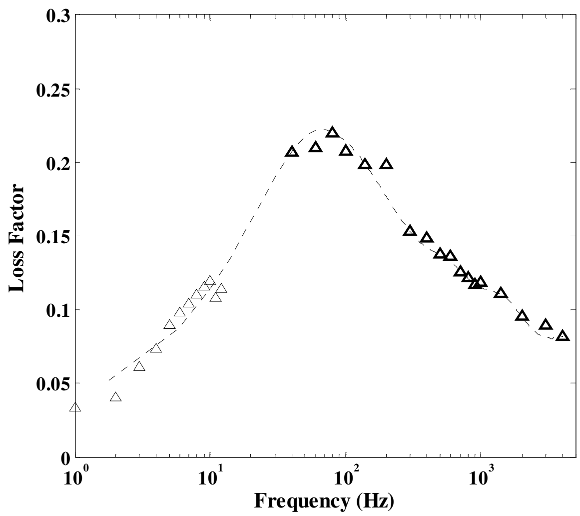

Figure 4-17. (a) Shear and viscous moduli and (b) loss modulus versus frequency for Sample 2 from the Rayleigh wave propagation method in the frequency range from 40 Hz to 4 kHz and those from the rheometry in the frequency range from 1 to 12 Hz. **□** : shear modulus from the Rayleigh wave method, 12 hours after curing; **○** : viscous modulus from the Rayleigh wave method, 12 hours after curing; □ : shear modulus from the Rayleigh wave method, 3 hours after curing; ○ : viscous modulus from the Rayleigh wave method, 3 hours after curing; □ : shear modulus from the rheometry; ○: viscous modulus from the rheometry; ▲: loss modulus from the Rayleigh wave method, 12 hours after curing; △: loss modulus from the rheometry; ....: regression for shear modulus from the Rayleigh wave method, 12 hours after curing; – – –: regression for viscous modulus from the Rayleigh wave method, 12 hours after curing; ______: regression for loss factor. (Regressions are to guide the eye)

(a)

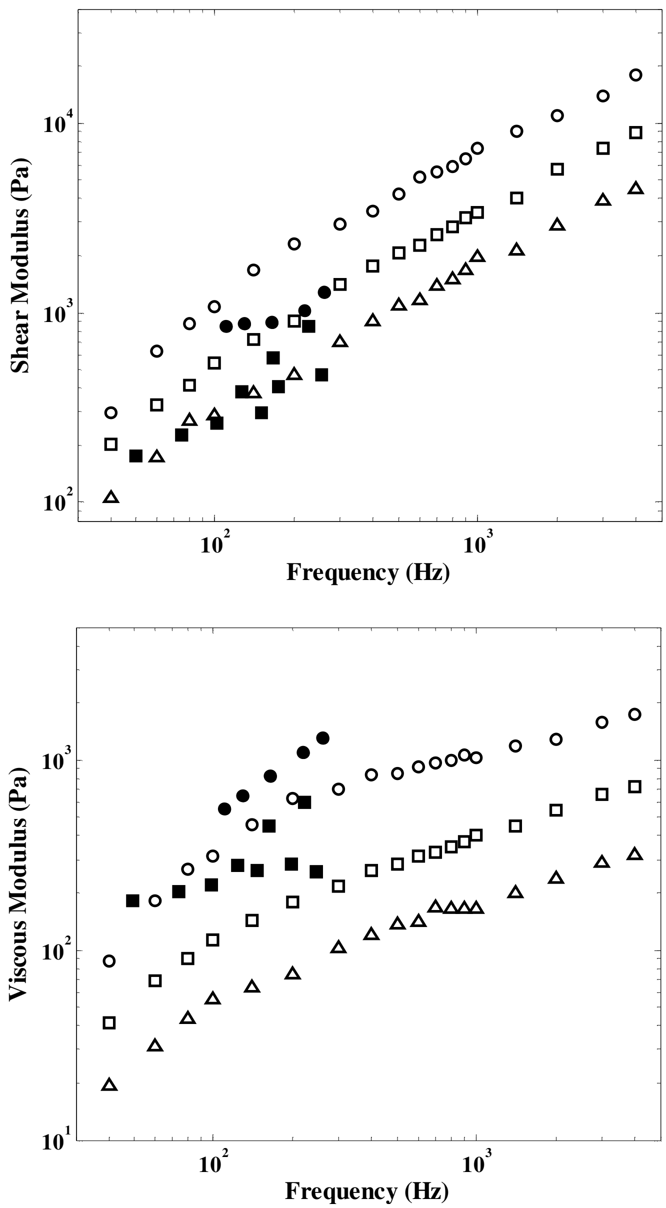

Figure 4-18. (a) Shear modulus and (b) viscous modulus versus frequency for three different hydrogels with different cross-linker concentrations in the frequency range from 400 Hz to 4 kHz. The moduli are compared with those of human vocal tissue obtained from *in vitro* and *in vivo* measurements. △: Sample 1; □ : Sample 2; ○ : Sample 3; ● : the mean value of three male subject's vocal fold tissue from *in vivo* measurements; ■ : the mean value of seven human vocal fold specimens obtained from *in vitro* measurements (Chan and Rodriguez, 2008).

(a)

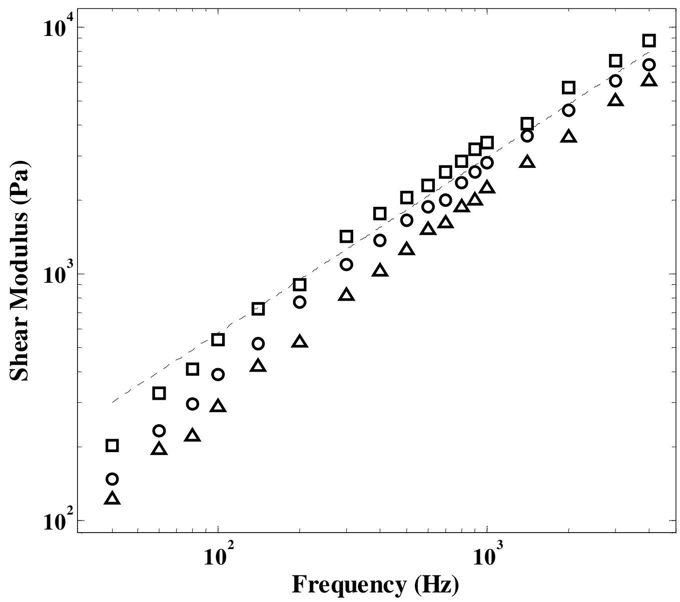

(b)

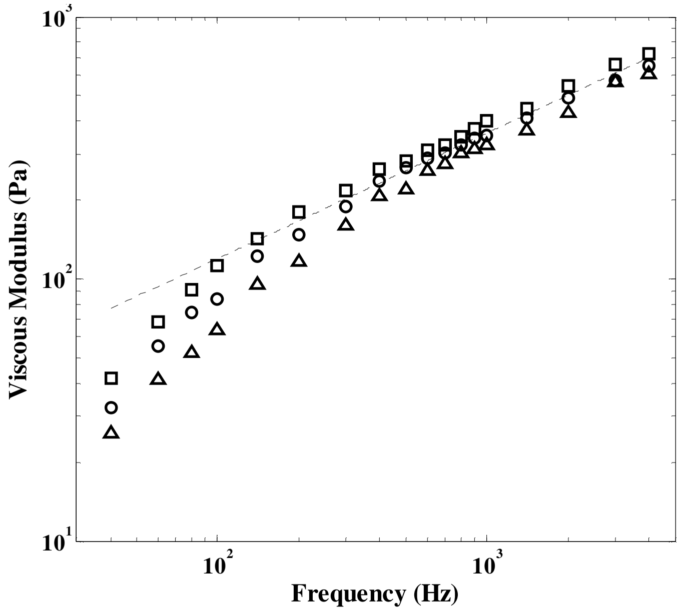

Figure 4-19. (a) Shear modulus and (b) viscous modulus versus frequency for three different hydrogels with different Ge concentrations in the frequency range from 400 Hz to 4 kHz. The moduli are compared with those of human vocal tissue obtained from *in vitro* and *in vivo* measurements. □ : Sample 2; ○ : Sample 4; Δ: Sample 5; ………: regression for an assumed case with 0.475% thiol-modified HA, 0.025% thiol-modified Ge, and 0.5% PEGDA.

CHAPTER 5
Conclusions and future works

5.1. Summary and conclusions

The main objective of this study was to develop novel experimental characterization methods based on wave propagation approaches to quantify the frequency-dependent viscoelastic properties of soft biomaterials and tissues. One application of such methods is in voice production. An integrated methodology was designed to characterize the shear modulus of human vocal fold tissue *in vivo* and fabricate an optimum injectable hydrogel with desirable viscoelastic properties required for the treatment of any specific patient's vocal fold tissue. This objective was achieved through the following specific accomplishments.

A novel experimental method based on Rayleigh wave propagation was developed for the quantification of the frequency-dependent viscoelastic properties of soft biomaterials at high frequencies. Soft silicone materials with characteristics similar to phonosurgical biomaterials and cadaveric human vocal folds were used for evaluation purposes. The complex elastic modulus and loss factor were determined at frequencies up to 4 kHz. Well-established longitudinal wave propagation and AFM-based nano-indentation methods were used to evaluate the Rayleigh wave propagation method. The longitudinal wave propagation method was first evaluated *qualitatively*. The influence of a static load and of the composition of the silicone rubber was investigated, and yielded results in excellent agreement with theoretical expectations for the class of polymers used. The results from the three methods were then *quantitatively* compared and cross-validated. The elastic modulus and loss factor trends were also in very good agreement with established dynamic viscoelastic models such as the Havriliak-Negami model (Havriliak and Negami, 1966).

A cost-effective and model-independent characterization method based on Rayleigh wave propagation was developed for quantifying the frequency-dependent viscoelastic properties of a small volume of soft biomaterials at high frequencies. A thin layer of the sample material, only a few millimetres thick, was required, in contrast with several centimetres for the previous method. This reduces the required sample volume, and consequently the cost of experiments, by a factor of 25 (96% saving). This method has the potential to be used for the characterization of injectable biomaterials used for vocal fold augmentation and repair such as commercial phonosurgical biomaterials (Cymetra, Radiesse, Juvederm, and Restylane) and hydrogels designed in our group (Heris *et al.*, 2012). Layered silicone rubber and gelatin samples consisting of a substrate with known properties under a thin layer of a soft material with unknown properties were fabricated and tested. Measurements were performed at frequencies up to 4 kHz. The results were found to be in good agreement with and improved upon those of Nenadic *et al*. (2011a).

A novel non-invasive method was developed for the *in vivo* measurements of the shear modulus of human vocal fold tissue during phonation. Four subjects underwent high speed digital and magnetic resonance imaging tests at different pitches, for fundamental frequencies in the range from 110 to 440 Hz. The images obtained from MRI were used to determine pixel size in those from HSDI. Using the high-speed images and an automatic image processing algorithm, the mucosal wave propagation speed was determined for different human subjects at different phonation pitches. The shear modulus of the subjects' vocal fold mucosa was then obtained using a surface (Rayleigh) wave propagation model and the measured wave speeds. A Voigt viscoelastic model was also used to calculate the complex shear modulus of the tissue including the shear elasticity and viscosity from the obtained shear wave speeds. The results, including the vocal fold edge displacement, mucosal wave speed and the mucosa shear modulus, were compared to those of previous studies from *in vitro* and *in vivo* measurements and found to be in good agreement. The obtained shear modulus increased with pitch. This was speculated to be because of the inherent viscoelastic properties of the tissue and the increased longitudinal tension applied to vocal folds at higher pitches. The magnitude of the obtained shear modulus and the rate of increase with pitch were considerably different for different subjects. This emphasizes the need for *in vivo* clinical assessments of any specific patients' vocal folds for diagnostic purposes or the evaluation of vocal fold treatment procedures.

Different cross-linked HA-Ge hydrogels with tuned mechanical and biological properties were fabricated for use as synthetic ECM biomaterials in vocal fold tissue engineering. The viscoelastic properties of the synthesized hydrogels were measured over a broad frequency range using the Rayleigh wave propagation method, and compared with those of human vocal fold tissue obtained from *in vivo* and *in vitro* measurements. The results revealed that HA-Ge hydrogels with appropriate concentrations of HA, Ge, and the cross-linker provide viscoelastic properties similar to those of human vocal fold tissue. More specifically, the values obtained for the shear and viscous moduli of the fabricated hydrogels were in the same range of those of human vocal fold tissue, and also their frequency-dependency, i.e., the increase of the moduli with frequency, approximately resembled that of the tissue. Furthermore, the Ge content of these hydrogels adjusts their biochemical properties. Therefore, HA-Ge hydrogels are strong potential candidates for use as injectable biomaterials in vocal fold tissue treatment. The physician can choose one of the synthesized hydrogels presented in this study or fabricate a specific HA-based biomaterial with desirable biomechanical and biological properties required for the treatment of any specific patient's vocal fold tissue. This completes the integrated methodology to design an optimum injectable hydrogel for the treatment of any specific patient's vocal fold tissue.

5.2. Future works

5.2.1. Wave propagation methods

Wave propagation methods have recently been introduced to characterize the mechanical properties of biomaterials and tissue. All of the methods developed so far assume that the propagation medium is homogeneous, isotropic, and linear. While this assumption may be acceptable for most of biomaterials such as the hydrogels fabricated and tested in this study, more sophisticated investigations are needed to model inhomogeneous and anisotropic soft tissues and take the nonlinearities into account.

Another aspect of these methods that needs profound attention and improvement is the characterization of biological media with complex geometries and boundaries. Most of the characterization methods developed based on wave propagation approaches are only capable to measure the mechanical properties of samples with simple geometry. For example, changes in the thickness of the tissue or biomaterial sample and the wave reflection from the sample boundaries are ignored in the modelling. Furthermore, most of these methods are based on the assumption of the propagation of only a single type of wave in the medium under study.

5.2.2. Inverse problem solution

In direct wave propagation problems, where the mechanical properties of the media are known and the displacement field is unknown, applying a new constraint such as one extra layer might not cause a substantial problem in the solution procedure. However, we are dealing with an inverse problem solution in characterization methods, where the displacement field is known and the mechanical properties of the medium are unknown. In our developed methods, the shear wavenumber and consequently the viscoelastic properties of the medium are obtained from a dispersion equation using the measured Rayleigh wavenumber. The dispersion equation for Rayleigh wave propagation in a uniform (non-layered) medium is a closed form equation. In contrast, it consists of two huge coupled nonlinear equations (the real and imaginary parts of the dispersion equation) for a layered media. As seen in the Appendix A, the dispersion equation is about 4 pages long, and thus the derivation of this equation was not possible manually. The Mathematica software was used to derive the dispersion equation. One can conclude that the realistic analytical modelling and inverse problem solution for biological tissues with complex nature and geometry is very difficult.

One way to tackle this problem is to implement finite element methods (FEM) to model and solve the inverse problem to develop characterization methods based on wave propagation approaches capable of the quantification of the mechanical properties of biomaterials and tissue with complex geometry and composition. In such integrated methodology, the external excitation and measured displacement or velocity filed on the sample surface is used as the boundary condition of the inverse problem. Then, an optimization problem is solved using the developed FEM model to estimate the mechanical properties of the medium.

5.2.3. Clinical studies

The results presented in this study for the shear modulus of human vocal fold tissue were obtained from only four subjects to present the developed *in vivo* measurement methodology and evaluate it. Further clinical studies involving a large number of subjects may be performed to investigate the changes in the mechanical properties of human vocal fold tissue due to different important parameters such as aging, gender, smoking, dehydration, and pathology.

Appendix A

The coefficient matrix of the system of equations developed in Eq. (2.21) is as follows:

$$\mathbf{C}=\begin{bmatrix} \left(2\hat{k}_R^2-\hat{k}_{s1}^2\right) & \left(2\hat{k}_R^2-\hat{k}_{s1}^2\right) & -2\hat{k}_R k_2 & 2\hat{k}_R k_2 & 0 & 0 \\ 2\hat{k}_R k_1 & -2\hat{k}_R k_1 & \left(2\hat{k}_R^2-\hat{k}_{s1}^2\right) & \left(2\hat{k}_R^2-\hat{k}_{s1}^2\right) & 0 & 0 \\ \left(2\hat{k}_R^2-\hat{k}_{s1}^2\right)\hat{\mu}_1 c_1^{-1} & \left(2\hat{k}_R^2-\hat{k}_{s1}^2\right)\hat{\mu}_1 c_1 & -2\hat{k}_R k_2 c_2^{-1} & 2\hat{k}_R k_2 c_2 & -\left(2\hat{k}_R^2-\hat{k}_{s2}^2\right)\hat{\mu}_2 c_3^{-1} & -2i\hat{k}_R k_4 \hat{\mu}_2 c_4 \\ 2\hat{k}_R k_1 \hat{\mu}_1 c_1^{-1} & -2\hat{k}_R k_1 \hat{\mu}_1 c_1 & \left(2\hat{k}_R^2-\hat{k}_{s1}^2\right)\hat{\mu}_1 c_2^{-1} & \left(2\hat{k}_R^2-\hat{k}_{s1}^2\right)\hat{\mu}_1 c_2 & 2i\hat{k}_R k_3 \hat{\mu}_2 c_3 & -\left(2\hat{k}_R^2-\hat{k}_{s2}^2\right)\hat{\mu}_2 c_4^{-1} \\ i\hat{k}_R c_1^{-1} & i\hat{k}_R c_1 & -ik_2 c_2^{-1} & ik_2 c_2 & -i\hat{k}_R c_3 & k_4 c_4 \\ -ik_1 c_1^{-1} & ik_1 c_1 & -i\hat{k}_R c_2^{-1} & -i\hat{k}_R c_2 & k_3 c_3 & i\hat{k}_R c_4 \end{bmatrix}, \tag{A.1}$$

where

$$c_1=e^{ik_1h},\ c_2=e^{ik_2h},\ c_3=e^{ik_3h},\ c_4=e^{ik_4h}. \tag{A.2}$$

The dispersion equation is given as follows:

$$\frac{c_3c_4}{(\alpha-i\beta)c_1c_2}\left\{-8\left[\frac{\rho\omega^2k_2}{\sqrt{\dfrac{\rho\omega^2}{\alpha-i\beta}}}\left(-2\left(\sqrt{\frac{\rho\omega^2}{\alpha-i\beta}}+1\right)\left(\alpha^2-2i\beta\alpha-\beta^2+2(\gamma+i\lambda)^2\right)(\gamma+i\lambda)^2-2k_3k_4\right.\right.\right.$$

$$\left(\frac{4(\gamma+i\lambda)^2\hat{\mu}_2^2}{\sqrt{\dfrac{\rho\omega^2}{\alpha-i\beta}}}+\left(-\alpha^2+2i\beta\alpha+\beta^2-4(\gamma+i\lambda)^2\right)\hat{\mu}_2+\left(\sqrt{\frac{\rho\omega^2}{\alpha-i\beta}}+1\right)\left(\alpha^2-2i\beta\alpha-\beta^2+2(\gamma+i\lambda)^2\right)\right)+$$

$$\left.\left(\alpha^2-2i\beta\alpha-\beta^2+4(\gamma+i\lambda)^2\right)\left(2(\gamma+i\lambda)^2+\hat{k}_{s2}^2\right)\mu_2-\frac{2\left(2(\gamma+i\lambda)^2+\hat{k}_{s2}^2\right)^2}{\sqrt{\frac{\rho\omega^2}{\alpha-i\beta}}}\hat{\mu}_2^2\right)-$$

$$2i(\alpha-i\beta)k_2^2k_3\hat{k}_{s2}^2\hat{\mu}_2+(i\alpha+\beta)\sqrt{\frac{\rho\omega^2}{\alpha-i\beta}}\left(\alpha^2-2i\beta\alpha-\beta^2+2(\gamma+i\lambda)^2\right)k_4\hat{k}_{s2}^2\hat{\mu}_2\Bigg]$$

$$\left(\alpha^2-2i\beta\alpha-\beta^2+2(\gamma+i\lambda)^2\right)c_1c_2k_1(\gamma+i\lambda)^2-c_2^2\left(4k_1k_2(\gamma+i\lambda)^2+\left(\alpha^2-2i\beta\alpha-\beta^2+2(\gamma+i\lambda)^2\right)^2\right)$$

$$\Big[4\rho\omega^2\gamma^6-4\alpha\hat{\mu}_2^2\gamma^6+4i\beta\hat{\mu}_2^2\gamma^6+24i\lambda\rho\omega^2\gamma^5-24i\alpha\lambda\hat{\mu}_2^2\gamma^5-24\beta\lambda\hat{\mu}_2^2\gamma^5+4\alpha\rho\omega^2\gamma^4-4\beta^2\rho\omega^2\gamma^4-$$
$$60\lambda^2\rho\omega^2\gamma^4-8i\alpha\beta\rho\omega^2\gamma^4+60\alpha\lambda^2\hat{\mu}_2^2\gamma^4-4\alpha k_{s2}^2\hat{\mu}_2^2\gamma^4+4i\beta k_{s2}^2\hat{\mu}_2^2\gamma^4-4\alpha k_3k_4\hat{\mu}_2^2\gamma^4+$$
$$4i\beta k_3k_4\hat{\mu}_2^2\gamma^4+4\rho\omega^2k_3k_4\gamma^4-80i\lambda^3\rho\omega^2\gamma^3+16i\alpha^2\lambda\rho\omega^2\gamma^3-16i\beta^2\lambda\rho\omega^2\gamma^3+32\alpha\beta\lambda\rho\omega^2\gamma^3+$$
$$80i\alpha\lambda^3\hat{\mu}_2^2\gamma^3+80\beta\lambda^3\hat{\mu}_2^2\gamma^3-16i\alpha\lambda\hat{k}_{s2}^2\hat{\mu}_2^2\gamma^3-16\beta\lambda\hat{k}_{s2}^2\mu_2^2\gamma^3-16i\alpha\lambda k_3k_4\hat{\mu}_2^2\gamma^3-16\beta\lambda k_3k_4\hat{\mu}_2^2\gamma^3+$$
$$16i\lambda\rho\omega^2k_3k_4\gamma^3+\alpha^4\rho\omega^2\gamma^2+\beta^4\rho\omega^2\gamma^2+60\lambda^4\rho\omega^2\gamma^2+4i\alpha\beta^3\rho\omega^2\gamma^2-6\alpha^2\beta^2\rho\omega^2\gamma^2-$$
$$24\alpha^2\lambda^2\rho\omega^2\gamma^2+24\beta^2\lambda^2\rho\omega^2\gamma^2+48i\alpha\beta\lambda^2\rho\omega^2\gamma^2-4i\alpha^3\beta\rho\omega^2\gamma^2-60\alpha\lambda^4\hat{\mu}_2^2\gamma^2+60i\beta\lambda^4\hat{\mu}_2^2\gamma^2-$$
$$\alpha\hat{k}_{s2}^4\mu_2^2\gamma^2+i\beta\hat{k}_{s2}^4\hat{\mu}_2^2\gamma^2+24\alpha\lambda^2\hat{k}_{s2}^2\hat{\mu}_2^2\gamma^2-24i\beta\lambda^2\hat{k}_{s2}^2\hat{\mu}_2^2\gamma^2+24\alpha\lambda^2k_3k_4\hat{\mu}_2^2\gamma^2-24i\beta\lambda^2k_3k_4\hat{\mu}_2^2\gamma^2+$$
$$4\alpha^2\rho\omega^2k_3k_4\gamma^2-4\beta^2\rho\omega^2k_3k_4\gamma^2-24\lambda^2\rho\omega^2k_3k_4\gamma^2-8i\alpha\beta\rho\omega^2k_3k_4\gamma^2-2i\alpha k_2k_3k_{s2}^2\hat{\mu}_2\gamma^2-$$
$$2\beta k_2k_3\hat{k}_{s2}^2\hat{\mu}_2\gamma^2+2i\alpha\sqrt{\frac{\rho\omega^2}{\alpha-i\beta}}k_2k_3\hat{k}_{s2}^2\hat{\mu}_2\gamma^2+2\beta\sqrt{\frac{\rho\omega^2}{\alpha-i\beta}}k_2k_3\hat{k}_{s2}^2\hat{\mu}_2\gamma^2+24i\lambda^5\rho\omega^2\gamma-$$
$$16i\alpha^2\lambda^3\rho\omega^2\gamma+16i\beta^2\lambda^3\rho\omega^2\gamma-32\alpha\beta\lambda^3\rho\omega^2\gamma+2i\alpha^4\lambda\rho\omega^2\gamma+2i\beta^4\lambda\rho\omega^2\gamma-8\alpha\beta^3\lambda\rho\omega^2\gamma-$$
$$12i\alpha^2\beta^2\lambda\rho\omega^2\gamma+8\alpha^3\beta\lambda\rho\omega^2\gamma-24i\alpha\lambda^5\hat{\mu}_2^2\gamma-24\beta\lambda^5\hat{\mu}_2^2\gamma-2i\alpha\lambda\hat{k}_{s2}^4\hat{\mu}_2^2\gamma-2\beta\lambda\hat{k}_{s2}^4\hat{\mu}_2^2\gamma+$$
$$16i\alpha\lambda^3\hat{k}_{s2}^2\hat{\mu}_2^2\gamma+16\beta\lambda^3\hat{k}_{s2}^2\hat{\mu}_2^2\gamma+16i\alpha\lambda^3k_3k_4\hat{\mu}_2^2\gamma+16\beta\lambda^3k_3k_4\hat{\mu}_2^2\gamma-16i\lambda^3\rho\omega^2k_3k_4\gamma+$$
$$8i\alpha^2\lambda\rho\omega^2k_3k_4\gamma-8i\beta^2\lambda\rho\omega^2k_3k_4\gamma+16\alpha\beta\lambda\rho\omega^2k_3k_4\gamma+4\alpha\lambda k_2k_3\hat{k}_{s2}^2\hat{\mu}_2\gamma-4i\beta\lambda k_2k_3\hat{k}_{s2}^2\hat{\mu}_2\gamma+$$
$$4i\beta\sqrt{\frac{\rho\omega^2}{\alpha-i\beta}}\lambda k_2k_3\hat{k}_{s2}^2\hat{\mu}_2\gamma-4\alpha\sqrt{\frac{\rho\omega^2}{\alpha-i\beta}}\lambda k_2k_3\hat{k}_{s2}^2\hat{\mu}_2\gamma-4\lambda^6\rho\omega^2+4\alpha^2\lambda^4\rho\omega^2-4\beta^2\lambda^4\rho\omega^2-$$
$$8i\alpha\beta\lambda^4\rho\omega^2-\alpha^4\lambda^2\rho\omega^2-\beta^4\lambda^2\rho\omega^2-4i\alpha\beta^3\lambda^2\rho\omega^2+6\alpha^2\beta^2\lambda^2\rho\omega^2+4i\alpha^3\beta\lambda^2\rho\omega^2+4\alpha\lambda^6\hat{\mu}_2^2-$$
$$4i\beta\lambda^6\hat{\mu}_2^2+\alpha\lambda^2\hat{k}_{s2}^4\hat{\mu}_2^2-i\beta\lambda^2\hat{k}_{s2}^4\hat{\mu}_2^2-4\alpha\lambda^4\hat{k}_{s2}^2\hat{\mu}_2^2+4i\beta\lambda^4\hat{k}_{s2}^2\hat{\mu}_2^2-4\alpha\lambda^4k_3k_4\hat{\mu}_2^2+4i\beta\lambda^4k_3k_4\hat{\mu}_2^2+$$
$$\alpha^4\rho\omega^2k_3k_4+\beta^4\rho\omega^2k_3k_4+4\lambda^4\rho\omega^2k_3k_4+4i\alpha\beta^3\rho\omega^2k_3k_4-6\alpha^2\beta^2\rho\omega^2k_3k_4-4\alpha^2\lambda^2\rho\omega^2k_3k_4+$$
$$4\beta^2\lambda^2\rho\omega^2k_3k_4+8i\alpha\beta\lambda^2\rho\omega^2k_3k_4-4i\alpha^3\beta\rho\omega^2k_3k_4+2i\alpha\lambda^2k_2k_3\hat{k}_{s2}^2\hat{\mu}_2^2+2\beta\lambda^2k_2k_3\hat{k}_{s2}^2\hat{\mu}_2^2+$$
$$i\alpha^3\sqrt{\frac{\rho\omega^2}{\alpha-i\beta}}k_2k_3\hat{k}_{s2}^2\hat{\mu}_2-\beta^3\sqrt{\frac{\rho\omega^2}{\alpha-i\beta}}k_2k_3\hat{k}_{s2}^2\hat{\mu}_2-3i\alpha\beta^2\sqrt{\frac{\rho\omega^2}{\alpha-i\beta}}k_2k_3\hat{k}_{s2}^2\hat{\mu}_2-$$

$$2i\alpha\lambda^2\sqrt{\frac{\rho\omega^2}{\alpha-i\beta}}k_2k_3\hat{k}_{s2}^2\hat{\mu}_2-2\beta\lambda^2\sqrt{\frac{\rho\omega^2}{\alpha-i\beta}}k_2k_3\hat{k}_{s2}^2\hat{\mu}_2+3\alpha^2\beta\sqrt{\frac{\rho\omega^2}{\alpha-i\beta}}k_2k_3\hat{k}_{s2}^2\hat{\mu}_2+$$

$$(\alpha-i\beta)k_1\left(k_2\left(-4k_3k_4\left(\sqrt{\frac{\rho\omega^2}{\alpha-i\beta}}-\hat{\mu}_2\right)(\mu_2-1)(\gamma+i\lambda)^2-\left(2(\gamma+i\lambda)^2\sqrt{\frac{\rho\omega^2}{\alpha-i\beta}}-\left(2(\gamma+i\lambda)^2+\hat{k}_{s2}^2\right)\hat{\mu}_2\right)\right.\right.$$

$$\left.\left.\left(\left(2(\gamma+i\lambda)^2+\hat{k}_{s2}^2\right)\hat{\mu}_2-2(\gamma+i\lambda)^2\right)\right)-i\left(\alpha^2-2i\beta\alpha-\beta^2+4(\gamma+i\lambda)^2\right)\sqrt{\frac{\rho\omega^2}{\alpha-i\beta}}k_4\hat{k}_{s2}^2\hat{\mu}_2\right)\Bigg]+$$

$$\left(\left(\alpha^2-2i\beta\alpha-\beta^2+2(\gamma+i\lambda)^2\right)^2-4(\gamma+i\lambda)^2k_1k_2\right)\Bigg[\Bigg(\left(\left(\alpha^2-2i\beta\alpha-\beta^2+2(\gamma+i\lambda)^2\right)^2\rho\omega^2-\right.$$

$$\left.\frac{2\left(\alpha^2-2i\beta\alpha-\beta^2+2(\gamma+i\lambda)^2\right)\rho\left(2(\gamma+i\lambda)^2+\hat{k}_{s2}^2\right)\hat{\mu}_2\omega^2}{\sqrt{\frac{\rho\omega^2}{\alpha-i\beta}}}+(\alpha-i\beta)\left(2(\gamma+i\lambda)^2+\hat{k}_{s2}^2\right)^2\hat{\mu}_2^2\right)$$

$$(\gamma+i\lambda)^2+k_3\left((\beta+i\alpha)\left(\sqrt{\frac{\rho\omega^2}{\alpha-i\beta}}(\alpha-i\beta)^2+2\left(\sqrt{\frac{\rho\omega^2}{\alpha-i\beta}}+1\right)\gamma^2-2\lambda^2\left(\sqrt{\frac{\rho\omega^2}{\alpha-i\beta}}+1\right)+\right.\right.$$

$$\left.\left.4i\left(\sqrt{\frac{\rho\omega^2}{\alpha-i\beta}}+1\right)\gamma\lambda\right)k_2\hat{\mu}_2\hat{k}_{s2}^2+k_4\left(\left(\alpha^2-2i\beta\alpha-\beta^2+2(\gamma+i\lambda)^2\right)^2\rho\omega^2-\right.$$

$$\left.\frac{4\left(\alpha^2-2i\beta\alpha-\beta^2+2(\gamma+i\lambda)^2\right)\rho\omega^2\hat{\mu}_2(\gamma+i\lambda)^2}{\sqrt{\frac{\rho\omega^2}{\alpha-i\beta}}}+4(\alpha-i\beta)\hat{\mu}_2^2(\gamma+i\lambda)^4\right)\Bigg)+$$

$$(\alpha-i\beta)k_1\left(k_2\left(-4k_3k_4\left(\sqrt{\frac{\rho\omega^2}{\alpha-i\beta}}-\hat{\mu}_2\right)(\hat{\mu}_2+1)(\gamma+i\lambda)^2-\left(2(\gamma+i\lambda)^2\sqrt{\frac{\rho\omega^2}{\alpha-i\beta}}-\left(2(\gamma+i\lambda)^2+\hat{k}_{s2}^2\right)\hat{\mu}_2\right)\right.\right.$$

$$\left.\left.\left(2(\gamma+i\lambda)^2+\left(2(\gamma+i\lambda)^2+\hat{k}_{s2}^2\right)\hat{\mu}_2\right)\right)-i(\alpha-i\beta)^3\sqrt{\frac{\rho\omega^2}{\alpha-i\beta}}k_3\hat{k}_{s2}^2\hat{\mu}_2\right)\Bigg]+$$

$$c_1^2\Bigg[c_2^2\left(\left(\alpha^2-2i\beta\alpha-\beta^2+2(\gamma+i\lambda)^2\right)^2-4(\gamma+i\lambda)^2k_1k_2\right)\left(4\rho\omega^2\gamma^6-4\alpha\hat{\mu}_2^2\gamma^6+4i\beta\hat{\mu}_2^2\gamma^6+24i\lambda\rho\omega^2\gamma^5-\right.$$

$$24i\alpha\lambda\hat{\mu}_2^2\gamma^5-24\beta\lambda\hat{\mu}_2^2\gamma^5+4\alpha^2\rho\omega^2\gamma^4-4\beta^2\rho\omega^2\gamma^4-60\lambda^2\rho\omega^2\gamma^4-8i\alpha\beta\rho\omega^2\gamma^4+60\alpha\lambda^2\hat{\mu}_2^2\gamma^4-$$

$$60i\beta\lambda\hat{\mu}_2^2\gamma^4-4\alpha\hat{k}_{s2}^2\hat{\mu}_2^2\gamma^4+4i\beta\hat{k}_{s2}^2\hat{\mu}_2^2\gamma^4-4\alpha k_3k_4\hat{\mu}_2^2\gamma^4+4i\beta k_3k_4\hat{\mu}_2^2\gamma^4+4\rho\omega^2k_3k_4\gamma^4-$$

$$80i\lambda^3\rho\omega^2\gamma^3+16i\alpha^2\lambda\rho\omega^2\gamma^3-16i\beta^2\lambda\rho\omega^2\gamma^3+32\alpha\beta\lambda\rho\omega^2\gamma^3+80i\alpha\lambda^3\hat{\mu}_2^2\gamma^3+80\beta\lambda^3\hat{\mu}_2^2\gamma^3-$$

$$16i\alpha\lambda\hat{k}_{s2}^{2}\hat{\mu}_2^2\gamma^3-16\beta\lambda\hat{k}_{s2}^{2}\hat{\mu}_2^2\gamma^3-16i\alpha\lambda k_3k_4\hat{\mu}_2^2\gamma^3-16\beta\lambda k_3k_4\hat{\mu}_2^2\gamma^3+16i\lambda\rho\omega^2k_3k_4\gamma^3+$$

$$\alpha^4\rho\omega^2\gamma^2+\beta^4\rho\omega^2\gamma^2+60\lambda^4\rho\omega^2\gamma^2+4i\alpha\beta^3\rho\omega^2\gamma^2-6\alpha^2\beta^2\rho\omega^2\gamma^2-24\alpha^2\lambda^2\rho\omega^2\gamma^2+$$

$$24\beta^2\lambda^2\rho\omega^2\gamma^2+48i\alpha\beta\lambda^2\rho\omega^2\gamma^2-4i\alpha^3\beta\rho\omega^2\gamma^2-60\alpha\lambda^4\hat{\mu}_2^2\gamma^2+60i\beta\lambda^4\hat{\mu}_2^2\gamma^2-\alpha\hat{k}_{s2}^{4}\hat{\mu}_2^2\gamma^2+$$

$$i\beta\hat{k}_{s2}^{4}\hat{\mu}_2^2\gamma^2+24\alpha\lambda^2\hat{k}_{s2}^{2}\hat{\mu}_2^2\gamma^2-24i\beta\lambda^2\hat{k}_{s2}^{2}\hat{\mu}_2^2\gamma^2+24\alpha\lambda^2k_3k_4\hat{\mu}_2^2\gamma^2-24i\beta\lambda^2k_3k_4\hat{\mu}_2^2\gamma^2+$$

$$4\alpha^2\rho\omega^2k_3k_4\gamma^2-4\beta^2\rho\omega^2k_3k_4\gamma^2-24\lambda^2\rho\omega^2k_3k_4\gamma^2-8i\alpha\beta\rho\omega^2k_3k_4\gamma^2-2i\alpha k_2k_3\hat{k}_{s2}^{2}\hat{\mu}_2\gamma^2-$$

$$2\beta k_2k_3\hat{k}_{s2}^{2}\hat{\mu}_2\gamma^2+2i\alpha\sqrt{\frac{\rho\omega^2}{\alpha-i\beta}}k_2k_3\hat{k}_{s2}^{2}\hat{\mu}_2\gamma^2+2\beta\sqrt{\frac{\rho\omega^2}{\alpha-i\beta}}k_2k_3\hat{k}_{s2}^{2}\hat{\mu}_2\gamma^2+24i\lambda^5\rho\omega^2\gamma-$$

$$16i\alpha^2\lambda^3\rho\omega^2\gamma+16\beta^2\lambda^3\rho\omega^2\gamma-32\alpha\beta\lambda^3\rho\omega^2\gamma+2i\alpha^4\lambda\rho\omega^2\gamma+2i\beta^4\lambda\rho\omega^2\gamma-8\alpha\beta^3\lambda\rho\omega^2\gamma-$$

$$12i\alpha^2\beta^2\lambda\rho\omega^2\gamma+8\alpha^3\beta\lambda\rho\omega^2\gamma-24i\alpha\lambda^5\hat{\mu}_2^2\gamma-24\beta\lambda^5\hat{\mu}_2^2\gamma-2i\alpha\lambda\hat{k}_{s2}^{4}\hat{\mu}_2^2\gamma-2\beta\lambda\hat{k}_{s2}^{4}\hat{\mu}_2^2\gamma+$$

$$16i\alpha\lambda^3\hat{k}_{s2}^{2}\hat{\mu}_2^2\gamma+16\beta\lambda^3\hat{k}_{s2}^{2}\hat{\mu}_2^2\gamma+16i\alpha\lambda^3k_3k_4\hat{\mu}_2^2\gamma+16\beta\lambda^3k_3k_4\hat{\mu}_2^2\gamma-16i\lambda^3\rho\omega^2k_3k_4\gamma+$$

$$8i\alpha^2\lambda\rho\omega^2k_3k_4\gamma-8i\beta^2\lambda\rho\omega^2k_3k_4\gamma+16\alpha\beta\lambda\rho\omega^2k_3k_4\gamma+4\alpha\lambda k_2k_3\hat{k}_{s2}^{2}\hat{\mu}_2\gamma-4i\beta\lambda k_2k_3\hat{k}_{s2}^{2}\hat{\mu}_2\gamma+$$

$$4i\beta\sqrt{\frac{\rho\omega^2}{\alpha-i\beta}}\lambda k_2k_3\hat{k}_{s2}^{2}\hat{\mu}_2\gamma-4\alpha\sqrt{\frac{\rho\omega^2}{\alpha-i\beta}}\lambda k_2k_3\hat{k}_{s2}^{2}\hat{\mu}_2\gamma-4\lambda^6\rho\omega^2+4\alpha^2\lambda^4\rho\omega^2-4\beta^2\lambda^4\rho\omega^2-$$

$$8i\alpha\beta\lambda^4\rho\omega^2-\alpha^4\lambda^2\rho\omega^2-\beta^4\lambda^2\rho\omega^2-4i\alpha\beta^3\lambda^2\rho\omega^2+6\alpha^2\beta^2\lambda^2\rho\omega^2+4i\alpha^3\beta\lambda^2\rho\omega^2+4\alpha\lambda^6\hat{\mu}_2^2-$$

$$4i\beta\lambda^6\hat{\mu}_2^2+\alpha\lambda^2\hat{k}_{s2}^{4}\hat{\mu}_2^2-i\beta\lambda^2\hat{k}_{s2}^{4}\hat{\mu}_2^2-4\alpha\lambda^4\hat{k}_{s2}^{2}\hat{\mu}_2^2+4i\beta\lambda^4\hat{k}_{s2}^{2}\hat{\mu}_2^2-4\alpha\lambda^4k_3k_4\hat{\mu}_2^2+4i\beta\lambda^4k_3k_4\hat{\mu}_2^2+$$

$$\alpha^4\rho\omega^2k_3k_4+\beta^4\rho\omega^2k_3k_4+4\lambda^4\rho\omega^2k_3k_4+4i\alpha\beta^3\rho\omega^2k_3k_4-6\alpha^2\beta^2\rho\omega^2k_3k_4-4\alpha^2\lambda^2\rho\omega^2k_3k_4+$$

$$4\beta^2\lambda^2\rho\omega^2k_3k_4+8i\alpha\beta\lambda^2\rho\omega^2k_3k_4-4i\alpha^3\beta\rho\omega^2k_3k_4+2i\alpha\lambda^2k_2k_3\hat{k}_{s2}^{2}\hat{\mu}_2+2\beta\lambda^2k_2k_3\hat{k}_{s2}^{2}\hat{\mu}_2+$$

$$i\alpha^3\sqrt{\frac{\rho\omega^2}{\alpha-i\beta}}k_2k_3\hat{k}_{s2}^{2}\hat{\mu}_2-\beta^3\sqrt{\frac{\rho\omega^2}{\alpha-i\beta}}k_2k_3\hat{k}_{s2}^{2}\hat{\mu}_2-3i\alpha\beta^2\sqrt{\frac{\rho\omega^2}{\alpha-i\beta}}k_2k_3\hat{k}_{s2}^{2}\hat{\mu}_2-$$

$$2i\alpha\lambda^2\sqrt{\frac{\rho\omega^2}{\alpha-i\beta}}k_2k_3\hat{k}_{s2}^{2}\hat{\mu}_2-2\beta\lambda^2\sqrt{\frac{\rho\omega^2}{\alpha-i\beta}}k_2k_3\hat{k}_{s2}^{2}\hat{\mu}_2+3\alpha^2\beta\sqrt{\frac{\rho\omega^2}{\alpha-i\beta}}k_2k_3\hat{k}_{s2}^{2}\hat{\mu}_2+(\alpha-i\beta)k_1$$

$$\Bigg(i\sqrt{\frac{\rho\omega^2}{\alpha-i\beta}}\left(\alpha^2-2i\beta\alpha-\beta^2+4(\gamma+i\lambda)^2\right)k_4\hat{k}_{s2}^{2}\hat{\mu}_2+k_2\Bigg(4k_3k_4\left(\sqrt{\frac{\rho\omega^2}{\alpha-i\beta}}-\hat{\mu}_2\right)(\hat{\mu}_2-1)(\gamma+i\lambda)^2+$$

$$\left(\left(2(\gamma+i\lambda)^2+\hat{k}_{s2}^{2}\right)\hat{\mu}_2-2(\gamma+i\lambda)^2\right)\left(2(\gamma+i\lambda)^2\sqrt{\frac{\rho\omega^2}{\alpha-i\beta}}-\left(2(\gamma+i\lambda)^2+\hat{k}_{s2}^{2}\right)\hat{\mu}_2\right)\Bigg)\Bigg)-$$

$$\left(4k_1k_2(\gamma+i\lambda)^2+\left(\alpha^2-2i\beta\alpha-\beta^2+2(\gamma+i\lambda)^2\right)^2\right)\Bigg(\Bigg(\Big(\left(\alpha^2-2i\beta\alpha-\beta^2+2(\gamma+i\lambda)^2\right)^2\rho\omega^2-$$

$$\frac{2\left(\alpha^2-2i\beta\alpha-\beta^2+2(\gamma+i\lambda)^2\right)\rho\left(2(\gamma+i\lambda)^2+\hat{k}_{s2}^2\right)\hat{\mu}_2\omega^2}{\sqrt{\frac{\rho\omega^2}{\alpha-i\beta}}}+(\alpha-i\beta)\left(2(\gamma+i\lambda)^2+\hat{k}_{s2}^2\right)^2\hat{\mu}_2^2\Big)$$

$$(\gamma+i\lambda)^2+k_3\left((\beta+i\alpha)\left(\sqrt{\frac{\rho\omega^2}{\alpha-i\beta}}(\alpha-i\beta)^2+2\left(\sqrt{\frac{\rho\omega^2}{\alpha-i\beta}}+1\right)\gamma^2-2\lambda^2\left(\sqrt{\frac{\rho\omega^2}{\alpha-i\beta}}+1\right)+\right.\right.$$

$$\left.4i\left(\sqrt{\frac{\rho\omega^2}{\alpha-i\beta}}+1\right)\gamma\lambda\right)k_2\hat{\mu}_2\hat{k}_{s2}^2+k_4\left(4(\alpha-i\beta)\hat{\mu}_2^2(\gamma+i\lambda)^4-\right.$$

$$\frac{4\left(\alpha^2-2i\beta\alpha-\beta^2+2(\gamma+i\lambda)^2\right)\rho\omega^2\hat{\mu}_2(\gamma+i\lambda)^2}{\sqrt{\frac{\rho\omega^2}{\alpha-i\beta}}}+\left(\alpha^2-2i\beta\alpha-\beta^2+2(\gamma+i\lambda)^2\right)^2\rho\omega^2\Big)\Big)+$$

$$(\alpha-i\beta)k_1\left(i\sqrt{\frac{\rho\omega^2}{\alpha-i\beta}}(\alpha-i\beta)^2k_4\hat{\mu}_2\hat{k}_{s2}^2+k_2\left(4k_3k_4\left(\sqrt{\frac{\rho\omega^2}{\alpha-i\beta}}-\hat{\mu}_2\right)(\hat{\mu}_2+1)(\gamma+i\lambda)^2+\right.\right.$$

$$\left.\left.\left.\left.\left(2(\gamma+i\lambda)^2+\left(2(\gamma+i\lambda)^2+\hat{k}_{s2}^2\right)\hat{\mu}_2\right)\left(2(\gamma+i\lambda)^2\sqrt{\frac{\rho\omega^2}{\alpha-i\beta}}-\left(2(\gamma+i\lambda)^2+\hat{k}_{s2}^2\right)\hat{\mu}_2\right)\right)\right)\right]\right\}=0.$$

(A.3)

Appendix B
List of contributions

1- **S. Kazemirad**, H.K. Heris, L. Mongeau, Experimental methods for the characterization of the frequency-dependent viscoelastic properties of soft tissues and material, *Journal of the Acoustical Society of America*, 133 (2013), 3186-3197.

2- **S. Kazemirad**, L. Mongeau, Rayleigh wave propagation method for the characterization of a thin layer of biomaterials, *Journal of the Acoustical Society of America*, 133 (2013), 4332-4342.

3- **S. Kazemirad**, H. Bakhshaee, L. Mongeau, K. Kost, Non-invasive *in vivo* measurement of the shear modulus of human vocal fold tissue, *Journal of Biomechanics*, 2013.

4- **S. Kazemirad**, H.K. Heris, L. Mongeau, Viscoelasticity of hyaluronic acid-gelatin hydrogels for vocal fold tissue engineering, *Laryngoscope*, in review.

5- **S. Kazemirad**, H. Bakhshaei, L. Mongeau, K. Kost, Wave methods for the measurement of the shear modulus of soft tissue and biomaterials, 19th Congress of the European Society of Biomechanics (ESB2013), August 2013, Patras, Greece.

6- **S. Kazemirad**, H. Bakhshaei, L. Mongeau, K. Kost, Non-invasive in vivo measurement of the shear modulus of human vocal fold tissue, 165th Meeting of the Acoustical Society of America (ICA2013), June 2013, Montreal, Canada.

7- **S. Kazemirad**, L. Mongeau, Rayleigh wave propagation method for the characterization of viscoelastic properties of biomaterials, 164th Meeting of the Acoustical Society of America, October 2012, Kansas City, USA.

8- **S. Kazemirad**, H. K. Heris, L. Mongeau, Quantifying the frequency-dependent viscoelastic properties of soft biomaterials, 8th International Conference on Voice Physiology and Biomechanics (ICVPB2012), July 2012, Erlangen, Germany.

9- N. Bufi, **S. Kazemirad**, H. Khadivi. A.K. Miri, L. Mongeau, Experimental methods to identify dynamic mechanical properties of vocal fold tissue, 18th international Congress on Sound and Vibration (ICSV18), July 2011, Rio de Janeiro, Brazil.

References

Achenbach, J. D. (**1973**). *Wave Propagation in Elastic Solids* (North-Holland, Amsterdam).

Bakhshaee, H. (**2013**). "Computational models of human laryx and vocal folds," in *Department of Mechanical Engineering* (McGill University, Montreal, Quebec).

Becker, S., Kniesburges, S., Müller, S., Delgado, A., Link, G., Kaltenbacher, M., and Döllinger, M. (**2009**). "Flow-structure-acoustic interaction in a human voice model," Journal of the Acoustical Society of America **125**, 1351-1361.

Benton, J. A., Deforest, C. A., Vivekanandan, V., and Anseth, K. S. (**2009**). "Photocrosslinking of gelatin macromers to synthesize porous hydrogels that promote valvular interstitial cell function," Tissue Engineering - Part A **15**, 3221-3230.

Berke, G. S. (**1992**). "Intraoperative measurement of the elastic modulus of the vocal fold. Part 1. Device development," Laryngoscope **102**, 760-769.

Berke, G. S., and Smith, M. E. (**1992**). "Intraoperative measurement of the elastic modulus of the vocal fold. Part 2. Preliminary results," Laryngoscope **102**, 770-778.

Boessenecker, A., Berry, D. A., Lohscheller, J., Eysholdt, U., and Doellinger, M. (**2007**). "Mucosal wave properties of a human vocal fold," Acta Acustica united with Acustica **93**, 815-823.

Borcherdt, R. D. (**2009**). *Viscoelastic Waves in Layered Media* (Cambridge University Press, New York).

Bufi, N., Kazemirad, S., Heris, H. K., Miri, A. K., and Mongeau, L. (**2011**). "Experimental methods to identify dynamic mechanical properties of vocal fold tissue," in *18th international Congress on Sound and Vibration, ICSV18 2011* (Rio de Janeiro, Brazil), pp. 926-933.

Butler, J. E., Hammond, T. H., and Gray, S. D. (**2001**). "Gender-related differences of hyaluronic acid distribution in the human vocal fold," Laryngoscope **111**, 907-911.

Cagniard, L. (**1962**). *Reflection and Refraction of Progressive Seismic Waves* (McGraw-Hill, New York, pp. 1-282).

Catheline, S., Gennisson, J. L., Delon, G., Fink, M., Sinkus, R., Abouelkaram, S., and Culioli, J. (**2004**). "Measurement of viscoelastic properties of homogeneous soft solid using transient elastography: An inverse problem approach," Journal of the Acoustical Society of America **116**, 3734-3741.

Caton, T., Thibeault, S. L., Klemuk, S., and Smith, M. E. (**2007**). "Viscoelasticity of hyaluronan and nonhyaluronan based vocal fold injectables: Implications for mucosal versus muscle use," Laryngoscope **117**, 516-521.

Chan, A., Mongeau, L., and Kost, K. (**2013**). "Vocal fold vibration measurements using laser Doppler velocimetry," Journal of the Acoustical Society of America **133**, 1667-1676.

Chan, R. W. (**2004**). "Measurements of vocal fold tissue viscoelasticity: Approaching the male phonatory frequency range," Journal of the Acoustical Society of America **115**, 3161-3170.

Chan, R. W., Gray, S. D., and Titze, I. R. (**2001**). "The importance of hyaluronic acid in vocal fold biomechanics," Otolaryngology - Head and Neck Surgery **124**, 607-614.

Chan, R. W., and Rodriguez, M. L. (**2008**). "A simple-shear rheometer for linear viscoelastic characterization of vocal fold tissues at phonatory frequencies," Journal of the Acoustical Society of America **124**, 1207-1219.

Chan, R. W., and Titze, I. R. (**1998**). "Viscosities of implantable biomaterials in vocal fold augmentation surgery," Laryngoscope **108**, 725-731.

Chan, R. W., and Titze, I. R. (**1999a**). "Hyaluronic acid (with fibronectin) as a bioimplant for the vocal fold mucosa," Laryngoscope **109**, 1142-1149.

Chan, R. W., and Titze, I. R. (**1999b**). "Viscoelastic shear properties of human vocal fold mucosa: Measurement methodology and empirical results," Journal of the Acoustical Society of America **106**, 2008-2021.

Chen, S., Fatemi, M., and Greenleaf, J. F. (**2004**). "Quantifying elasticity and viscosity from measurement of shear wave speed dispersion," Journal of the Acoustical Society of America **115**, 2781-2785.

Chen, S., Urban, M. W., Pislaru, C., Kinnick, R., Zheng, Y., Yao, A., and Greenleaf, J. F. (**2009**). "Shearwave dispersion ultrasound vibrometry (SDUV) for measuring tissue elasticity and viscosity," IEEE transactions on ultrasonics, ferroelectrics, and frequency control **56**, 55-62.

Dailey, S. H., Tateya, I., Montequin, D., Welham, N. V., and Goodyer, E. (**2009**). "Viscoelastic Measurements of Vocal Folds Using the Linear Skin Rheometer," Journal of Voice **23**, 143-150.

Drechsel, J. S. (**2007**). "Characterization of synthetic, self-oscillating vocal fold models," in *Department of Mechanical Engineering* (Brigham Young University).

Duflo, S., Thibeault, S. L., Li, W., Shu, X. Z., and Prestwich, G. D. (**2006a**). "Vocal fold tissue repair in vivo using a synthetic extracellular matrix," Tissue Engineering **12**, 2171-2180.

Duflo, S., Thibeault, S. L., Li, W., Xiao, Z. S., and Prestwich, G. (**2006b**). "Effect of a synthetic extracellular matrix on vocal fold lamina propria gene expression in early wound healing," Tissue Engineering **12**, 3201-3207.

Ewing, W. M., Jardetzky, W. S., and Press, F. (**1957**). *Elastic Waves in Layered Media* (McGraw-Hill Book Company Inc., New York).

Ferry, J. D. (**1980**). *Viscoelastic properties of polymers* (John Wiley & Sons, New York).

George, N. A., de Mul, F. F., Qiu, Q., Rakhorst, G., and Schutte, H. K. (**2008**). "Depth-kymography: high-speed calibrated 3D imaging of human vocal fold vibration dynamics," Physics in Medicine and Biology **53**, 2667-2675.

Ghosh, K., Shu, X. Z., Mou, R., Lombardi, J., Prestwich, G. D., Rafailovich, M. H., and Clark, R. A. F. (**2005**). "Rheological characterization of in situ cross-linkable hysluronan hydrogels," Biomacromolecules **6**, 2857-2865.

Goodyer, E., Hemmerich, S., Müller, F., Kobler, J. B., and Hess, M. (**2007a**). "The shear modulus of the human vocal fold, preliminary results from 20 larynxes," European Archives of Oto-Rhino-Laryngology **264**, 45-50.

Goodyer, E., Muller, F., Bramer, B., Chauhan, D., and Hess, M. (**2006**). "In vivo measurement of the elastic properties of the human vocal fold," European Archives of Oto-Rhino-Laryngology **263**, 455-462.

Goodyer, E., Müller, F., Licht, K., and Hess, M. (**2007b**). "In vivo measurement of the shear modulus of the human vocal fold: Interim results from eight patients," European Archives of Oto-Rhino-Laryngology **264**, 631-635.

Goodyer, E., Welham, N. V., Choi, S. H., Yamashita, M., and Dailey, S. H. (**2009**). "The Shear Modulus of the Human Vocal Fold in a Transverse Direction," Journal of Voice **23**, 151-155.

Goodyer, E. N., Gunter, H., Masaki, A., and Kobler, J. (**2003**). "Mapping the visco-elastic properties of the vocal fold," in *AQL 2003* (Hamburg).

Graff, K. F. (**1975**). *Wave Motion in Elastic Solids* (Ohio State University Press, Columbus).

Greenleaf, J. F., Fatemi, M., and Insana, M. (**2003**). "Selected methods for imaging elastic properties of biological tissues," Annual Review of Biomedical Engineering **5**, 57-78.

Hahn, M. S., Teply, B. A., Stevens, M. M., Zeitels, S. M., and Langer, R. (**2006**). "Collagen composite hydrogels for vocal fold lamina propria restoration," Biomaterials **27**, 1104-1109.

Havriliak, S., and Negami, S. (**1966**). "A complex plane analysis of a-dispersions in some polymer systems, in transitions and relaxations in polymers," Journal of Polymer Science Part C **14**, 99–117.

Heris, H. K. (**2013**). "Investigation of a hyaluronic acid-gelatin crosslinked microgel-hydrogel extracellular matrix for superficial lamina propria restoration in scarred vocal folds " in *Department of Mechanical Engineering* (McGill University, Montreal, Quebec).

Heris, H. K., Rahmat, M., and Mongeau, L. (**2012**). "Characterization of a Hierarchical Network of Hyaluronic Acid/Gelatin Composite for use as a Smart Injectable Biomaterial," Macromolecular Bioscience **12**, 202-210.

Hertegård, S., Hallén, L., Laurent, C., Lindström, E., Olofsson, K., Testad, P., and Dahlqvist, Å. (**2002**). "Cross-linked hyaluronan used as augmentation substance for treatment of glottal insufficiency: Safety aspects and vocal fold function," Laryngoscope **112**, 2211-2219.

Hertegård, S., Hallén, L., Laurent, C., Lindström, E., Olofsson, K., Testad, P., and Dahlqvist, Å. (**2004**). "Cross-linked hyaluronan versus collagen for injection treatment of glottal insufficiency: 2-Year follow-up," Acta Oto-Laryngologica **124**, 1208-1214.

Hess, M. M., Mueller, F., Kobler, J. B., Zeitels, S. M., and Goodyer, E. (**2006**). "Measurements of vocal fold elasticity using the linear skin rheometer," Folia Phoniatrica et Logopaedica **58**, 207-216.

Jha, A. K., Hule, R. A., Jiao, T., Teller, S. S., Clifton, R. J., Duncan, R. L., Pochan, D. J., and Jia, X. (**2009**). "Structural analysis and mechanical characterization of hyaluronic acid-based doubly cross-linked networks," Macromolecules **42**, 537-546.

Kanai, H. (**2005**). "Propagation of spontaneously actuated pulsive vibration in human heart wall and in vivo viscoelasticity estimation," IEEE transactions on ultrasonics, ferroelectrics, and frequency control **52**, 1931-1942.

Kazemirad, S., Bakhshaee, H., Mongeau, L., and Kost, K. (**in review**). "Non-invasive in vivo measurement of the shear modulus of human vocal fold tissue," Journal of Biomechanics.

Kimura, M., Mau, T., and Chan, R. W. (**2010**). "Viscoelastic properties of phonosurgical biomaterials at phonatory frequencies," Laryngoscope **120**, 764-768.

Klemuk, S. A., and Titze, I. R. (**2004**). "Viscoelastic properties of three vocal-fold injectable biomaterials at low audio frequencies," Laryngoscope **114**, 1597-1603.

Kundu, T. (**2004**). *Ultrasonic Nondestructive Evaluation: Engineering and Biological Material Characterization* (CRC Press, Boca Raton).

Lakes, R. S. (**2009**). *Viscoelastic Materials* (Cambridge University Press, New York).

Lebl, M. D. A., Martins, J. R. M., Nader, H. B., Simões, M. D. J., and De Biase, N. (**2007**). "Concentration and distribution of hyaluronic acid in human vocal folds," Laryngoscope **117**, 595-599.

Link, G., Kaltenbacher, M., Breuer, M., and Döllinger, M. (**2009**). "A 2D finite-element scheme for fluid-solid-acoustic interactions and its application to human phonation," Computer Methods in Applied Mechanics and Engineering **198**, 3321-3334.

Madigosky, W. M., and Lee, G. F. (**1983**). "Improved resonance technique for materials characterization," Journal of the Acoustical Society of America **73**, 1374-1377.

Nenadic, I. Z., Urban, M. W., Aristizabal, S., Mitchell, S. A., Humphrey, T. C., and Greenleaf, J. F. (**2011a**). "On Lamb and Rayleigh wave convergence in viscoelastic tissues," Physics in Medicine and Biology **56**, 6723-6738.

Nenadic, I. Z., Urban, M. W., Mitchell, S. A., and Greenleaf, J. F. (**2011b**). "Lamb wave dispersion ultrasound vibrometry (LDUV) method for quantifying mechanical properties of viscoelastic solids," Physics in Medicine and Biology **56**, 2245-2264.

Pao, Y.-H., and Mow, C.-C. (**1973**). *Diffraction of Elastic Waves and Dynamic Stress Concentrations* (Crane, Russak & Company Inc., New York).

Park, J., Siegmund, T., and Mongeau, L. (**2003**). "Viscoelastic properties of foamed thermoplastic vulcanizates and their dependence on void fraction," Cellular Polymers **22**, 137-156.

Pritz, T. (**1982**). "Transfer function method for investigating the complex modulus of acoustic materials: Rod-like specimen," Journal of Sound and Vibration **81**, 359-376.

Rousseau, B., Hirano, S., Chan, R. W., Welham, N. V., Thibeault, S. L., Ford, C. N., and Bless, D. M. (**2004**). "Characterization of chronic vocal fold scarringin a rabbit model," Journal of Voice **18**, 116-124.

Royston, T. J., Mansy, H. A., and Sandler, R. H. (**1999**). "Excitation and propagation of surface waves on a viscoelastic half-space with application to medical diagnosis," Journal of the Acoustical Society of America **106**, 3678-3686.

Scholte, J. G. (**1947**). "The range of existence of Rayleigh and Stoneley waves," Geophysical Journal International **5**, 120–126.

Shu, X. Z., Liu, Y., Palumbo, F., and Prestwich, G. D. (**2003**). "Disulfide-crosslinked hyaluronan-gelatin hydrogel films: A covalent mimic of the extracellular matrix for in vitro cell growth," Biomaterials **24**, 3825-3834.

Shu, X. Z., and Prestwich, G. D. (**2004**). "Therapeutic Biomaterials from Chemically-Modified Hyaluronan," in *Chemistry and Biology of Hyaluronan*, edited by H. G. Garg, and C. A. Hales (Elsevier Press, Amsterdam), pp. 475-504.

Sinkus, R., Tanter, M., Xydeas, T., Catheline, S., Bercoff, J., and Fink, M. (**2005**). "Viscoelastic shear properties of in vivo breast lesions measured by MR elastography," Magnetic Resonance Imaging **23**, 159-165.

Stevens, K. N., and Hirano, M. (**1981**). *Vocal Fold Physiology* (University of Tokyo Press, Tokyo, Japan).

Thibeault, S. L., Gray, S. D., Bless, D. M., Chan, R. W., and Ford, C. N. (**2002**). "Histologic and rheologic characterization of vocal fold scarring," Journal of Voice **16**, 96-104.

Thibeault, S. L., Klemuk, S. A., Chen, X., and Quinchia Johnson, B. H. (**2011**). "In vivo engineering of the vocal fold ECM with injectable HA hydrogels - Late effects on tissue repair and biomechanics in a rabbit model," Journal of Voice **25**, 249-253.

Titze, I. R. (**1994**). *Principles of Voice Production* (Prentice-Hall, Englewood Cliffs).

Titze, I. R., Klemuk, S. A., and Gray, S. (**2004**). "Methodology for rheological testing of engineered biomaterials at low audio frequencies," Journal of the Acoustical Society of America **115**, 392-401.

Tran, Q. T., Berke, G. S., Gerratt, B. R., and Kreiman, J. (**1993**). "Measurement of Young's modulus in the in vivo human vocal folds," Annals of Otology, Rhinology and Laryngology **102**, 584-591.

Van Krevelen, D. W., and Hoftyzer, P. J. (**1972**). *Properties of Polymers: Correlations with Chemical Structure* (Elsevier, Amsterdam, pp. 1-427).

Vanderhooft, J. L., Alcoutlabi, M., Magda, J. J., and Prestwich, G. D. (**2009**). "Rheological properties of cross-linked hyaluronan-gelatin hydrogels for tissue engineering," Macromolecular Bioscience **9**, 20-28.

Vappou, J., Maleke, C., and Konofagou, E. E. (**2009**). "Quantitative viscoelastic parameters measured by harmonic motion imaging," Physics in Medicine and Biology **54**, 3579-3594.

Verdolini, K., and Ramig, L. O. (**2001**). "Review: Occupational risks for voice problems," Logopedics Phoniatrics Vocology **26**, 37-46.

Ward, P. D., Thibeault, S. L., and Gray, S. D. (**2002**). "Hyaluronic acid: Its role in voice," Journal of Voice **16**, 303-309.

Yamakoshi, Y., Sato, J., and Sato, T. (**1990**). "Ultrasonic imaging of internal vibration of soft tissue under forced vibration," IEEE transactions on ultrasonics, ferroelectrics, and frequency control **37**, 45-53.

Zörner, S., Kaltenbacher, M., Lerch, R., Sutor, A., and Döllinger, M. (**2010**). "Measurement of the elasticity modulus of soft tissues," Journal of Biomechanics **43**, 1540-1545.